A study of pseudomorphism and the growth of palladium on (111) gold and silver.

~~AN INVESTIGATION OF THE GROWTH~~ A STUDY OF PSEUDOMORPHISM AND THE GROWTH OF ~~THIN~~ PALLADIUM ~~FILMS~~ ON (111) SILVER AND GOLD

by

G.N. Burland

A Thesis Submitted for the Degree of
DOCTOR OF PHILOSOPHY
of the University of London

Department of Physics
Imperial College of Science and Technology
London SW7

ACKNOWLEDGEMENTS

I should like to thank my colleagues in the Electron Diffraction Group of the Physics Department, Imperial College, for numerous enlightening discussions and practical assistance. In particular, I should like to express my gratitude to Professor M. Blackman and Dr P.J. Dobson, under whose supervision this work was carried out.

In addition, I am indebted to the Science Research Council for the provision of a maintenance grant, and to Tina Richardson for typing this thesis.

G.N. Burland

CONTENTS

		Page
Abstract		8
CHAPTER 1 :	Introduction	10
CHAPTER 2 :	Interfacial Structures and Pseudomorphism.	12
2.1	Pseudomorphism and Crystal Interfaces.	12
2.2	Dislocations and interfacial Structure.	15
2.3	Theoretical calculations of the structure of Low Misfit Interfaces.	19
2.3.1	The models used in calculations.	20
2.3.2	General results of calculations.	22
2.3.3	A criticism of the models used for calculations.	23
CHAPTER 3 :	A Review of the Application of Experimental Methods in the Study of Pseudomorphism.	26
3.1	The information required for the Study of Pseudomorphism.	26
3.2	Reflection High Energy Electron Diffraction : RHEED.	28
3.2.1	Kinematic Diffraction Theory.	30
3.2.2	Refraction of electrons by the inner potential of the crystal.	34
3.2.3	Dynamical Diffraction Theory.	34
3.2.4	Relaxation of the Diffraction Conditions and the Reciprocal Lattice Spot Size.	37
3.3	Interpretation of RHEED patterns.	39
3.3.1	Measurement of the Lattice Spacing.	39
3.3.2	Broadening of diffraction features.	41

		Page
3.3.3	The streaking of diffraction features.	42
3.3.4	Diffraction from bicrystals, the contribution from multiple scattering and diffractions of dislocation array.	43
3.4	Transmission Electron Microscopy: limitations of the technique.	48
3.4.1	Problem of specimen mounting.	48
3.4.2	Surface Sensitivity.	49
3.4.3	Ultra High Vacuum.	50
3.4.4	Techniques for Chemical Analysis	50
3.5	The use of the electron microscope to determine misfit.	51
3.5.1	Transmission Electron Diffraction.	51
3.5.2	Imaging dislocations in the electron microscope to determine misfit.	52
3.5.3	The determination of misfit in the electron microscope using Moire fringes.	54
3.6	Topographic information from electron microscopy studies.	57
3.6.1	Dark field microscopy.	57
3.6.2	Thickness fringes.	58
3.6.3	Absorption contrast.	58
3.6.4	Surface step resolution.	58
3.6.5	Replication Method.	59
3.7	Analytical Techniques and Electron Microscopy.	59
3.8	The Quartz Crystal Microbalance.	61
3.9	Auger Electron Spectroscopy: AES	63
3.9.1	Factors effecting the quantification of Auger Electron production.	65
3.9.2	Factors effecting the emission and detection of created Auger electrons.	67
3.9.3	The Auger Spectrum.	69

			Page
	3.9.4	Multi-component specimens.	70
CHAPTER 4 :		A Review of Experimental Results of Pseudomorphism.	72
	4.1	Introduction.	72
	4.2	Non-insitu report of pseudo-morphism since 1956.	72
	4.2.1	Chemical Attack.	73
	4.2.2	Diffusion processes.	74
	4.2.3	Further evidence that non-insitu experiments produce anomalous results in the film growth experiment.	76
	4.2.4	Conclusion.	77
	4.3	Insitu Investigations of Pseudo-morphism.	80
	4.3.1	Conclusion	84
CHAPTER 5 :		Experimental Procedures.	85
	5.1	Introduction	85
	5.2	Materials and Specimen Preparation.	85
	5.2.1	(111)Silver Substrate Preparation.	86
	5.2.2	Gold Substrate Preparation.	86
	5.3	The Application of RHEED.	89
	5.3.1	Lattice Spacing Changes.	89
	5.3.2	Crystallinity of Specimens.	92
	5.4	Application of Quartz Crystal Microbalance.	93
	5.4.1	Linearity of Frequency Change.	93
	5.4.2	Absolute Deposit Thickness Deter-mination.	94
	5.5	The Application of Auger Electron Spectroscopy to the Present Study.	95
	5.5.1	Experimental System Employed.	95
	5.5.2	Auger Transitions Observed.	96

			Page
	5.6	A Method of Investigating the Mode of Growth Using Auger Electron Spectroscopy.	102
	5.6.1	The Method of Calculation of Auger Signal Strengths.	102
	5.6.2	The Predicted Auger Signal Strengths.	108
	5.7	Scanning Electron Microscope used in conjunction with Auger Electron Spectroscopy.	111
CHAPTER 6:		The Growth of Palladium on Silver.	113
	6.1	Introduction.	113
	6.2	Results for Room Temperature Depositions.	114
	6.3	Results Indicating the role of Diffusion at Elevated Temperatures.	120
	6.4	Discussion of Growth of Palladium on Silver.	120
	6.5	Conclusions.	125
CHAPTER 7:		The Growth of Palladium on Gold.	126
	7.1	Introduction.	126
	7.2	The Growth of Palladium on (111) Gold at Room Temperatures.	127
	7.3	Results of annealing experiments at elevated temperatures on palladium.	130
	7.4	Discussion of Growth of Palladium on (111) Gold at room temperature.	133
	7.5	Discussion of Results of Annealine Bicrystals Grown at Room Temperature T >550K.	134

		Page
7.6	Results for the Growth of Palladium on (111) Gold at 600K.	136
7.7	Discussion of the growth of Palladium on annealed and Au Bicrystals at 600K.	140
7.8	Discussion of the results of the present work in relation to other investigations on the same system.	142
7.9	Conclusions.	144
REFERENCES:		145

ABSTRACT

An experimental investigation has been carried out of the growth of vapour deposited overlayers of palladium on (111) silver and gold substrates. The experiments were performed under ultra-high vacuum conditions and in situ observations were made with Reflection High Energy Electron Diffraction R.H.E.E.D., and Auger Electron Spectroscopy A.E.S.

For all the conditions investigated the overlayers were found to grow epitaxially in parallel orientation with the substrate. Accurate R.H.E.E.D. measurements of the specimen surface lattice spacing were obtained as a function of overlayer film thickness. The thinnest overlayers deposited at room temperature were elastically strained to match the substrate and the strain was found to decrease continuously with increased film thickness.

By interpretation of the R.H.E.E.D. patterns and by correlation of A.E.S. data with the quantity of material deposited, the mode of growth of the overlayer was determined. Overlayers deposited at room temperature grew initially in a layer by layer mode maintaining a sharp interface with the substrate.

Observations carried out after annealing the films to temperatures > 550K demonstrated the actions of diffusion processes at higher temperatures. These observations indicate that the assumption of immobility made in similar investigations at elevated temperatures are of questionable validity.

CHAPTER 1

Introduction

The epitaxial growth of deposit crystals strained to match the substrate (pseudomorphism) has been widely reported and has gained acceptance as a phenomenon frequently occurring at interfaces of low natural misfit.

The approach throughout this study is to question the assumptions and observations of pseudomorphism. At the outset criteria were developed by which pseudomorphic systems could be identified. These criteria were then related to the design requirements of experiments capable of establishing pseudomorphism. The aim of the present investigation was to determine the existence of pseudomorphism in a low misfit system, examining critically the influence of diffusion processes on the results.

The general concepts and definitions related to interfacial phenomena are outlined in Chapter Two. The range of possible interfacial structures are presented and the concept of interfacial dislocations examined. The basic properties of pseudomorphic systems are introduced with the models used for calculations related to the phenomena.

Techniques which have been used in experimental investigations of pseudomorphism are discussed in Chapter Three in relation to the criteria developed to establish pseudomorphic systems. Transmission electron microscopy and reflection high energy electron diffraction are examined in particular,

the inherent surface sensitivity of RHEED is considered to provide an advantage over TEM in identification experiments.

The experimental evidence for pseudomorphism is reviewed in Chapter Four, in which non-insitu studies areshown to be subject to an unacceptable number of uncontrolled factors. A number of in situ investigations are considered to demonstrate the existence of pseudomorphism. However it is considered very necessary to examine carefully the role of diffusion in all experiments.

The application of the available experimental techniques in the present investigation is described in Chapter Five.

The experimental growth of Pd/Ag and Pd/Au as determined in the present study is described in Chapters 5,6 and 7. Evidence of pseudomorphic strains is presented and Auger electron spectroscopy is successfully applied to demonstrate a two-dimensional growth mode in the case of films grown at room temperature. A major change in specimen configuration is observed at elevated temperatures.

CHAPTER 2

Interfacial Structures and Pseudomorphism

2.1 Pseudomorphism and crystal interfaces

The atomic configuration across the plane interface of two crystals A + B changes periodically with displacement in the interface. We shall be concerned with a simple case illustrated in Fig. 2.1 in which the interfacial planes having a rectangular symmetry.

The natural misfit M_o is the parameter which characterises the difference in atomic spacing when a_o and b_o are the corresponding values for the bulk crystals

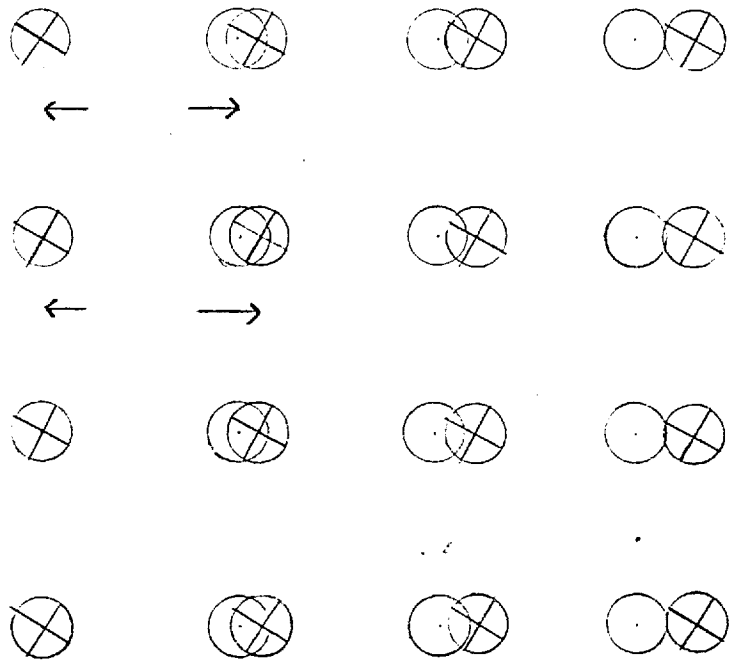
$$M_o = \frac{b_o - a_o}{a_o} \qquad 2.1$$

The misfit M is then defined by

$$M = \frac{b-a}{a} \qquad 2.2$$

where a and b are the average observed spacings corresponding to a_o and b_o. The period of the variation of the interface configuration is aN when $aN = (N \mp 1)b$ 2.3 where N is an integer such that equation 2.3 is a good approximation. The interaction of the crystals via the A-B bonding produces a periodic interfacial potential U(x) of period Na, the forces resulting from which necessitate the existence of reactional forces associated with small atomic displacements in both crystals.

The small displacements are determined by the equilibrium of the interfacial and reactional forces and must vary with the period Na.



Atoms of lattice B

Atoms of lattice A

Planes of AB interface with mismatch along one axis only

Figure 2.1

The energy of formation of the crystalline interface per unit area E_I may be written

$$E_I = E_{AB} + E_{BB} + E_{AA} \qquad 2.4$$

where E_{AB} is the interaction energy of the A-B bonding/unit area.

E_{AA} and E_{BB} are the increases in the energies of the crystals A and B due to the existence of the deformation discussed above.

We shall consider crystal B to be in the form of a thin film of thickness h growing on a crystal A of large dimensions.

Since the energy of a system containing an overall strain is given by

$$\text{Strain energy} = \text{constant} \times \text{strain}^2 \times \text{volume of material strained}$$

Any overall strain ε in the bi-crystal will occur preferentially in the overlayer.

$$\varepsilon = \frac{b_o - b}{b_o} \qquad 2.5$$

Since $a_o \simeq b_o >> b_o - b$.
a relation between the strain and the misfit is obtained

$$\varepsilon \simeq \frac{b_o - b}{a_o} = M_o - M \qquad 2.6$$

The term E_{BB} of equation 2.4 will increase with ε and h whereas E_{AB} will be a minimum when $\varepsilon = M_o$: i.e. the overlayer

is deformed to match the substrate.

It follows that a thin overlayer may minimize the energy of the bi-crystal via E_I by growing pseudomorphically strained to match the substrate. Since E_{BB} is also dependent on a film thickness h, as h increases E_{BB} will dominate the right hand side of equation 2.4 and the strain ε of the pseudomorphic layer will reduce to maintain equilibrium.

2.2. Dislocations and interfacial structure

From the geometrical similarity of the structures illustrated in figures 2.2 and 2.3. it is seen that the interface represented in figure 2.3. may be described as an array of dislocations. The structures represented in figures 2.2., 2.3. and 2.4. form one period of the periodic interfacial structure. It is also clear that the same Burgers vector may be associated with these three structures. The misfit M accommodated by all these structures is

$$M = \frac{NG-Na}{Na} = \frac{b}{s} \qquad 2.7$$

where $\underline{b}$ is the Burgers vector of the dislocations

s is the separation of the dislocations.

From equations 2.6. and 2.7. it is evident that misfit at an interface is accommodated by a combination of elastic strain and dislocation:

$$M_o = \varepsilon + \frac{b}{s} \qquad 2.8$$

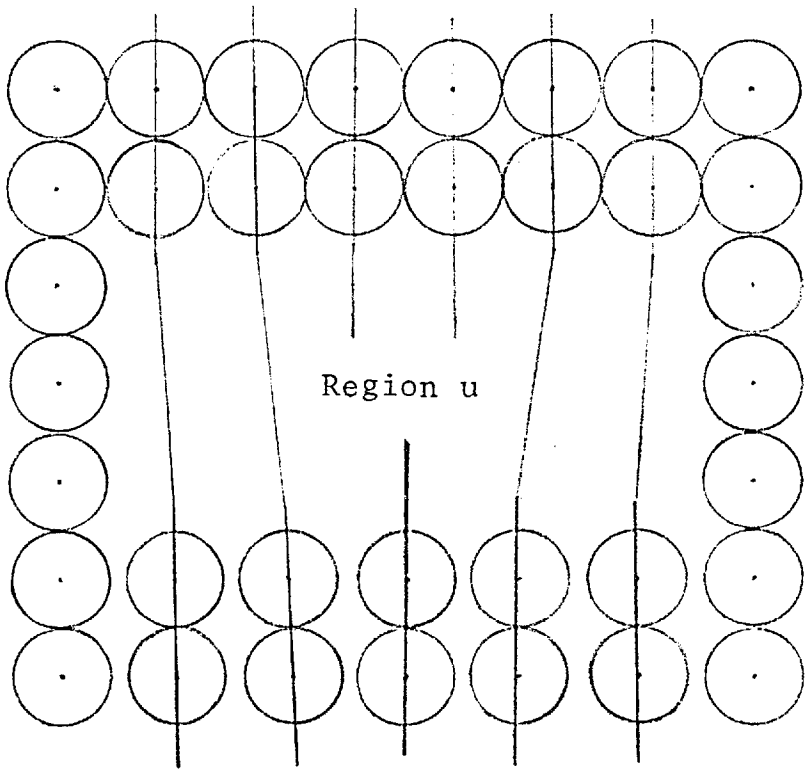


Figure 2.2

Representation of the atomic arrangement around an edge dislocation. A section normal to the line of the dislocation. The distortion of planes normal to the section is illustrated.

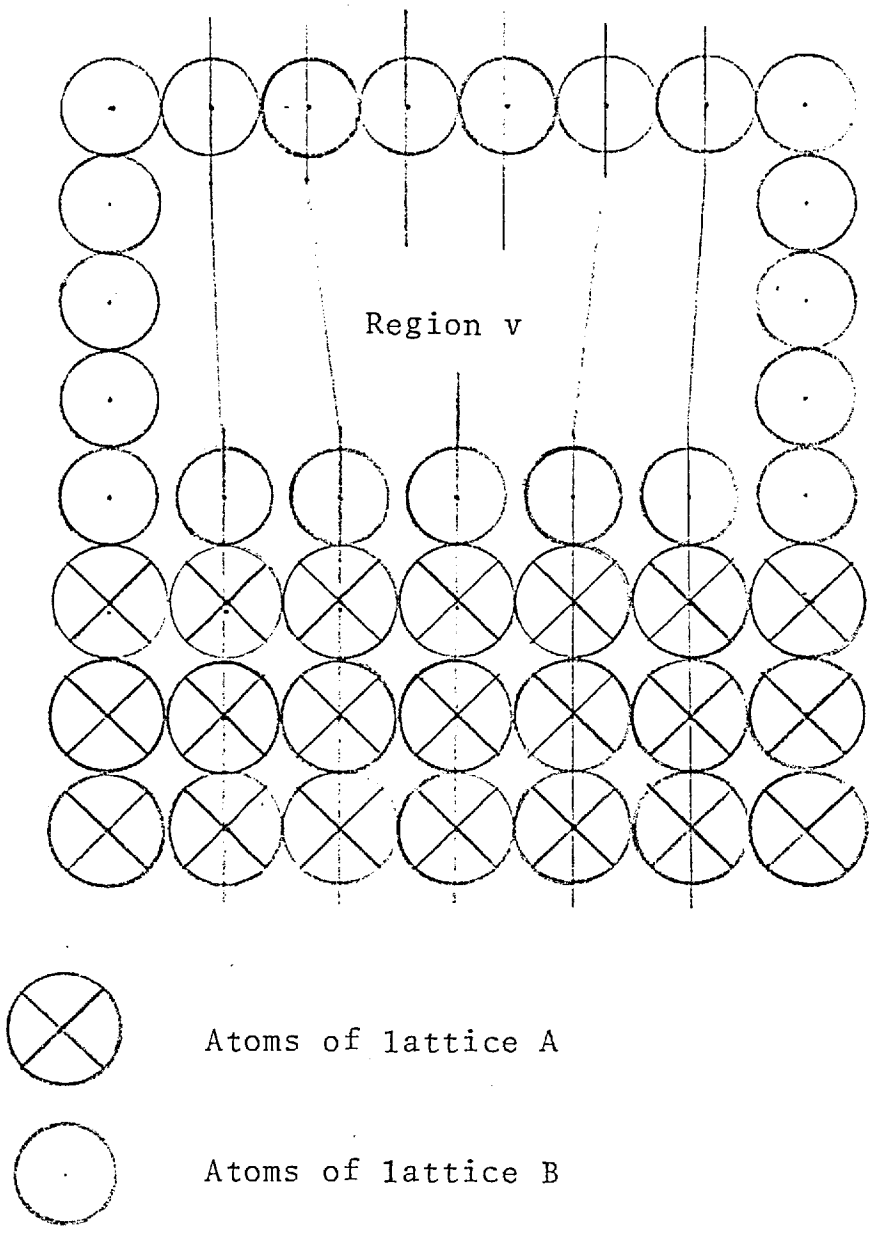


Figure 2.3

Atomic structure of a plane perpendicular to an AB interface, one atomic layer of B having a pseudomorphic configuration.

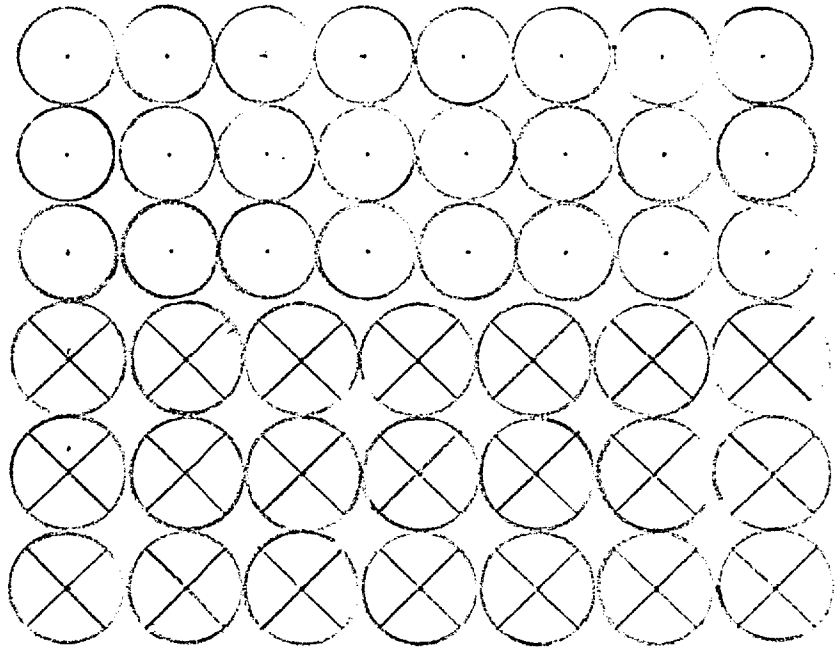


Figure 2.4

An atomic plane perpendicular to an AB interface

(a) Between non-interacting crystals
(b) Between rigid crystals.

Hence we may say that the interfacial energy E_I is composed of a strain energy component $E_{(\varepsilon)}$ and a dislocation energy component $E_{(D)}$.

$$E_I = E_D + E_\varepsilon. \qquad 2.9$$

Regions u and v of figures 2.2 and 2.3 contain similar deformations of the crystal lattice and are large compared with any deformations associated with the interface of figure 2.4. Consequently the energy E_{BB} of regions u and v will be similar and larger than E_{AA} or E_{BB} associated with the structure of figure 2.4. If the interfacial energy of the structure of figure 2.4 is lower than that of figure 2.3 it would be energetically favourable for a film, which grew pseudomorphically while very thin, to adopt the structure of figure 2.4 on thickening. The occurrence of such a transformation requires the removal of holes from formerly pseudomorphic planes and hence a degree of atomic mobility. The potential energy gradient associated with the transformation would assist in providing a driving force for the diffusion process.

2.3. Theoretical Calculations of the Structure of Low Misfit Interfaces

A number of workers have examined theoretically the properties of crystalline interfaces, of the type discussed above. The important parameters include the average elastic strain ε and the interfacial energy E_I. Exact calculations are not possible because the form of the interatomic potentials $V_{AA}(r)$ $V_{BB}(r)$ $V_{AB}(r)$ are not known and the number of

variables, the individual atomic displacements are large.

In section 2.3.1 the models used in calculations are outlined. The general results obtained are presented in section 2.3.2. How well the models used correspond to an actual physical situation is considered in section 2.3.3.

2.3.1. The models used in calculations

The different models with which calculations have been made are outlined below:

(a) Van der Merwe 1

Van der MERWE (1970) obtained an expression for E_{AB} by assuming a simple form for the interatomic potential variations V_I in the interfacial atomic plane of B. In order to determine the energies E_{AA} and E_{BB} he treated the crystals A and B as isotropic elastic media subjected to local strains. By requiring that each atom be in equilibrium under the influence of the elastic and interfacial forces an expression for the displacement of each atom was found. The interfacial energy E_I is then obtained by substitution as a function of the elastic moduli, the amplitude of the chosen interfacial potential, V_I the misfit and the film thickness.

(b) Van der Merwe 2

This method Van der MERWE (1950, 1963a,b) treats the calculations of E_{AB} as well as E_{AA} and E_{BB} as elasticity problems, by ascribing elastic moduli to the interface and applying a periodic shear wave there. The problem may be solved after imposing boundary conditions at the interface

and surfaces of the crystals.

(c) Ying

YING (1970) has made calculations with the same model as Van der Merwe 1. He has however not made Van der Merwe's assumption that the interatomic distance within the interfacial planes must change slowly with position. These calculations add nothing to those of Van der Merwe in the primary area of study of this work. They do however examine overlayer systems which are commensurate but not pseudomorphic.

Such studies are particularly relevant to the investigation of submonolayer absorbates and are developed to examine their lattice vibrational spectrum.

(d) Fletcher

FLETCHER (1967) and FLETCHER & LODGE (1975) have followed Van der Merwe in treating the strain energies E_{AA} and E_{BB} as resulting from the action of a periodic interfacial shear wave on an elastic medium. For the calculation of the interaction energy E_{AB} however he assumed a model potential for $V_{AB}(r)$ and evaluated E_{AB} as the sum of the individual contributions. In doing this Fletcher has made use of a Morse potential and an ab initio potential for aluminium.

(e) Matthews

MATTHEWS (1975) has calculated the equilibrium strain in thin overlayers by an alternative method. This requires the determination of a mechanism by which misfit dislocations

may be introduced into a pseudomorphic film. The forces imposed by the stress field which favour the formation of dislocations may thus be specified. The expression for ε the mean overlayer strain is then obtained by examining the equilibrium of the stress field forces and the forces which oppose the formation of dislocations.

2.3.2. General Results of calculations

It is shown that a pseudomorphic structure is energetically favourable in thin films provided that certain conditions are satisfied. Pseudomorphism is found to be favoured by strong interfacial bonding A-B relative to the A-A and B-B bonding. A small misfit M_o is shown to be a prerequisite for pseudomorphism and in the case of the A-A, B-B and A-B bonding having equal strength the inequality, $M_o < \sim 0.1$ is found to be a condition for pseudomorphic growth.

There is a critical film thickness h_c such that thicker films at equilibrium contain misfit dislocations.

The interfacial energy E_I is found to increase with misfit M_o and with the strength of the interfacial bonding AB. Fletcher refined the calculation and was able to show that cusps occurred in the interfacial energy curve as both a function of misfit and angular rotation of the crystals. This may be understood to occur when a larger number of interface atoms, as a result of a particular transformation, occupy sites closer to those of the other lattice hence lowering the energy of the structure.

2.3.3. A Criticism of the models used for Calculations

The application of the models outlined in section 2.3.1. is restricted to cases in which the following restrictions may be accepted.

(i) The interface is planar.

(ii) The lateral dimensions of the interface are large so edge effects may be neglected.

(iii) The film is homogeneously thick.

(iv) The crystals A and B are mutually insoluble.

(v) Either there is a non-zero mismatch in one interfacial direction or the strains in two mutually perpendicular directions produce no interaction.

The structure and interfacial energy of 3D islands has also been examined, CANBRERA (1964), JESSER & KUHLMANN WILSDORF (1967), JESSER & Van der MERWE (1971) and others, but island deposits are not considered in chapter two.

The five major approximations of the calculations of section 2.3.1. which may affect their entire validity are as follows:

(1) A rigid substrate

The requirement that the stress varies continuously across the interface proves this to be an incorrect physical assumption.

Calculations by BALL (1970a,b) show that the relaxation of a substrate substantially reduces the interfacial energy.

This result remains generally true in the case of very thin overlayers on thick substrates. The energy E_{AA} may only be considered negligible in the case of a thin pseudomorphic layer on a thick substrate. E_{AA} then increases in proportion to the dislocation density.

(2) Overlayer strains do not change from layer to layer

This assumption only corresponds to a true physical situation in the case of pseudomorphism or overlayers one atom thick, ie monolayers. The use of this approximation outside the above regime is not valid.

(3) The Component of the Interfacial Interaction normal to the interface is zero

A calculation allowing a uniform displacement of the interfacial planes normal to the interface has been made by Van der MERWE (1963a,b) using a parabolic interatomic potential V_I. He showed that the contribution to the interfacial energy E_I from this source was $\simeq$ 10% and was independent of the natural misfit. This contribution to E_I results from a force other than first nearest neighbours.

(4) The range of the interaction V_{AB} has been limited to planes adjacent to the interface

This is an incorrect physical assumption since it partially neglects the contribution of non first nearest neighbour forces. NIEDERMAYER (1975) has demonstrated this contribution by showing the binding energy of sodium absorbed on tungsten to change over the first four atomic layers. An

effect of increasing the range of the interaction will be to enhance the difference of the interfacial energy between monoatomic overgrowths and overgrowths several monolayers thick.

(5) The use of isotropic elasticity theory

The application of continuum elasticity theory to problems of strains in solids while inexact is very widely adopted. Several specific problems in its application will be noted. Isotropic elastic modulii have been used in the calculation whereas the dislocation energies obtained using anisotropic theory show variations from isotropic values of ≃ 20% ESHELBY J.D. (1949).

Bulk values of the elastic modulii have been used for the special cases of thin films, the interface and strained films, all of which will modify the bulk value.

The adoption of elastic modulii for the interface assumed to be equal to the average of the substrate and overlayer values is an arbitrary procedure. In general this is probably only partially justified for deposit substrate combinations which form ideal solid solutions.

CHAPTER 3

A review of the application of experimental methods in the study of pseudomorphism

3.1. The information required for the study of pseudomorphism

The study of pseudomorphism has largely consisted of the identification of the systems in which the phenomenon is observed. The simple theories discussed in section 2.3. associated its occurrence with low misfit, thin deposits and strong interfacial bonding. These theoretical results have been supported by the experimental observations of MATTHEWS (1970) β Co/Ca, YAGI et al (1971) Pd/Au and many others.

Pseudomorphism is however still not well understood for several reasons:

(1) Conflicting results and their interpretation have led to a dispute over the identification e.g. KUNZ et al (1969), GRADMANN (1964, 1966) Ni/Cu and MATTHEWS (1966), YAGI et al (1971) Pd/Au.

(2) Experimental data which adequately characterises the interfacial bonding has not been available.

(3) It has not been possible to produce a theoretical treatment of the problems using a realistic model.

Recently in addition to identifying pseudomorphic systems emphasis has been placed on the study of the transition from a strained pseudomorphic state to the unstrained state as the overlayer thickness is increased. YAGI et al (1971); STOWELL & CHERNS (1975).

To classify a particular deposit/substrate combination as pseudomorphic the following criteria must be satisfied:-

(a) The deposit must have the same structure and interatomic spacing as the substrate, i.e. show that M = 0.

(b) The presence of an actual deposit must be ascertained. Since no change in the lattice spacing would also be observed in the trivial case of there being no deposit.

(c) Contamination of the specimen must be prevented or the extent and effect of the contamination established.

(d) Diffusion processes must be monitored and accounted for in the interpretation of the observations.

Although pseudomorphism is established by considering the above criteria, in order to produce a model, a knowledge of the mode of growth is necessary ie: the Volmer Weber mode - three-dimensional, the Frank van der Merwe mode - two-dimensional and the Stranski Krastanov mode, BAUER (1958).

A technique of structural observation is therefore obviously required in studies of pseudomorphism; this usually involves electron microscopy. The criteria (b) (c) and (d) require a method of chemical analysis and to satisfy (c) ultra high vacuum U.H.V. procedures and great care in experimental construction is necessary. The techniques must be applied in situ to limit uncertainties arising in the interpretation of the results.

Because pseudomorphism is only expected to occur in thin film deposits a high degree of surface sensitivity is required in all the techniques used.

3.2. Reflection High Energy Electron Diffraction : RHEED

RHEED is a technique of electron diffraction which makes use of electron beams of energy greater than 10 keV incident on specimens of grazing angles in the range 0-5°. The total elastic cross section Q for the scattering of high energy electrons depends on the electron energy E and the atomic number of the scattering material Z.

The elastic mean free paths of 40 keV electrons in Aluminium and Gold obtained by calculation are 305 + 28Å respectively MISELL (1973). These values correspond to a penetration of the specimen by a beam incident at 5° of 55Å and 4Å. Although multiple elastic scattering allows a fraction of the beam to interact with the specimen at much greater depths, in all but the thinnest specimens most emitted electrons emerge from the specimen face on which they were incident. The differential cross section for the scattering of high energy electrons has a strong maxima for small angles of scattering, < 5° from the incident beam, and hence the diffraction pattern is conveniently displayed on a small fluorescent screen adjacent to the straight through beam. The nature of the specimen surface will determine whether the diffraction pattern is a true reflection pattern or as a result of surface roughness a "reflection" transmission pattern Fig. 3.1a,b. The small beam penetration depth provides a surface sensitivity comparable to LEED and in principle a technique for depth profiling the structure by varying the angle of incidence or beam energy. NEWMAN, PASHLEY (1955).

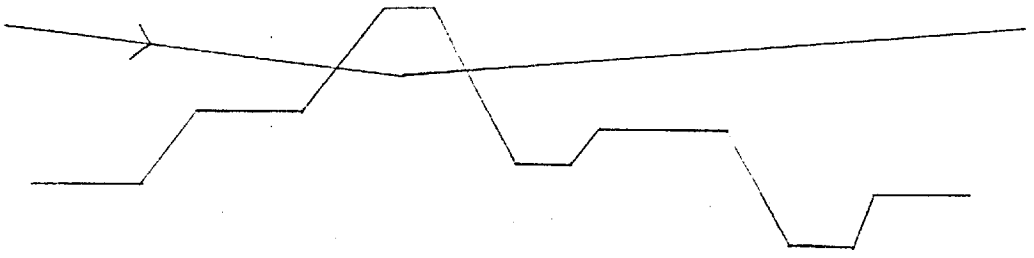


Figure 3.1a
Transmission "Reflection" Diffraction

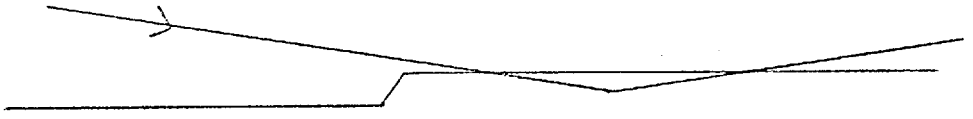


Figure 3.1b
True Reflection Diffraction

3.2.1. Kinematic Diffraction Theory

The problem of predicting the elastic scattering of electrons may be approached by the solution of the Shrodinger equation

$$(\nabla^2 + \underline{k}^2 - U(\underline{r}))\psi(\underline{r}) = 0 \qquad (3.1)$$

Where U(r) is the scattering potential.

This is equivalent to the integral equation

$$\psi(\underline{r}) = \exp(i\underline{k}.\underline{r}) - \frac{1}{4\pi} \int \exp(i\underline{k}.|r-\acute{r}|)\, U(\acute{\underline{r}})\psi(\acute{\underline{r}})\, \frac{1}{|r-\acute{r}|}\, d\acute{\underline{r}} \qquad (3.2)$$

Where, for elastic scattering, $|\underline{k}| = |\underline{k}_o|$ and $\exp(i\underline{k}_o.\underline{r})$ represents the incident plane wave. $\psi(\underline{r})$ is the resultant wave function at the point having position vector $\underline{r}$ expressed as the summation of the spherical waves of different phases originating from scattering events from points having position vectors $\acute{\underline{r}}$. The amplitude of the spherical waves being determined by the scattering power of the potential at the point of scattering $U(\acute{\underline{r}})$ and amplitude of the incident wave $\psi(\acute{\underline{r}})$.

Since we are interested in the resultant at distances r large compared with the sample dimensions we may approximate the denominator $|r-\acute{r}| = r$ and rewrite equation 3.2 as equation 3.3:

$$\psi(\underline{r}) = \exp(i\underline{k}_o.\underline{r}) - \exp(ikr)\frac{1}{4\pi r} \times \int \exp(i\underline{k}.\underline{f}) U(\underline{f})\ \psi(\underline{f})\ d\underline{f} \qquad (3.3)$$

In the kinematic approximation it is assumed that the incident wave is unattenuated and hence that the incident wave at each scattering point $\psi(\underline{f}) = e^{i\underline{k}_o.\underline{r}}$. For a crystal $U(\underline{f})$ is periodic having a potential distribution within a unit cell $\phi(\underline{f})$ as its basis. The scattering due to the whole crystal is the scattering for a single unit cell transposed throughout the crystal.

$\phi(\underline{f})$ the scattering potential of the unit cell may be written in equation 3.4 as the summation of the scattering potentials ϕ_j of the j atoms which make up the unit cell. The position of the j^{th} atom being specified by the vector $\underline{r}_j$ within the cell.

$$\phi(\underline{f}) = \sum_j \phi_j(\underline{f}-\underline{r}_j) \qquad (3.4)$$

The position of each unit cell within the crystal $\underline{f}$ is written as

$$\underline{f} = m_1\underline{a}_1 + m_2\underline{a}_2 + m_3\underline{a}_3 \qquad (3.5)$$

where $\underline{a}_1$, $\underline{a}_2$ and $\underline{a}_3$ are the vectors of the unit cell, and m_1, m_2 and m_3 are integers which specify the position of the unit cell along each of the three crystallographic axis.

The scattered wave function from a parallelipiped crystal consisting of M_1 M_2 and M_3 unit cells is given by equation 3.6.

$$\psi(\underline{r}) = \exp(ikr)\,\frac{1}{4\pi r}\int_{\text{unit cells}} \exp(i(\underline{k}-\underline{k}_o).\underline{f})\,\phi(\underline{f})\,d\underline{f}$$

$$\times \sum_{m_1=0}^{M_1-1}\sum_{m_2=0}^{M_2-1}\sum_{m_3=0}^{M_3-1} \exp(i(\underline{k}-\underline{k}_o).(m_1\underline{a}_1+m_2\underline{a}_2+m_3\underline{a}_3)) \qquad (3.6)$$

or may be written as

$$\psi(\underline{f}) = \exp(i\,kr)\,\frac{1}{4\pi}\,F(\underline{k}-\underline{k}_o) \times G(\underline{k}-\underline{k}_o) \qquad (3.7)$$

where $F(\underline{k}-\underline{k}_o)$ is termed the structure amplitude and $G(\underline{k}-\underline{k}_o)$ the lattice amplitude.

We may write $(\underline{k}-\underline{k}_o)$ in terms of the reciprocal lattice vector b_j of the diffracting crystal.

$$2\pi\,\underline{H}_i = \underline{k} - \underline{k}_o = k_1\underline{b}_1 + k_2\underline{b}_2 + k_3\underline{b}_3 \qquad (3.8)$$

where the reciprocal lattice vectors are defined by

$$\underline{a}_i \cdot \underline{b}_j = \delta_{ij} \qquad (3.9)$$

The summation of equation 3.6 may then be rewritten as

$$\sum_{m=0}^{M_i-1} \exp(-ik_j m_i) = \frac{\sin(\frac{M_i k_j}{2})}{\sin(\frac{k_j}{2})} \times \exp(-\tfrac{1}{2}(M-1)k_j) \qquad (3.10)$$

The intensity distribution $|\psi(\underline{r})|^2$ is proportional to $|G(\underline{k}-\underline{k}_o)|^2$ and from equation 3.10 and 3.6.

$$|G(\underline{k}-\underline{k}_o)|^2 = \frac{\mathrm{Sin}^2\tfrac{1}{2}M_1k_1}{\mathrm{Sin}^2\tfrac{1}{2}\,k_1}\quad\frac{\mathrm{Sin}^2\tfrac{1}{2}M_2k_2}{\mathrm{Sin}^2\tfrac{1}{2}\,k_2}\quad\frac{\mathrm{Sin}^2\tfrac{1}{2}M_3k_3}{\mathrm{Sin}^2\tfrac{1}{2}\,k_3} \qquad (3.11)$$

The function $|G(\underline{k}-\underline{k}_o)|^2$ has strong maxima for integral values of k_1 k_2 and k_3 i.e. diffracted beams containing the majority of the elastically scattered electrons exist for discrete values of $\underline{k}$ such that the values of k_1 k_2 and k_3 of equation 3.8. are integers.

$$\underline{k}-\underline{k}_o = k_1\underline{b}_1 + k_2\underline{b}_2 + k_3\underline{b}_3 = H_{iDIFF}$$

when k_1 k_2 k_3 are all integers (3.12)

For a particular crystal structure, some integral values of k_1 k_2 k_3 correspond to zero values of the structure factor $|F(\underline{k}-\underline{k}_o)|^2$ equation 3.7. The associated diffracted beams do not then occur.

From equation 3.12 H_{iDIFF} is a reciprocal lattice vector and a graphical construction (the Ewald sphere construction) of the diffraction conditions in reciprocal space is possible.

A sphere (the Ewald sphere) of radius $\frac{|\underline{k}_o|}{2\pi}$ is drawn in the reciprocal lattice passing through a reciprocal lattice point which has $\frac{k_o}{2\pi}$ for its radius. All other reciprocal lattice points which intersect the sphere define by their radii the possible diffracted beam directions. Figure 3.2. For the electron energies used in RHEED, the sphere radius

is very large compared with the dimensions of the reciprocal lattice and for small scattering angles the Ewald sphere approximates to a plane Figure 3.3.

The diffraction pattern observed on a fluorescent screen corresponds to the projection of the reciprocal lattice points intersected by the Ewald sphere over the camera length L.

3.2.2. Refraction of Electrons by the Inner Potential of the Crystal

The inner potential of the specimen crystal accelerates the electrons on entering the crystal from the vacuum producing a difference in the electron wavelength in and out of the crystal. This gives rise to refraction at the crystal surface. Figure 3.4.

3.2.3. Dynamical Diffraction Theory

The strong scattering of electrons by matter means that the kinematic approximation used above does not agree well with experiment. A correct analysis of the scattering would include the attenuation of the incident beam, and allow the diffracted beams to be subjected to further scattering. Such a theory predicts the formation of a dynamic equilibrium between the intensities of the incident and diffracted beams which are now a complicated function of the crystal dimensions. In this more complete analysis diffraction maxima H_{iDIFF} equation 3.12 which are forbidden by zero values of the structure factor may occur if diffracted beams H_{jDIFF} and H_{kDIFF} exist such that

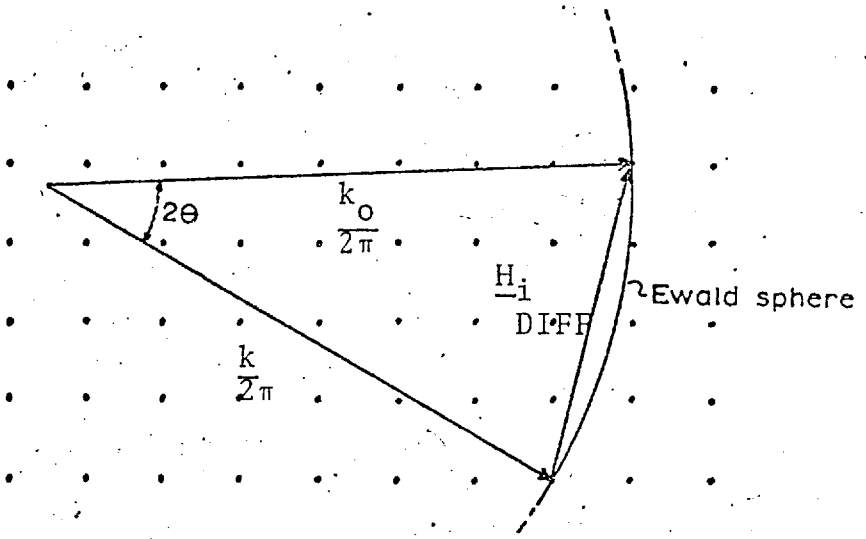


Figure 3.2

The Ewald sphere construction

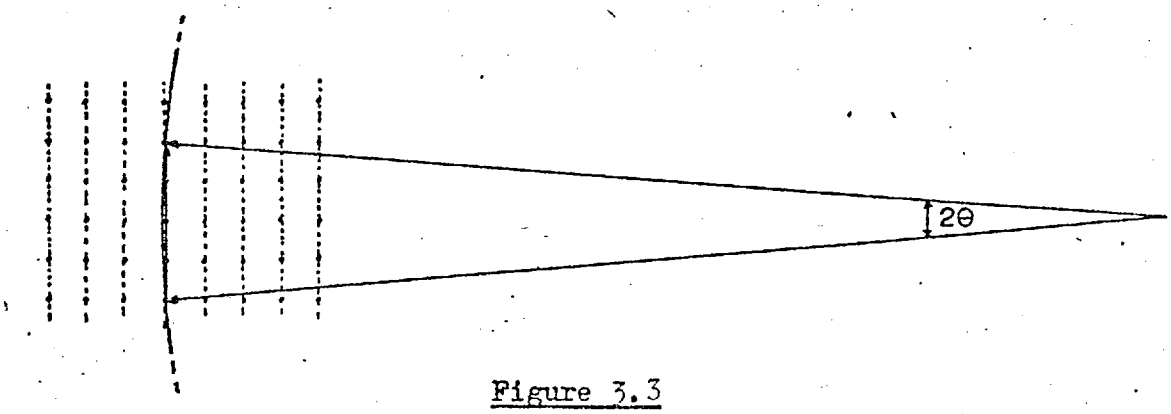


Figure 3.3

Ewald sphere construction applied to RHEED

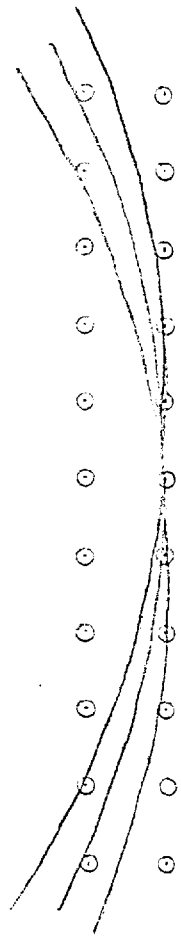


Figure 3.5

Ewald sphere construction for three slightly different incidence angles.

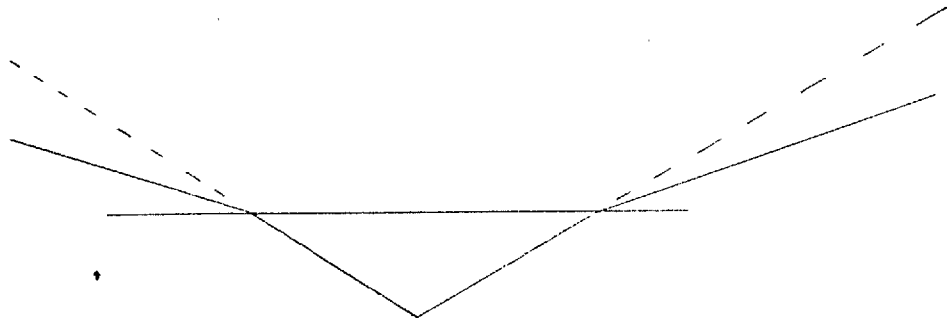


Figure 3.4

Refraction of crystal surface in RHEED

$$\underline{H}_{iDIFF} = \underline{H}_{jDIFF} + \underline{H}_{kDIFF} \qquad (3.13)$$

The dynamical formulation of diffraction theory also allows small deviations from the condition for strong diffraction equation 3.12.

The instantaneous atomic separation varies as a result of thermal vibrations. The effect of this variation may be incorporated in diffraction theory by the use of equation 3.14 which results from the convolution of the probability distribution function of the vibrating atom $e^{-\underline{\delta}_i^2 . \underline{k}_i^2}$ with $G(\underline{k}-\underline{k}_o)$ from equation 3.6.

Hence
$$G(\underline{k}-\underline{k}_o)_{vib} = \sum_{m_1 0}^{M_1 - 1} \sum_{m_2 0}^{M_2 - 1} \sum_{m_3 0}^{M_3 - 1} \exp i(\underline{k}-\underline{k}_o)$$

$$[(m_1+\delta_i)\underline{a}_1 + (m_2+\delta_2)\underline{a}_2 + (m_3+\delta_3)\underline{a}_3] \qquad (3.14)$$

where δ_i are the components of the instantaneous displacement of the atoms from their mean positions.

3.2.4. Relaxation of the Diffraction Conditions and the Reciprocal Lattice Spot Size

As a result of a number of effects discussed below strong diffraction may occur for small deviations from the diffraction condition. equation 3.12.

The effect of crystal size thermal vibration and local disorder in allowing these small deviations may be represented in the Ewald sphere construction by allowing the reciprocal lattice points to occupy a finite volume. The

Ewald sphere then intercepts many more reciprocal lattice spots and many more diffracted beams result.

The function $|G(\underline{k}-\underline{k}_o)|^2$ of equation 3.11 has now zero values within a region $\pm \frac{k_i}{M_i}$ of the reciprocal lattice point. Strong diffractions occur in directions thus defined. The extent of this region is dependent on M_i, the size and shape of the crystal. This has the effect of reducing the intensity of the diffracted beams and increasing the reciprocal lattice spot size. This form is valid if either the atomic displacements are small or their amplitudes obey a Gaussian distribution.

The angular width of the electron beam may be represented in the Ewald sphere construction by a range of incident beam directions Fig. 3.5. This may lead to the intersection of the Ewald sphere by reciprocal lattice points which would not otherwise occur, i.e. giving an apparent increase in spot size.

Aspects of crystal structure which lead to a range of atomic spacings produce broadened diffraction features. This effect is expected to result from elastic strains, alloying and crystal disorder.

The presence of a range of electron energies in a imperfectly monochromated electron beam is equivalent to a range of radii of the Ewald sphere. This effect is usually insignificant because accelerating voltages of high stability are used (variation 1 part in 2×10^5).

3.3. Interpretation of RHEED Patterns

A great deal of information about the structure of the specimen surface may be obtained from the geometry of RHEED patterns. For example, the crystal type, the orientations present and the lattice parameter and, in some circumstances, details of the topography, i.e. the flatness and crystal sizes may be determined. Because of the complexity of the application of dynamical diffraction theory to RHEED little attempt has been made to make use of quantitative RHEED intensity measurements to examine the properties of materials. Consideration has been given however to determining the relaxation and the lattice spacing normal to the surface MENADUE (1972) but little success has been achieved.

The direct crystal lattice and the orientations present can be determined by recording diffraction patterns for different orientations of the incident beam with respect to the crystal azimuthal directions.

3.3.1. Measurement of the Lattice Spacing

The separation of diffraction features recorded on a plane screen may be related to the dimensions of the reciprocal lattice and hence the direct lattice Figure 3.6a,b.

From Figure 3.6b it is seen that

$$\tan 2\theta = \frac{r}{L} \qquad (3.15)$$

From Figure 3.6a

$$\sin \theta = \frac{H}{2} \lambda \qquad (3.16)$$

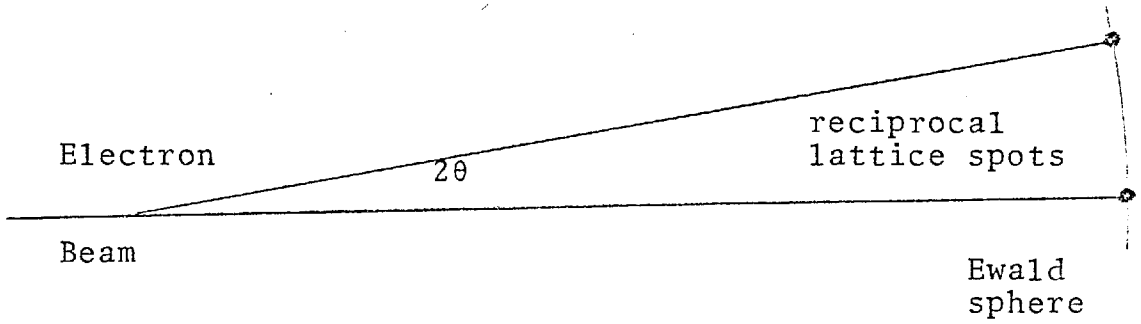


Figure 3.6a

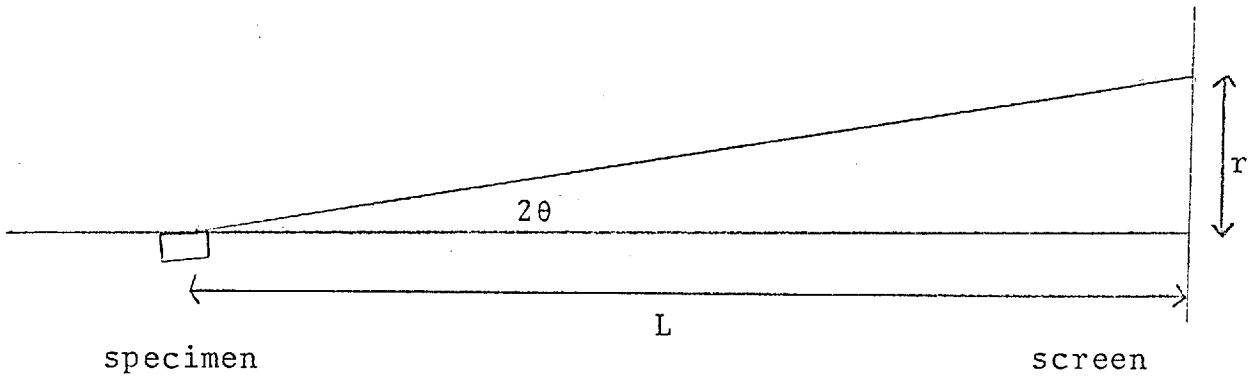


Figure 3.6b

The geometries of (a) Ewald sphere construction.
(b) the projection of the diffracted beams onto the fluorescent screen.

Therefore $$\frac{L\lambda}{2} \frac{\tan 2\theta}{\sin\theta} = rd \qquad (3.17)$$

Expanding the trignometric functions as power series in θ may be shown that

$$L\lambda = rd \left(1 - \frac{3}{8} \frac{r^2}{L^2} + \frac{37}{138} \frac{r^4}{L^4}\right) \qquad (3.18)$$

since $L >> r$.

The equation $L\lambda = rd$ is sufficient for many applications. For typical experimental values of L and r $\frac{3}{8} \frac{r^2}{L^2} \simeq 0.001$.

3.3.2. Broadening of Diffraction Features

A number of aspects of specimen structure were considered in section 3.2.4 which gave rise to the broadening of diffraction features. The difficulty of distinguishing the different contributions to the broadening severely limits the usefulness as an experimental technique. The same effects have been monitored in X-ray diffraction with much greater success TAYLOR (1961).

Mosaic structures have been examined by observing the resultant broadening of electron diffraction features, VAINSHTEIN (1968). This may be understood as resulting from a single well defined incident beam acting on a superposition of reciprocal lattices rotated through small angles with respect to one another.

The dimensions of crystallites in the plane of the specimen surface may be estimated when they are sufficiently small i.e. < 100Å, to cause greater broadening than the other effects acting.

Elastic strains and disorder have been associated with the observations of broadened diffraction features but no quantitative analysis has been possible.

3.3.3. The Streaking of Diffraction Features

The elongation of diffraction features normal to the crystal surface in true reflection RHEED patterns is much greater than the broadening observed in other directions. This may result from a combination of effects, specimen topography, surface thermal vibrations, planar defects and refraction.

For diffraction from an atomically flat surface the limited beam penetration may be thought of as diffraction from a crystal having a small dimension normal to the surface. This gives rise to a streaking of diffraction features in the same direction. This has the effect of modulating the diffraction streaks obtained from a flat surface according to the topography of a real surface. Multiple elastic scattering gives rise to contributions to the diffracted beams from considerable depth in the crystal and prevents any simple analysis of the effect.

The crystal surface is expected to allow localised additional vibrations normal to the surface. The amplitudes of these vibrations though dependent on the particular surface plane may be up to twice that of the bulk. The diffraction features become smaller and more modulated as the number of atomic planes making a substantial contribution to the diffracted intensity increases. The contribution of diffracted waves arising from planes more than a few monatomic layers below the

exit surface is enhanced by the presence of steps. Figure 3.7.

The thermal vibrations may then produce an increased thermal broadening of the diffraction features.

Stacking faults and other planar defects give rise to streaks in reciprocal space normal to their plane and therefore may contribute to the extension of diffraction spots into streaks.

Diffraction at stepped surfaces gives rise to two diffracted beams for each reciprocal lattice point as a result of refraction effects Figure 3.8a,b. If these beams are already broadened they may overlap in the diffraction pattern.

Quantitatively, the contributions of the effects discussed above to the streaking of diffraction features have not been distinguished. Qualitatively, it is possible to distinguish many subtle changes in the intensity distribution of the diffraction features in the course of an experiment. It is probable that these largely reflect differences in topography and crystallite size. Little progress has however been made in obtaining quantitative information about the surface roughness from these observations.

The spectrum of distinguishable diffraction features and the surface sensitivity of RHEED suggest that a very sensitive technique for the investigation of surface topography might be developed.

3.3.4. Diffraction from Bicrystals, The Contribution from Multiple Scattering and Diffraction and Dislocation Array

Bicrystals produce separate diffraction features from the substrate and deposit when the deposit is thin. This allows

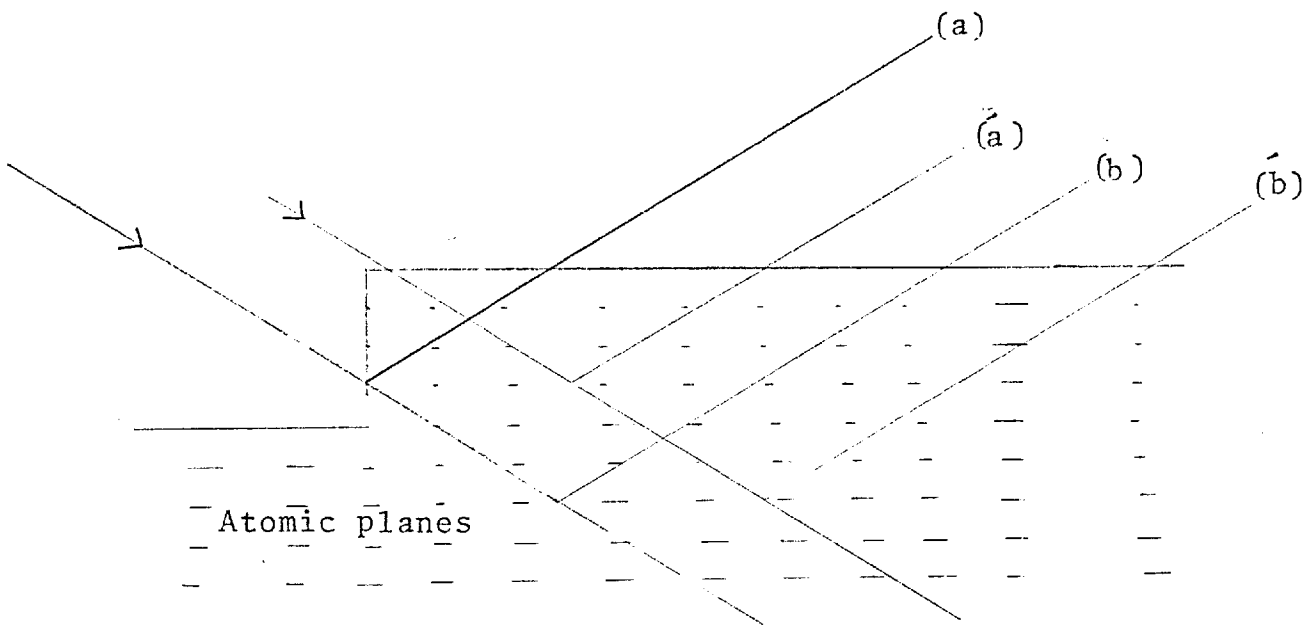


Figure 3.7

Diffraction from a stepped surface.

Diffracted beams (a)+(a') and (b)+(b') results from scattering at equal depths below the exit surface. The total path of (b) in the specimen is less than that of (a) and if both are greater than the mean free path for elastic scattering, (b) will be the stronger beam.

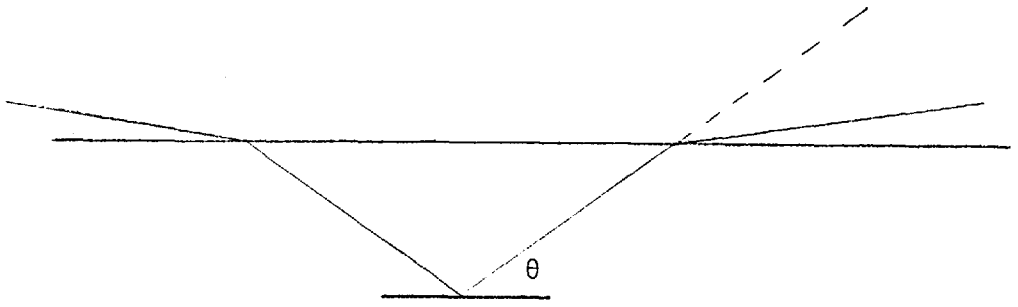


Figure 3.8a

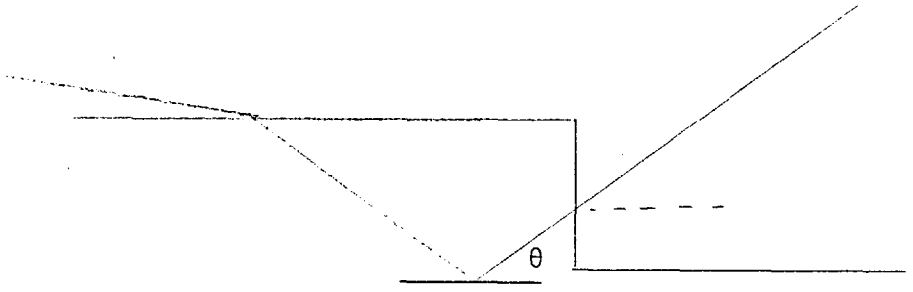


Figure 3.8b

Refraction effect of a stepped surface.

(a) Refraction at glancing angles
(b) Negligible refraction effect for normal angles of incidence.

the determination of their relative orientation. Elastic strains may also be investigated by measurement of the diffraction pattern. If the misfit of the system M_o is small or there are significant elastic strains it may not be possible to resolve individual diffraction features and composite broadened features result. Similarly broadened features would be observed in the case of alloys having a compositional gradient normal to the surface.

Multiple diffraction leads to a complicated array of additional diffracted beams. The multiple scattering events may occur, within a single phase, between phases e.g. substrate and deposit O, between a normal phase and reciprocal lattice points which are associated with stacking faults. HORNG & VOOK (1976) have shown that relatively high angle scattering $\simeq 12^{o}$ involving reciprocal lattice points in the 2nd Laue zone Figure 3.9. must be included when determining the additional features that may result. There has been a much prolonged discussion over the origin in particular cases of diffraction features which may result from both multiple scattering and diffraction by an array of regularly spaced dislocations. Recently SASS et al (1975, 1976) have demonstrated that certain features occur as a result of scattering by dislocations rather than multiple diffraction. This investigation made use of separately prepared crystals brought together to form a bicrystal and hence provides a favourable case for the formation of highly regular dislocation arrays. The non-equilibrium conditions which frequently prevail during film growth might be expected to produce insufficiently regular dislocations to produce strong diffractions. HORNG & VOOK (1976) has shown this to be the case in Ag/Cu films and the additional diffraction features observed, to result from double diffractions.

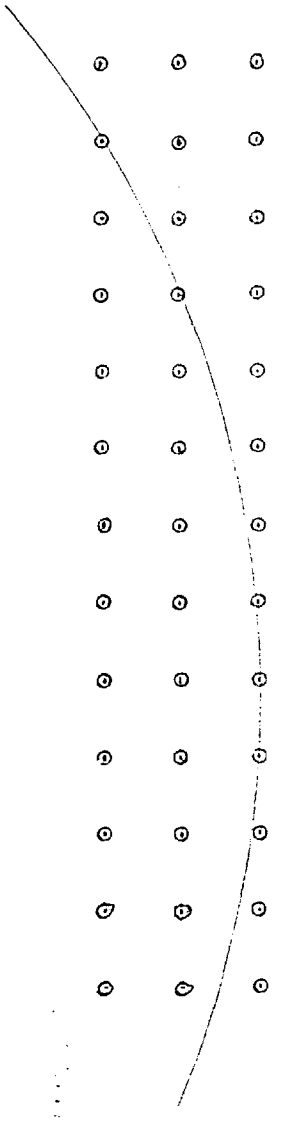


Figure 3.9

Diffraction conditions satisfied by intersection of Ewald sphere by reciprocal lattice point of 2nd Laue zone.

In the examination of low misfit systems multiple diffraction features cannot be resolved since they occur very close to the primary substrate and overlayer features. They therefore may contribute to the apparent width of the primary features which are often already dominated by broadening from other effects.

3.4. Transmission Electron Microscopy, Limitations of the Technique

3.4.1. Problems of Specimen Mounting

The problem of producing self-supported specimens which allow the transmission of an electron beam is a limitation of the technique.

The defect and impurity content of specimens may be influenced by the method of preparations. Ideally the concentrations of both should be monitored and their influence on subsequent observations established.

The different techniques of specimen production allow two distinct procedures in electron microscopy.

Specimen preparation for *in* situ electron microscopy

The examination of overlayers grown inside the microscope.

Specimens for in situ experiments may be produced by two methods:

(i) The growth of substrates on cleaned bases which are thin enough ~ 100 Å to allow transmission. Allowing both substrate and deposit to be grown inside the microscope.

(ii) The growth of substrates on thick bases which must be stripped before the substrate is mounted in the microscope. Only the deposit is grown in situ by this method.

Better control of contamination is achieved by adopting (i) above. The second method requires the use of in situ cleaning of the substrate which is not always possible in the electron microscope.

The preparation of specimens outside the microscope.

In the case of studies of pseudomorphism this has generally involved the preparation of both the substrate and overlayer by vapour deposition on thick single crystal bases in technical vacuum conditions ~ 10^{-5} Pa . The specimens have thus been transported through air and exposed to a stripping agent (water or acid) before being mounted in the microscope. This procedure will allow the possibility of heavy contamination and of the partial removal of the specimen during the stripping process.

Both the stripping process and techniques of cleaning very thin bases have been observed to affect the defect content of specimens. POPPA (1972).

3.4.2. Surface Sensitivity fo Electron Microscope

(a) The transmission nature of the technique leads in many modes of operation to a low contribution to the intensity from thin deposits. Typically a thin deposit of several Å

thickness on a substrate several 100 Å thick will contribute 1-5% of the total intensity.
(For materials of similar atomic number).

CHERNS (1974) has demonstrated the possibility of examining the surface via surface specific contrast effects. However the inherently low intensities produced have so far prevented their successful application.

3.4.3. Ultra High Vacuum in the Electron Microscope

(b) The attainment of UHV conditions within the microscope has proved difficult and expensive and consequently very few microscopes have the capability. Therefore possible contamination effects may always be present.

3.4.4. Techniques for Chemical Analysis in the Electron Microscope

(c) In conventional electron microscopes the inclusion of additional experimental techniques within the microscope has not been possible because of limitations of space. This has meant that the only technique of chemical analysis available has been X-ray fluorescence in which the fluorescence is excited by the electron beam of the microscope.

This problem is further discussed in Section 3.7.

3.5. The Use of the Electron Microscope to Determine Misfit

Three methods are available to obtain the lattice spacing and hence misfit.

(i) Transmission electron diffraction
(ii) Imaging of Moire fringes
(iii) Imaging of periodic dislocation networks.

3.5.1. Transmission Electron Diffraction: TED

The transmission of the electron beam through both the substrate and the deposit will produce diffraction patterns arising from both these regions. By measurements of the separation of the features of these two patterns the misfit may be obtained by a method very similar to that used with RHEED Section 3.3.1.

A problem of resolution arises however in the case of small misfts when the separation of the diffracted beams from the overlayer and substrate is similar to the width of the diffracted beams. This problem is made worse by the low relative intensity of the overlayer beam and may prevent the measurement of small misfits.

CHAMBERS & JACKSON (1975) in an investigation of this type found the method unsuitable for misfits of less than 1-5%. Abnormaly large diffraction features are frequently observed in patterns obtained from thin overlayer films. These features which are often ascribed to increased crystal disorder or small crystal sizes have a detrimental effect on the resolution of mismatch discussed above.

If separate diffraction features can be resolved an increase in the camera length may improve the accuracy in the determination of misfit. This is made use of in transmission high resolution electron diffraction : THRED in which the microscope projector lens is used to enlarge the diffraction pattern FERRIER & MURRAY (1966). The only measurements of misfit in relation to pseudomorphism using TED made use of this facility KUNTZE et al (1969), CHAMBERS & JACKSON (1975).

CHAMBERS & JACKSON (1975) concluded that the technique could not be used because of a lack of resolution in the case of 2D deposits of Cu on Ni having a misfit less than 1.5%. They were unable to apply the technique to 3D deposits since a value of misfit averaged over a large number of islands was obtained. In the case of 2D deposits of larger misfit the uncertainty was equivalent to a misfit uncertainty of ± 0.05%.

3.5.2. Imaging Dislocations in the Electron Microscope to Determine the Misfit

It has been shown Section 2.2 that a non-zero mismatch at a crystal interface is associated with a periodic set of interfacial dislocations. By imaging the dislocations and determining their Burgers vectors the misfit which they accommodate may be determined.

$$M_r = \sum_i \rho_i \, \underline{b}_i \cdot \hat{\underline{r}} \qquad (3.19)$$

where

$\underline{r}$ is a direction in the interfacial plane.

i is the label of dislocations having different Burgers vectors.

$\underline{b}_i$ is the Burgers vector of the dislocation.

ρ_i is the line density of dislocations.

The crystal planes in the region of a dislocation are slightly misorientated with respect to those of the perfect crystal. Diffraction occurring at these planes will necessarily be of different intensities. Hence contrast appears in both the incident, transmitted and diffracted beams which if imaged reveal dislocations. The contrast and resolution of the images will depend on the magnitude of the atomic displacements and the region over which they extend. Therefore, the contrast and resolution will be dependent on the mismatch and the interfacial bonding.

The contrast must appear complementary in dark and bright field micrographs. The study of dislocations via their image contrast in a specialised topic in which dynamical effects are important. A knowledge of the limits of resolution in situations encountered in studies of pseudomorphism would be of great value in discussion when dislocations are not observed. These considerations are beyond the scope of the present work.

The Burgers vector of a dislocation is determined using the condition of invisibility equation 3.10. HIRSCH et al (1965)

$$\underline{b}_i \cdot \underline{g} = 0. \qquad (3.20)$$

where $\underline{b}$ is the Burgers vector of the dislocation.

$\underline{g}$ is the reciprocal lattice vector of a diffracted beam for which the dislocation is not visible.

The dislocations are imaged in dark field using different diffracted beams until one is selected for which the dislocation is not resolved. The direction of the Burgers vector is then determined from the above diffraction conditions.

The invisibility condition is understood by noting that when $\underline{g}.\underline{b} = 0$ the diffracting planes are normal to the Burgers vector and no variation in the atomic spacing of these planes would be expected.

3.5.3. Determination of Misfit in the Electron Microscope using Moiré Fringes

Moiré fringes result from the superpositions of two wave systems whose phases vary with a different periodicity. MENTER (1958).

Two interfering plane waves $ae^{i\,2\pi\underline{s}.\underline{r}}$, $be^{i2\pi\underline{t}.\underline{r}}$ superimpose to give a resultant wave ψ

$$\psi = ae^{i2\pi\underline{s}.\underline{r}} + be^{i2\pi\underline{t}.\underline{r}} \qquad (3.21)$$

where a,b are the amplitudes of the two waves.

$\underline{s},\underline{t}$ are the wave vectors of the two waves.

$\underline{r}$ is the propagation vector of two waves.

The intensity $I = \psi\psi^* = a^2 + b^2 + 2ab \cos 2\pi r(\underline{s}.\underline{t})$ (3.22) of the resultant wave includes cosine fringes which are called Moiré fringes.

In the electron microscope Moiré fringes may be formed by the interference of electron waves arising from diffraction in different regions of the specimen. For fringes to appear the different specimen regions must either contain different structures or a single structure in different orientations providing different phase periodicities. In studies of pseudomorphism we are generally concerned with different crystal structures in a single parallel orientation. Beams arising from diffraction at two parallel sets of planes in the substrate and deposit are selected to form a Moire image.

The diffracted waves may then be represented by

$ae^{i2\pi\underline{k}'.\underline{r}}$, $be^{i2\pi\underline{k}''.\underline{r}}$ where $\underline{k}'$ and $\underline{k}''$ are the wave vectors of the two diffracted beams. If $\underline{k}$ is the wave vector of the incident beam and $\underline{g}'$ and $\underline{g}''$ the reciprocal lattice vectors of the diffraction processes giving rise to $\underline{k}'$ and $\underline{k}''$ then

$$\underline{k}' = \underline{k}'' + \underline{g}' \qquad \underline{k}'' = \underline{k} + \underline{g}'' \tag{3.23}$$

The cosine fringes produced in equation 3.22 have a fringe spacing F

$$F\alpha \frac{1}{g'-g''} = \frac{d'\,d''}{d''-d'} \tag{3.24}$$

where d' and d'' are the plane spacings of the crystal planes giving rise to the diffraction. Hence from F the mismatch

may be determined.

Two considerations must lead to practical limits on the application of the technique to studies of low misfit thin deposit films.

(i) As the fringe spacing increases corresponding to small misfits the fringe contrast is reduced.

(ii) If the diffracted beam arising from the substrate is very much stronger than that from the over-layer. The fringes will represent a correspondingly small fluctuation on a large constant background. $a^2 + b^2 >> 2ab$.

(iii) Both random and periodic deviations from a perfect crystal structure will reduce fringe contrast.

Moiré fringes have frequently been observed and by application of equation 3.24 made use of in the measurement of mismatch. YAGI (1971), CHAMBERS & JACKSON (1975). YAGI (1971) has pointed out that if the mismatch is accommodated entirely by interfacial dislocations the mismatch determined by observation of Moiré fringes and dislocation images should be equal. While this was not observed by MATTHEWS (1966), YAGI (1971) has demonstrated this correspondence.

3.6. Topographic information from Electron Microscopy Studies

A number of electron microscopy techniques may provide topographical information:

1. Dark field microscopy
2. Thickness fringes.
3. Absorption contrast.
4. Surface step resolution. (CHERNS, 1974)
5. Replication methods.

While the application of these methods to thick films has provided a great deal of information, their power when applied to low misfit thin deposits is greatly reduced. Other than the particularly favourable situations of deposits having a well defined 3D growth mode or an atomic number considerably higher than that of the substrate, the mode of growth and topographic detail is generally not resolved.

3.6.1. Dark Field Microscopy: This technique makes use of a specimen image formed from a diffracted beam rather than the transmitted deviated beam. The electron micrographs obtained identity regions of the specimen which contribute to the diffracted beam. From a diffracted beam associated with the deposit the distribution of the deposit on the substrate is obtained. In the case of low natural misfit or highly strained specimens it may not be possible to resolve the overlayer diffracted beams with the result that the technique cannot be applied. Providing the diffracted beams are resolved the technique will distinguish between two and three dimensional growth. The existence however of a ≃ monolayer coverage in addition to 3D islands [Stranski Krastanov growth

mode] would probably not be resolved. In order to determine the deposit thickness a comparison of the experimental and calculated intensities would be required. Such a procedure lies beyond the present development of the technique.

3.6.2. Thickness Fringes: Calculation of transmitted intensities show a oscillating dependence on film thickness. HIRSCH et al (1965). The periodicity of this variation which depends on the extinction distance and the deviation from the Bragg condition is of the order of 100Å. Thickness fringes of this type are observed but the contrast varies much too slowly for the resolution of the structure of very thin films.

3.6.3. Absorption Contrast: For deposit thickness small compared with the specimen thickness the absorption contrast is low and is insufficient to examine the topography of thin films.

3.6.4. Surface Step Resolution: By resolving additional diffraction features which occur when specimen thickness contains an incomplete unit cell CHERNS (1974) has developed a surface specific technique of electron microscopy. Forming dark field micrographs from these diffracted beams single atomic steps are claimed to have been resolved between regions of the specimen which contain an incomplete cell and those which do not. The resolution of this technique is very high but has yet to be widely applied. The results remain somewhat controversial.

3.6.5. Replication Methods: Specimens for replication are coated with a material which is readily removable from the specimen and which reproduces the specimen surface structure. BRADLEY (1965) On removal the replica, coating material, is examined using absorption contrast, by transmission electron microscopy. The technique is advantageous when the specimen is too thick to be examined directly by electron microscopy but has the disadvantage that further experimentation on the same specimen is largely prevented. A shadowing method may be used, depositing replica at a angle $\theta \neq 90^{o}$, to enhance the surface structure enabling steps to be identified more readily Figure 3.10. Although the technique has been widely used when examining the slightly more gross aspects of surface structure and in favourable circumstances single atomic steps have been resolved the determination of the technique is not used for mode of growth of very thin films.

3.7. Analytical Techniques and Electron Microscopy

Design constraints acting in conventional electron microscopes have prevented the inclusion of additional apparatus required for analytical techniques such as Auger Electron Spectroscopy AES. Two techniques, X-ray micro-analysis and more recently electron energy low spectroscopy have been developed for use in the electron microscope, making use of the microscope beam as the probe. X-ray microanalysis in particular is capable of high resolution quantitative analysis of specimens and has been successfully used to measure in-situ the thickness of thin films. CHERNS & STOWELL (1976).

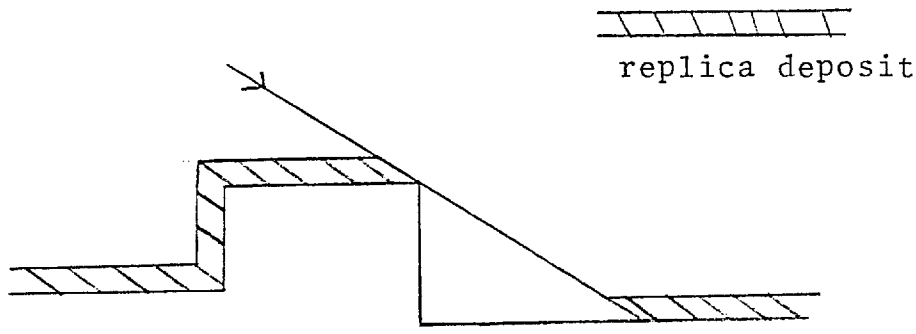


Figure 3.10

Shadowing technique in replica production. Step constant is increased due to shadowing effect, replica thick on one side of island thin on the other.

Some difficulty has arisen however with elements of atomic number < 12 due to their weak x-ray emission.

The weak attenuation by the specimen of both the emitted x-rays and the high energy electron beam has made the technique insensitive to the distribution of the components within the specimen. A number of attempts have been made to overcome this problem. SEWELL P.B., MITCHELL D.F., COHEN, M. (1969) have made use of glancing incidence electron beams and have achieved considerable surface sensitivity detecting the presence of $\frac{1}{10}$ of a monolayer of carbon on the surface of Iron.

However these modifications have not been applied in the electron microscope. The lack of a surface sensitive technique of chemical analysis in the electron microscope has meant that contamination and diffusion effects cannot be adequately monitored in such studies.

3.8. The Quartz Crystal Microbalance

The piezoelectric induced oscillations of a quartz crystal are made use of in the construction of a microbalance. The change in resonant frequency of an oscillatory crystal is measured to determine the mass loading.

The frequency change Δf of a crystal resulting from a change in the mass load has been shown by SAUERBREY (1959, 1964) to be given by equation 3.25

$$\Delta f = \frac{k\ f\ \Delta M}{At} \qquad (3.25)$$

and $$\frac{1}{t} = k' f \qquad (3.26)$$

where t is the crystal thickness
A the electrode area
ΔM the change in mass loading
f the resonant frequency of the crystal
Δf the change in frequency resulting from ΔM.

The frequency of f and the constants k, k' depend on the type of crystal cut and the accuracy to which the cut has been made. These expressions for the crystal frequency are true provided the deposited film can be treated as an extension of the quartz crystal. This is a good approximation if the film thickness is small compared with that of the crystal CHI SHUI LU (1975). For small mass loadings it is seen that Δf has a linear dependence on ΔM, this has been shown to hold with a 2% for mass loadings of up to 2×10^{-2} kg m^{-2} CHI SHUI LU (1975). EERNISSE (1972) has developed an expression for the resonant frequency which includes vibrations within the deposited film. This has been applied in the experimental investigation of strains imposed on the crystal. The frequency of a typical unloaded crystal used in this technique is ≃ few *MHz*.

A mass change detection limit of 1×10^{-11} kg $m^{-2} \simeq 10^{-4}$ monoatomic layers has been determined by WARNER and STOCKBRIDGE (1963). This limit arises from the dual problems of the stabilisation and measurement of the crystal frequency. In ultra high vacuum conditions using a lightly loaded crystal the main problem of frequency stabilisation is the effect of temperature fluctuations. The temperature dependence of crystal frequency is non-linear and may change in sign. To minimise this effect AT cut crystals operating in a thickness

shear mode are used.

The temperature coefficient of such crystals is dependent on the cut of the crystal and has a maximum value of ≃ 1 part in 10^6 of frequency k^{-1}. To achieve the highest sensitivity to mass changes, WARNER & STOCKBRIDGE (1963), the temperature was stabilised to ± 0.1K. This degree of stabilisation is not easily achieved and limits the application of the technique.

The measurement of frequency change was performed by the timing of beats between the monitor crystal and a master oscillator. The measurement of frequency changes of 1 part in 10^{11} were just possible with the available technology.

Uncontrolled sorption gives rise to frequency changes. Inhomogeneous deposits may give rise to a more complicated frequency dependence and in extreme cases severely damp the resonance.

3.9. Auger Electron Spectroscopy : AES

AES is a surface sensitive technique of chemical analysis. An electron beam of typical energy 1.5-3 keV is used to stimulate specimen atoms to excited or ionised states. These subsequently relax with the emission of an Auger electron or a photon.

The Auger electron production process may be labelled WXY Fig. 3.11 where W indicates the energy level of the initial core state hole created by the incident electrons. The excited atom then relaxes by an electron transition from energy

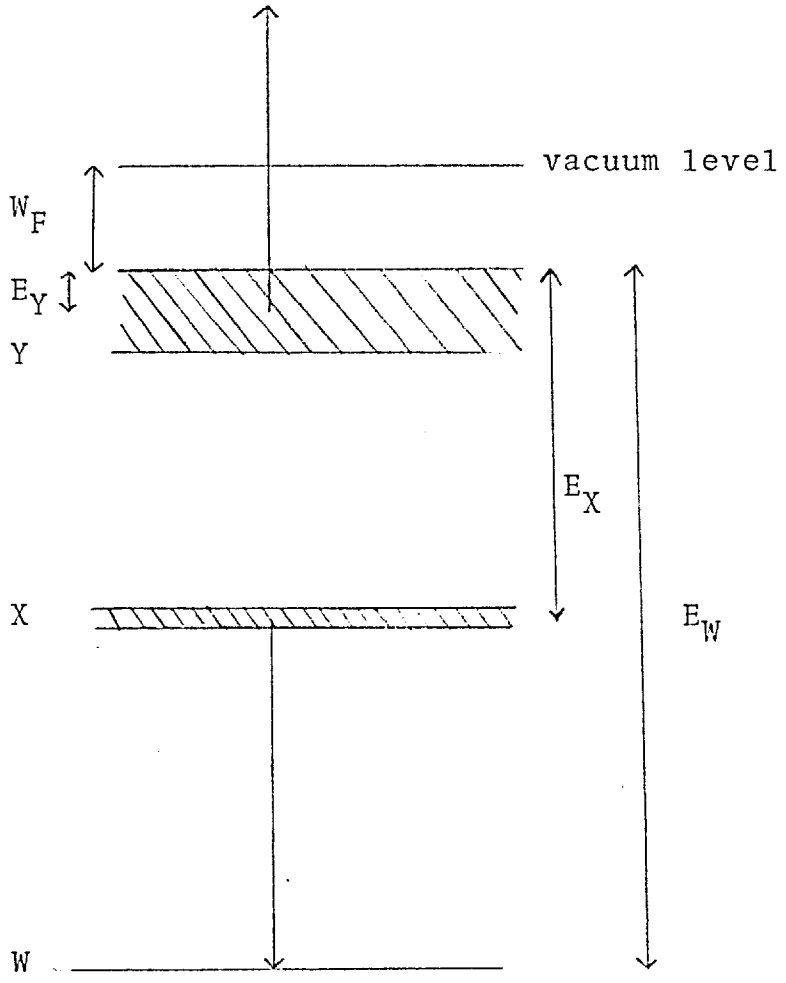


Figure 3.11

Energy level diagram of Auger electron emission from an atom in a solid.

level X to fill the hole. The excess energy is released by ejecting an electron from energy level Y from the atom. The kinetic energy E_k is given by equation 3.27

$$E_k = E_W - E_X - E_Y \qquad 3.27$$

A useful first approximation for E_{kin} is obtained using atomic energy levels for a free neutral atom. These must be modified for application to a solid and corrections applied for core hole screening and other effects resulting from the atom's excited state. In the case of a solid, the following equation is often useful.

$$E_k = E_W - E_X - E_Y - W_F \qquad 3.28$$

Where W_F is the work function of the emitting surface and the binding energies are referred to the Fermi level.

The technique is highly surface sensitive due to the low mean free path of the Auger electrons. These low energies (20-1200) eV ensures that the major portion of those emitted come from the surface region, POWELL (1974).

3.9.1. Factors Affecting the Quantification of Auger Electrons Production

The total number of Auger electrons created is determined by the number of ionisation and excitation events occurring and the probability that the atoms will relax by radiationless transitions.

An expression for the probability p of the relaxation of an excited state by photo emission has been obtained by BURHOP (1952). viz.

$$p = \frac{1}{1 + \frac{a}{z^4}} \qquad (3.29)$$

where z is the atomic number
a is a constant dependent on the electron shell containing the hole.

For Auger transitions of experimental interest p is generally ≤ 0.01 and the formation of a hole can be considered equivalent to the production of an Auger electron.

BETHE (1930) has obtained, for each electron subshell, an expression for the total cross-section of all excitation and ionisation processes (equations 3.30 and 3.31):

$$Q^e_{nc} = \frac{\pi e^4}{E_p E_{nc}} Z_{nc} b_{nc} \ell n\left[\frac{4E_p}{B_{nc}}\right] \qquad (3.30)$$

$$Q^i_{nc} = \frac{\pi e^4}{E_p E_{nc}} Z_{nc} C_{nc} \ell n\left[\frac{4E_p}{C_{nc}}\right] \qquad (3.31)$$

where Q^e_{nc} and Q^i_{nc} are the cross-sections for excitations and ionisation of the nc subshell.

e is the electronic change.
E_{nc} is the binding energy of the electrons in the shell described by the quantum numbers nc.
E_p is the primary beam energy.
Z_{nc} is the number of electrons in the nc shell.
B_{nc} is $\simeq E_{nc}$.
C_{nc} is $\simeq 0.1\ E_{nc}$.

b_{nc} and c_{nc} are constants calculated by BETHE (1930) assuming hydrogen-like wave functions.

The form of the cross-section as a function of $\frac{E_p}{E_{nc}}$ is illustrated in Figure 3.12.

The contributions to hole production of the primary incident electrons and the secondary scattered electrons is often considered separately.

Expression for the cross-section for hole formation such as equations 3.30 and 3.31 may be used in calculating the contribution to Auger electron production of the primary electrons. The attenuation of the primary beam is accounted for most simply by applying an exponential decay law with a characteristic inelastic mean free path. The mean free path of electrons depends on their energy and the atomic number of the scatterer. POWELL (1974).

The secondary electron distribution changes with position in the specimen and is generally unknown. This has prevented a similar direct calculation of the contribution of the secondary electrons to hole formation.

3.9.2. Factors Affecting the Emission and Detection of Created Auger Electrons

The fraction of the created Auger electrons which are detected depends upon their attentuation within the specimen and the collector geometry. The probability of escape of an Auger electron is dependent on its position of origin. Thus providing AES with a sensitivity to the distribution of an element with respect to the specimen surface.

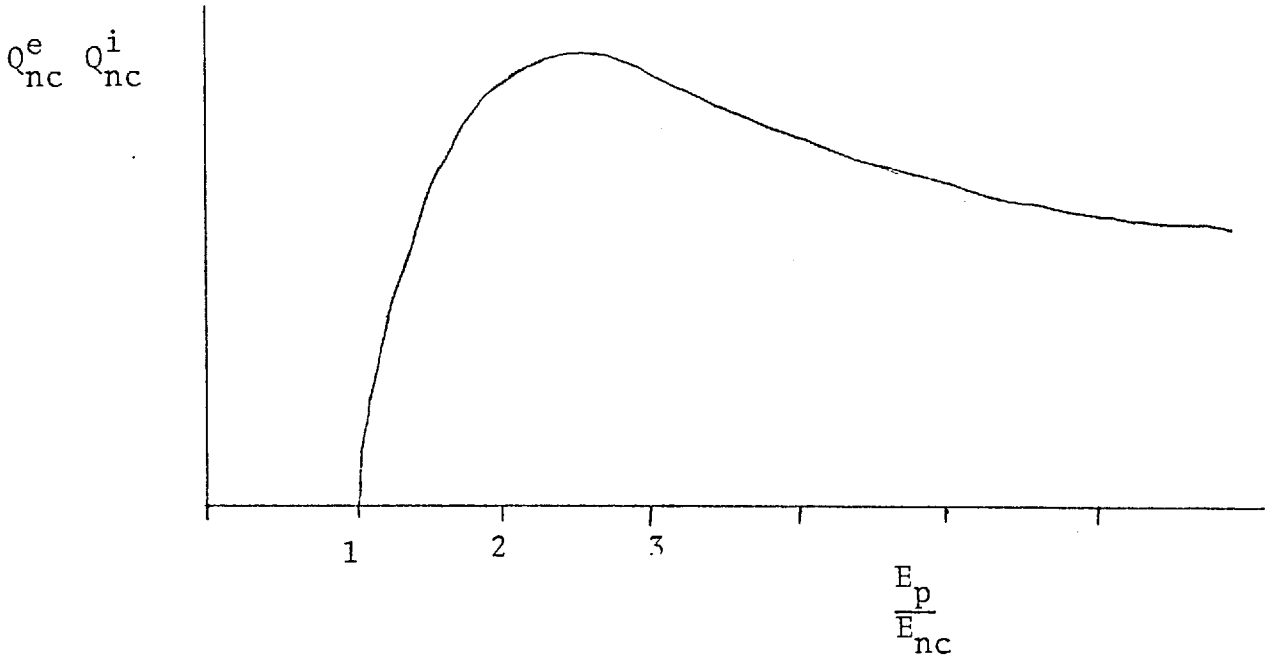


Figure 3.12

The form of the functions given in equations 3.30 and 3.31. The exact shape and position of the maximum depends on the functions B_{nc} and C_{nc}.

The number of Auger electrons created and their distribution within the surface region of the specimen is greatly altered by the variation of energy and angle of incidence of the primary beam HARRIS (1969), NEAVE et al (1972) and MEYER, VRAKKING (1974). These variables also alter the relative contribution of secondary electrons to hole production.

GALLON (1972) and VRAKKING, MEYER (1975) have attempted to determine experimentally this contribution. It is accommodated numerically by replacing the primary current I_p by an effective current rI_p where r is the back scattering factor defined by BISHOP, RIVIERE (1969); $\frac{r-1}{r}$ is then the fraction of emitted Auger electrons stimulated by secondaries. Calculations of Auger electron emission current are greatly complicated by the effect of surface roughness which severely inhibits useful calculation.

3.9.3. The Auger Spectrum

The total Auger current of each atomic species forms a line spectrum, electrons being emitted at the different characteristic energies allowed (equation 3.27). The distribution of the current between the different lines of the spectrum is determined by the distribution of the holes between the different core levels possible and the transition probabilities for the decay of hole states via the available X and Y states. The initial hole distribution is determined by equations 3.30 and 3.31, this may however be modified by Koster-Kronig transitions. Koster Kronig transitions for a sub-group of Auger transitions, those which in the

final state have transferred the hole to a more weakly bound subshell of the same electron shell. The calculation of transition probabilities required to determine the final form of the spectrum is beyond the scope of this work.

The emission lines of an Auger spectrum may be several electrons both wide and contain contributions to this width from:

Instrumental effects particularly the superposition of a modulating voltage on the retarding grid of some forms of energy analysers.

The width of the valence band causes a range of values of E_k to be allowed when the X or Y' states are in the valence band.

Low energy losses e.g. plasmon losses broadens the electron energy distribution while escaping from the specimen.

Lifetime broadening, the short life of hole states $\sim 10^{-16}$ secs causes an uncertainty in the emitted electron energy, given by the uncertainty principle.

3.9.4. Multi-component Specimens

As a result of the strong attentuation of emitted Auger electrons within the sample section. The detected Auger signal strengths from multicomponent specimens are highly sensitive to the distribution of different atomic species with respect to the specimen surface. This sensitivity has been made use of by many workers to determine the 'mode of growth' of overlayers e.g. JACKSON et al (1973) and to investi-

gate the surface enrichments of alloys e.g. McDAVID & FAIN (1975).

The primary beam energy and its angle of incidence together with the energy of the Auger transition examined are useful variables with which this sensitivity may be enhanced.

CHAPTER 4

4.1. A Review of Experimental Reports of Pseudomorphism

Introduction

This review will be concerned only with reports of pseudomorphism in thin film metal-metal systems. Pseudomorphism has been observed particularly by YAGI (1974, 1975) in thin films of a number of semiconducting compounds. Much of this work is referred to by YAGI (1974, 1975). In addition to the above, relatively thick pseudomorphic films of doped semiconductors have been grown. These have a very small natural misfit ≤ 0.001. A large body of work on the pseudomorphic growth of precipitation and inclusions in metallic alloys has also been omitted; this has been reviewed by MATTHEWS (1973).

It has been found convenient to consider separately those investigations carried out in situ and those not. PASHLEY (1956) re-examined all the existing reports of pseudomorphic growth in thin films and was able to demonstrate that in all cases the evidence had been misinterpreted. It was concluded that although the principle of pseudomorphism was sound there was then no experimental evidence for its occurrence.

4.2. Non-in situ Reports of Pseudomorphism since 1956

The results considered in this section are listed in Tables 1A, 1B. The conditions under which these investigations were carried out cause the results to be subject to uncertain-

ties regarding the effects of mechanical handling, chemical attack by the atmosphere and the stripping solutions. In addition there is the possibility of diffusion effects particularly in the experiments performed at elevated temperatures.

Many of the above factors do not appear to have been considered by these research workers and furthermore the apparatus was not easily capable of chemical analysis on the scale required to detect chemical attack or diffusion. Evidence of chemical attack and diffusion pertinent to the experiments in Tables 1A, 1B will now be considered.

4.2.1. Chemical Attack

At present we have little knowledge of many of the chemical reactions of interest in the system considered. Individual cases which have been investigated will therefore be presented.

RHODIN (1950, 1951) has shown that thin films of oxide form in minutes on the surface of copper single crystals exposed to oxygen partial pressures as low as 10^{-1} p_a at temperatures of 78K and above.

KRUGER & YOLKEN (1964) found thin oxide films to form at room temperature on iron at partial pressures of 10^{-4} p_a oxygen. The rapid oxidation of iron at room temperature on exposure to small quantities of oxygen ~ 100 langmuirs has been further demonstrated by SEWELL et al (1972) and SIMMONS & DWYER (1975) who made use of modern techniques for surface studies under controlled conditions.

It has not been possible to find data on the low temperature oxidation of cobalt. CHATTOPADHYAY & MEASOR (1969) have shown however that thin oxide films form on cobalt in a few minutes when cobalt is exposed to oxygen at 600K. The oxidation was shown to follow a direct logarithmic law and to be independent of oxygen partial pressure. A search of the literature for information about the chemical actions of water on pure metals failed to locate data comparable with that discussed above for the action of oxygen on such surfaces. It is considered however that the combination of water and air form a very complex active environment. During the stripping process used in the investigation listed in Tables 1A,B the specimens are exposed to such an environment. It is expected that significant changes occur at the specimen surface during this stripping process, and that only the relatively unreactive elements Ag, Au, Pt and Pd might be expected to remain unaffected.

4.2.2. Diffusion Processes

Diffusion processes in thin films are often more complicated that those occurring in large crystals. The structure of thin films frequently provide a high concentration of paths i.e. grain boundaries, dislocations and surfaces, which have a diffusion coefficient much greater than that of the bulk, BALLUFFI, BLAKELY (1975). Potential energy gradients which modify the diffusion coefficient frequently occur in thin films. These may result from elastic strains

and atomic species concentration gradients, BALLUFFI, BLAKELY (1975).

When the substrate is the lower surface energy component of the bi-crystal, surface and grain boundary diffusion may lead to the coating of the deposit grain surfaces by the substrate species. This phenomenon has been observed to occur in a number of systems including Ni/Ag and Cu/Ag GIBSON, DOBSON (1975) and Ni/Cu GIBSON, DOBSON at temperatures above 475K. These observations are closely associated with the more widely observed phenomenon of surface and grain boundary segregation in alloys, McDAVID, FAIN (1975) and STODDART et al (1975).

Diffusion may also occur during the period of film growth. The release of the energy of condensation may provide the initial deposit atoms with sufficient energy to penetrate the surface layer of the substrate. The diffusion by the substrate into the deposit planes by surface and grain boundary processes while the deposit planes are incompletely formed may also occur during deposition. This would require that the relevant inter-site jump times be less than the time for monolayer formation.

The only data available for low temperature surface diffusion, suggests that this may sometimes be the case. Such data is obtained from field ion microscopy observations. A value of $\sim 1\text{Å}^2$ sec.$^{-1}$ for the mean square displacement of tungsten adatoms on a (211) tungsten single crystal has been obtained EHRLICH (1974).

The factors introduced above may vary greatly for different systems and also depend on the conditions of film formation. It may however be expected that in some thin film specimens inter-diffusion will proceed at much higher rates than predicted by simple extrapolation from bulk diffusion data. The coating of the surface by the substrate species may also occur. The overall inter-diffusion of very thin films has not been widely investigated but enhanced diffusion has been observed. BOYKO et al (1968).

The specimen configurations can also be changed by the interaction of some component of the system with the gas environment. It has been observed in many alloy systems that one component may preferentially segregate to the surface and react with the gas environment. The reaction product may then form thin films which overlay the specimen. HALES (1976).

4.2.3. Further Evidence that Non-in situ Experiments Produce Anomalous Results in Thin Film Growth Experiments

Inconsistencies observed among the results of different workers demonstrate that the uncontrolled conditions of non-in situ experiments give rise to anomalous results.

In their investigations of the Ni/Cu system KUNTZE et al (1969) reported a very much larger value of h_c (the thickness to which the overlayer grew pseudomorphically) than was observed by MATTHEWS & CRAWFORD (1970) and GRADMANN (1966). This difference probably results from the different effects of contamination on film formation in the

experiments of KUNTZE et al (1969) which were performed at pressures of $5 > 10^{-4}$ Pa.

The three-dimensional growth observed by MATTHEWS (1972a) for Cu/Ni disagrees with the results of CHAMBERS & JACKSON (1975) who performed an in situ study. Similarly MATTHEWS (1966) observed the three-dimensional growth of Pd/Au which conflicts with the evidence of YAGI et al (1971) and CHERNS & STOWELL (1975) made in situ studies which showed that Pd grows two-dimensionally on Au.

4.2.4. Conclusion

From the evidence of sections 4.2.1., 4.2.2., and 4.2.3. it is expected that diffusion and chemical reaction are active in many of the non-in situ investigations listed in Table IA,B.

These processes are capable of substantially altering the assumed configuration of the specimens examined. Although the case for reinterpretation of the results varies for different systems it is considered that the experiments reported in Table IA,B cannot be accepted as providing strong evidence for the occurrence of pseudomorphism.

TABLE 1A : DETAILS OF NON-IN SITU INVESTIGATIONS IN WHICH OVERLAYERS HAVE BEEN REPORTED TO GROW 2-DIMENSIONALLY AND PSEUDOMORPHICALLY ON (001) SUBSTRATES

			Natural Misfit M_o	Critical Thickness h_c A^o	Substrate Temperature K
	Au/Ag	Matthews (1966)	-0.002	250-300	625
	Pt/Au	Matthews & Jesser (1967)	-0.039	10	300-575
	Fe/Cu	Jesser & Matthews (1967, 1968b)	-0.005	20	300
	Fe/Au	Wasserman & Jablonski (1970)	-0.006	10-20	675
	Co/Cu	Jesser & Matthews (1968a)	-0.019	20	300
[1]	Co/Cu	Matthews (1970)	-0.019	18	300
	Co/Cu	Federenko & Vincent (1971)	-0.019	13	525-625
	Co/Ni	Jesser & Matthews (1968c)	0.005	20	300
[1]	Ni/Cu	Matthews & Crawford (1970)	-0.026	15	300
[2][3]	Ni/Cu	Kuntze et al (1969)	-0.026	80	300-635
	Cr/Ni	Jesser & Matthews (1968d)		10	300

TABLE 1B : DETAILS OF NON-IN *SITU* INVESTIGATIONS IN WHICH OVERLAYERS HAVE BEEN REPORTED TO GROW AS ISLANDS ON (001) SUBSTRATES

		Natural Misfit M_o	Substrate Temperature K
Fe/Cu	Jesser & Matthews (1968b)	-0.005	675
Co/Cu	Jesser & Matthews (1968a)	-0.019	625
Cu/Ni	Matthews (1972a)	0.026	300

A. In all cases listed the specimen has been removed from a base by stripping. Electron microscopy observations were made use of in all these experiments. The base pressure of these investigations lay in the range $(5\times10^{-5}\text{-}3\times10^{-7})$pa.

[1] X-ray microanalysis was made use of in this investigation.
[2] THRED was made use of in this investigation.
[3] The base pressure in this investigation was 5×10^{-4} pa.

4.3. In situ Investigations of Pseudomorphism

The experimental observations considered in this section are listed in Table II. The in situ nature of these studies carried out under good vacuum conditions ~ 10^{-7} Pa and better, leads one to suppose that the results will be unaffected by contamination. The investigation of the growth of Au/Pd, Pd/Au YAGI et al (1971) was carried out at 10^{-4} Pa, the relatively unreactive material used suggests that the results may be little affected by contamination, although this is not certain.

Of the criteria developed, section 3.1, to test the validity of reports of pseudomorphism only the effects of diffusion were uncontrolled in these experiments and require further consideration.

The results obtained in the present study, section 7.2, 7.3 show that over most of the temperature range investigated by YAGI et al (1971), CHERNS & STOWELL (1975a,b: 1976), in their studies of the Pd/Au system, the temperature was not sufficient to bring about changes by diffusion effects. Their results obtained over the entire temperature range investigated are consistent with those obtained at room temperature in the present study.

The results of CHAMBERS & JACKSON (1975) for Cu on Ni would be expected to be free of major diffusion effects at room temperature, and this is shown to be the case by the monitoring of the surface chemical composition with A.E.S. In the case of experiments performed at 575K A.E.S. also demonstrated that diffusion did not occur during the period of observation.

TABLE II - DETAILS OF IN. *SITU* EXPERIMENTS IN WHICH THE TWO-DIMENSIONAL PSEUDOMORPHIC GROWTH OF THIN FILMS HAS BEEN REPORTED.

			Natural Misfit M_o	Critical Thickness h_c A^o	Substrate Temp. K	Pressure pa	Experimental Techniques
	Na/W(001)	Mlynczak & Niedermeyer (1975)	-0.040	300	230-375	10^{-8}	R.H.E.E.D (Desorption Spectra)
	Pd/Au(001)	Cherns & Stowell (1975,a,b: 1976)	-0.048	10	300-575	10^{-6}	E.M. + X.F.
	Pd/Au(111)		-0.048	6			
	Pd/Au(111)	Yagi et al (1971)	-0.048		575-675	10^{-4}	E.M. A.E.S.
	Au/Pd(111)		0.048				
	Au/Pd(001		0.048	10			
	Cu/Ni(001)	Chambers & Jackson (1975)	0.026	6-9	300	$5x10^{-6}$	E.M., A.E.S.
[1]	Cu/Ni(001)		0.026		575		T.H.R.E.D.
	Ni/Cu(111)	Gradmann (1966)	-0.026	10	510	10^{-6}	R.H.E.E.D., XF
[2]	Fe/Cu(111)	Gradmann et al (1976)	-0.005		300-675	$5x10^{-8}$	L.E.E.D., AES
	Au/Ag(001)	Yagi et al (1976)	-0.002				E.M.
	Pd/Ag(001)		-0.048				
	Pt/Au(001)		-0.039				
	Pt/Au(111)		-0.039				
	Pt/Ag(001)		-0.040				

Table II continued...

		Natural Misfit M_o	Critical Thickness h_c A^o	Substrate Temp. K	Pressure pa	Experimental Techniques
Pd/Cu(001)	Yagi et al (1976)	-0.076				E.M.
Pt/Cu(001)		0.085				
Cu/Au(111)		-0.114				
Au/Cu(111)		0.128				

[1] Mode of growth Stranski-Krastanov.

[2] Mode of growth observed to be dependent on substrate temperature and evaporation changing 2-dimensional to 3-dimensional.

The experiment of MLYNCZAK & NIEDERMEYER (1975) on Na/Cu (100) did not include a method of chemical analysis. But thermal desorption studies carried out were entirely consistent with sodium existing as an overlayer film. The absorption of sodium into grain boundaries of the substrate was not possible because a tungsten single crystal was used, although at the temperatures investigated sodium is mobile and tungsten is immobile.

The results of GRADMANN (1966) for Ni/Cu at 510K lie in the temperature range for which GIBSON & DOBSON showed diffusion to occur in this system. However the very short time ~ 100 seconds, in which the experiments were completed probably precluded significant changes occurring.

In his studies of the growth of Fe on Cu (111) over a large temperature range 300-675K GRADMANN et al (1976) found thin films of Fe normally stable in the body-centred cubic α phase, grew pseudomorphically in the face-centred cubic γ phase. The thickness to which the Fe grew pseudomorphically was observed to increase and the island coverage to decrease with increased temperature. These results were explained as due to the increased stability of the γ Fe phase near its transition temperature and as a nucleation theory effect discussed recently by MARKOV & KAISCHEW (1976).

Interdiffusion was not considered in the interpretation of these experiments and no observations were made able to resolve diffusion effects. Although the time in which these experiments were completed was very short further considerations of the role of diffusion is necessary.

In particular the extent of diffusion processes occurring during deposition and the possibility of the copper coating the Iron must be considered.

YAGI et al (1976) has recently reported pseudomorphism in a large number of systems including Au/Cu and Cu/Au. However few experimental details were included. These reports greatly extend the range of mismatch M_o for which pseudomorphism has been reported to include Au/Cu 0.128. The importance of considering diffusion is emphasised by YAGI et al (1976) who notes that all the systems in which he has reported pseudomorphism are mutually soluble combinations whereas pseudomorphism has not been reported in bicrystals of insoluble materials. Therefore no conclusion about the validity of these latest claims should be made without further information.

4.3.1. Conclusion

Pseudomorphic growth has been convincingly demonstrated in a number of in situ experiments. Consideration must always be given to the effect of diffusion on the reported results.

CHAPTER 5

Experimental Procedures

5.1. Introduction

The experiments described in the present work were carried out in a stainless steel UHV system described by GIBSON (1973). The apparatus contained facilities for the structural examination of specimens using LEED and RHEED. Chemical analysis was performed by AES using a retarding field analyser. *In* situ evaporation from three different sources was possible and quartz crystal oscillators were available to monitor the deposition rate of two of these. A base pressure of 5×10^{-8} Pa was routinely achieved.

5.2. Materials and Specimen Preparation

All evaporant used were supplied by Johnson Matthey and were 99.99% pure. Palladium was deposited by direct sublimation from a heated wire and by evaporation from tungsten baskets. Silver and Gold were in all cases evaporated from tungsten baskets. Air cleaved Muscovite mica formed the base for all specimens. The mica was orientated by electron diffraction observations and then cut so that an azimuthal direction was approximately parallel to the specimen edges.

5.2.1. (111) Silver Substrate Preparation

Pashley (1959) has described the production of atomically flat, epitaxially orientated (111) Silver single crystals on mica. His procedure was adopted for the present work. Silver was deposited in a standard high vacuum evaporation plant onto air cleaved mica maintained at ~ 575K at a pressure of ~ $10^{-3}\rho a$. Films of 1-2 x 10^{3}Å were grown in a period of a few minutes. After cooling, the silver specimens were transferred to a U.H.V. system and outgassed at temperatures of up to 625K. Subsequently further silver was deposited under U.H.V. conditions onto the specimen maintained at 575K. A series of such depositions were carried out until examination with A.E.S. indicated a relatively clean surface, Fig. 5.1. The RHEED patterns obtained from these silver substrates figure 5.2. display characteristically elongated diffraction streaks which are believed to indicate the atomic flatness of the silver surface DICKSON et al (1965).

5.2.2. Gold Substrate Preparation

Gold substrates were prepared in a number of different ways. The Gold substrates obtained often contained regions of 30^{o} misorientation and some polycrystallinity together with higher contaminant levels than were observed for silver substrates. A procedure similar to that described above for the production of silver substrates section 5.2.1. was investigated. Gold was deposited directly on to air

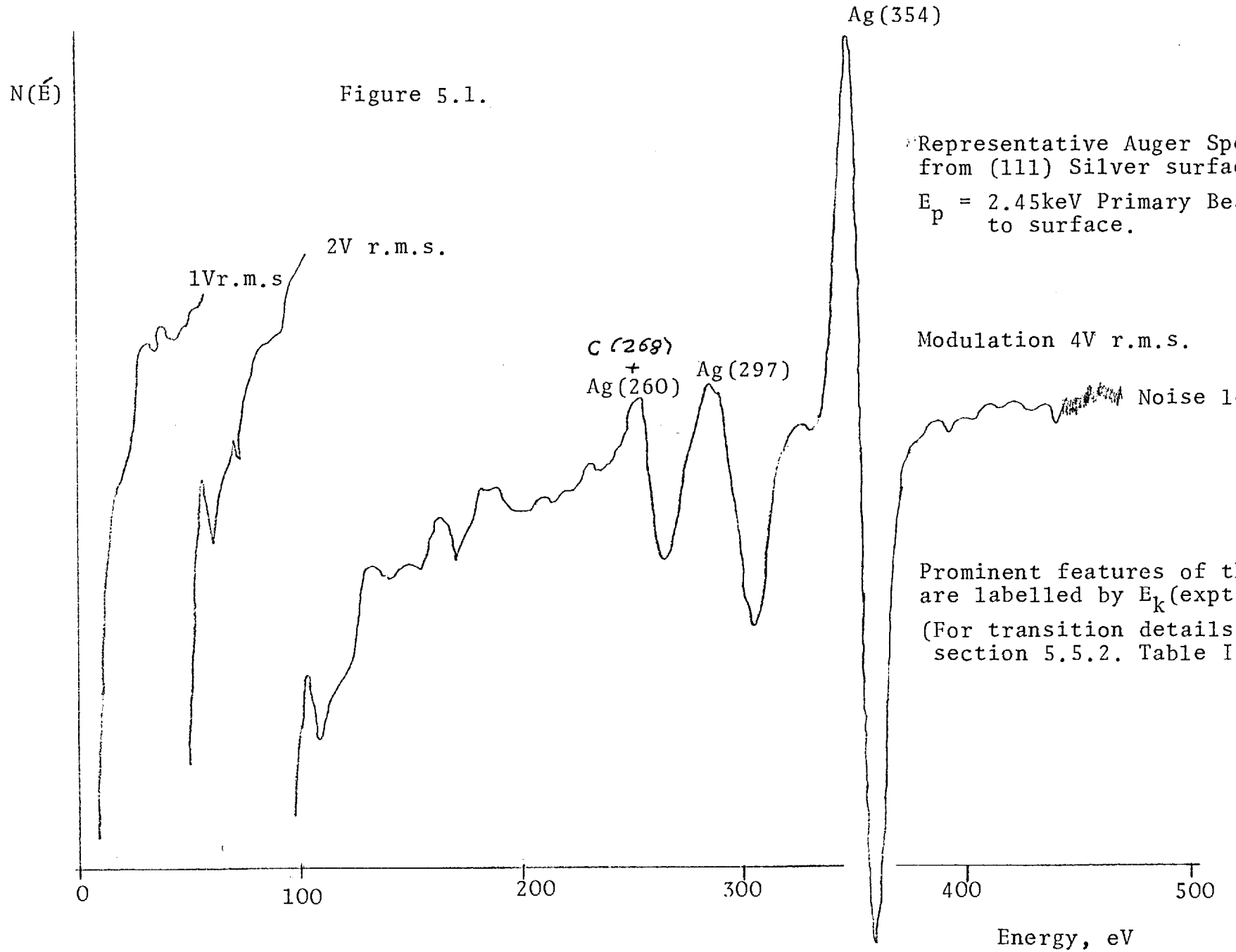


Figure 5.1.

Representative Auger Spectrum from (111) Silver surface.

E_p = 2.45keV Primary Beam at 30° to surface.

Modulation 4V r.m.s.

Noise level

Prominent features of the spectrum are labelled by E_k(expt)

(For transition details see section 5.5.2. Table I).

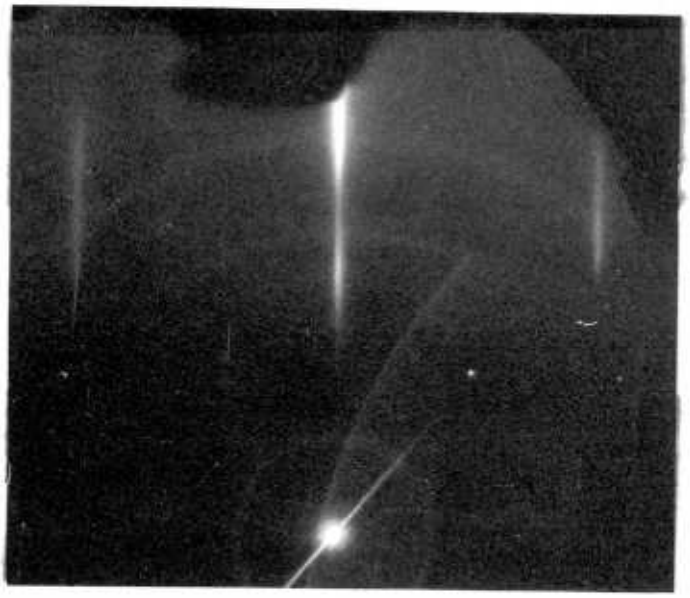


Figure 5.2.

RHEED pattern from (111) silver substrate
E_p = 37 keV, <211> azimuth ; $\alpha = 1.5^o$.

cleaved mica over a range of substrate temperatures between 500K and 800K, a temperature of 675K was found to give the most satisfactory results. Gold was also deposited in U.H.V. at room temperature onto silver palladium and gold palladium multilayer structures.

It was sometimes observed that the diffracted intensity from (111) gold surface and was substantially lower than that observed from similar silver and palladium surfaces. The diffracted intensity was then observed to increase substantially on the deposition of a few monolayers of palladium. These low intensity diffraction features may have been connected with a sizeable contaminant peak observed in the corresponding Auger spectrum, which was speculatively attributed to the potassium $L_3M_{2,3}\,M_{2,3}$ transition.

5.3. The Application of RHEED

RHEED patterns were displayed on a phosphor screen and photographically recorded with a camera placed outside the vacuum system. Overlayers were grown in stages and diffraction patterns for comparison were recorded before and after each deposition.

5.3.1. Lattice Spacing Changes

Changes of the lattice parameter of the specimen surface were obtained from measurements made with a travelling microscope of the separation of the recorded diffraction features Section 3.3.1. The misfit were obtained directly using the relationship

$$\frac{r_s - r}{r_s} = \frac{a - a_s}{a} \simeq M \qquad (5.1)$$

when M is small.

where r_s = the separation of the recorded diffraction features of the substrate

r = the separation of diffraction features after the deposition of an overlayer

a_s = the lattice parameter of the substrate

a = the lattice parameter of the overlayer.

Within the accuracy of the present investigation the effects of curvature of the Ewald sphere need not be considered Section 3.3.1. Since FCC crystal structures were observed throughout it was always possible to record diffraction features having the same indices, and hence the simple relationship of equation 5.1 could be applied. If this analysis is to be valid the electron wavelength λ, the camera length L and the distance of the recording camera from the fluorescent screen must all remain constant during the period in which diffraction patterns are being recorded. A high accuracy was achieved by ensuring that only one experimental or instrumental variable was changed between the recording of diffraction patterns.

The electron wavelength λ is determined by the accelarating voltage V applied to the electron gun. The specifications of the Brandenburg Model 853 EHT power supply was sufficient to maintain λ constant within the resolution of the experiment (the voltage stability was <2 parts in 10^5). The distance between the camera and fluorescent screen was maintained constant by the construction of a special camera holder Figure 5.3. The exposure of a specimen of finite breadth to a glancing incidence beam

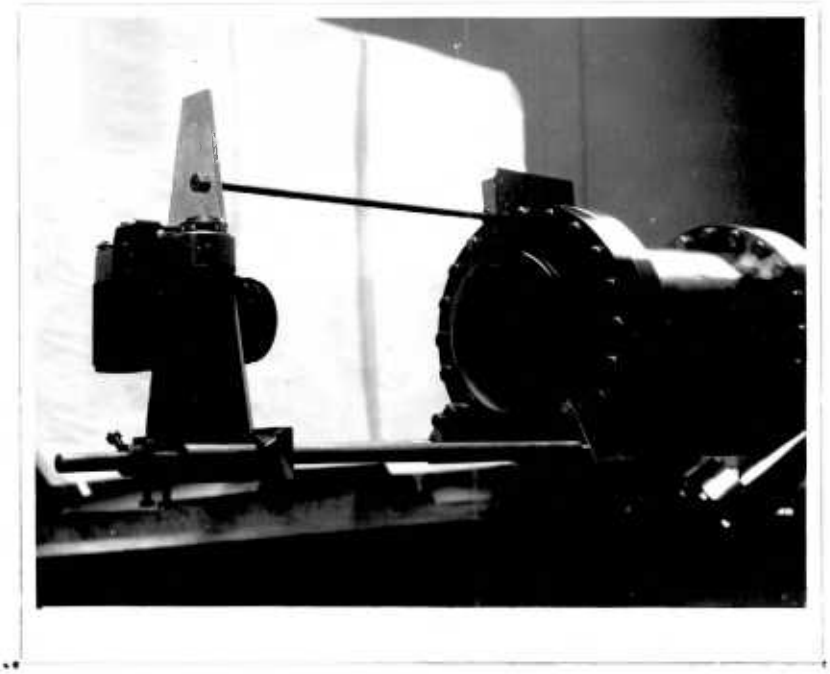


Fig. 5.3: The mounting of the camera used to photograph the RHEED screen

produces an uncertainty in the camera length equal to the specimen breadth. This error was reduced by using narrow specimens (~ 2mm) and extending the camera length to 600mm. The percentage error thus obtained $\leq \pm 0.2\%$ is an upper limit since in order to produce a high intensity diffraction pattern it is expected that the beam would be repeatedly positioned to intersect the full breadth of the specimen.

The limiting source of error in these experiments is believed to be a measurement error associated with aligning the travelling microscope with the centre of the diffraction features. This error will vary slightly with the size of individual diffraction features and the form of their intensity distribution. Repeated measurement of the dimensions of an individual diffraction pattern produced an error of ± 0.2-0.3%. This would give rise to an error in the determination of misfit changes of $\pm$ (0.3-0.4)%.

This is in good agreement with the observed errors and support the conclusion that other sources of error have been reduced to a lower level.

5.3.2. Crystallinity of Specimens

A number of diffraction patterns of distinct appearance could be distinguished and were obtained reproducibly during each experimental run. The extension of diffraction features normal to the specimen surface varied over a range between almost continuous streaks and sharp

spots characteristic of transmission RHEED patterns. This variation was attributed largely to changes in specimen topography Section 3.3.3.

The size of diffraction features in the plane of the specimen surface also varied. These variations resulted from a combination of changes of crystallite sizes, specimen topography and the degree of crystalline disorder, the effects of which cannot easily be distinguished (Section 3.3.2).

5.4. Application of Quartz Crystal Microbalance

A quartz crystal microbalance was used in the present work to control and monitor the increments of film thickness deposited. Marconi type 20 1670-A crystals (6 MHz) were used and were re-mounted with U.H.V. compatable materials. The oscillation frequency was measured with a RCS 301 digital frequency counter which was accurate to 1 part in 10^7.

The main application of the film thickness data obtained was to provide a measure against which changes in RHEED and AES data could be examined. For this purpose the linearity of the measurement and its absolute accuracy shall be considered separately.

5.4.1. Linearity of Frequency Change

It is found from the observations of other workers that for mass loadings of less than 2×10^{-2} Kg m^{-2} the frequency changes linearly to within 2% CWI SHU LU (1975).

A major problem in this present work was the radiative heating of the crystals by the evaporators which caused a reversible frequency change equivalent to the deposition of a film several Å thick. The problem was largely overcome by recording the crystal frequency at a time after the evaporation when the crystal had cooled. Measurement errors then arise from small longer term frequency drifts of the crystal. The relative magnitude of these errors decreases with increasing deposit thickness and are ≈ ±20% for monatomic (average thickness) films of Ag, Pd or Au.

5.4.2. Absolute Deposit Thickness Determination

In order to obtain an absolute measurement of the deposit film thickness a calibration experiment must be performed to take account of the anisotropy of the evaporation source and the different distances from the source of the monitor quartz crystal and the specimen substrate.

The calibration experiment was carried out by placing a second (assumed) identical quartz crystal microbalance in the specimen position. By comparing the frequency change of the two crystal microbalances and determining the area of their crystal surfaces exposed to the vapour, the geometrical corrections were determined.

Equal sticking coefficients were assumed throughout the calibration experiment on the two quartz crystal surfaces. This was ensured experimentally by depositing a thin film

of evaporant on both quartz oscillators prior to the calibration.

For the measurement of the deposit film thickness it was assumed that the sticking coefficients at the monitor crystal and the substrate were equal. After formation of complete, uniform coverage on the substrate crystal this would occur because the evaporant would be depositing onto itself at both surfaces. The Auger electron emission from the specimen monitored at stages during film growth suggest that the sticking coefficient remained constant at all stages of film growth (Section 5.6.2).

The mass frequency coefficient of the monitor crystals was extracted from data supplied by Edwards High Vacuum Ltd for a commercial film thickness monitor which makes use of the same quartz crystals. From this data and the calibration a frequency change of 29±7 cycles was obtained for the deposition of 2.25Å (one monoatomic layer) of palladium. This was in good agreement with a value of 28± 4 cycles obtained by fitting experimentally obtained Auger data for palladium deposited on silver, to the calculated dependence of the Auger signal on film thickness Section 5.6.2.

5.5. The Application of Auger Electron Spectroscopy to the Present Study

5.5.1. Experimental System Employed

AES was carried out in the present work using a Vacuum Generator 3-grid LEED optical system as a retarding field analyser. A 2 keV glancing incidence electron gun was usually employed although a normal incidence LEED gun was also available.

The Auger electron emission typically represents $\simeq \frac{1}{100}$ of the total secondary electron emission at a given energy. HARRIS (1968) has shown that the signal to noise ratio for Auger detection is substantially improved by detecting a first derivative of the secondary electron spectrum. Provided the background secondary electron spectrum is relatively smooth. TAYLOR (1969) has shown that the peak-to-peak height of the first derivative is approximately proportional to the Auger current. The detection of this signal in the present work was achieved by the superposition of a small sinusoidal modulation voltage on the retarding grid potential which was swept over the required range. The component of the output from the retarding field analyser modulated by the second harmonic of the applied voltage was extracted by phase sensitive detection. The amplitude of this signal has been shown to be proportional to the required first derivative of the electron energy distribution. The sensitivity and resolution of this detection system has been discussed by TAYLOR (1969).

5.5.2. Auger Transitions Observed

The silver, gold and palladium Auger peaks observed in the present work are listed in Tables I and II. The theoretical transition energies are obtained from COGHLAN, CLAUSING (1973). The transitions listed are those expected to produce strong Auger peaks. This selection is made by considering the electron mutliplicities COGHLAN, CLAUSING (1973) and the transition rates compiled by McGUIRE (1972). Representative Auger spectra are reproduced in Figures 5.1. and 5.4. for Ag and Pd.

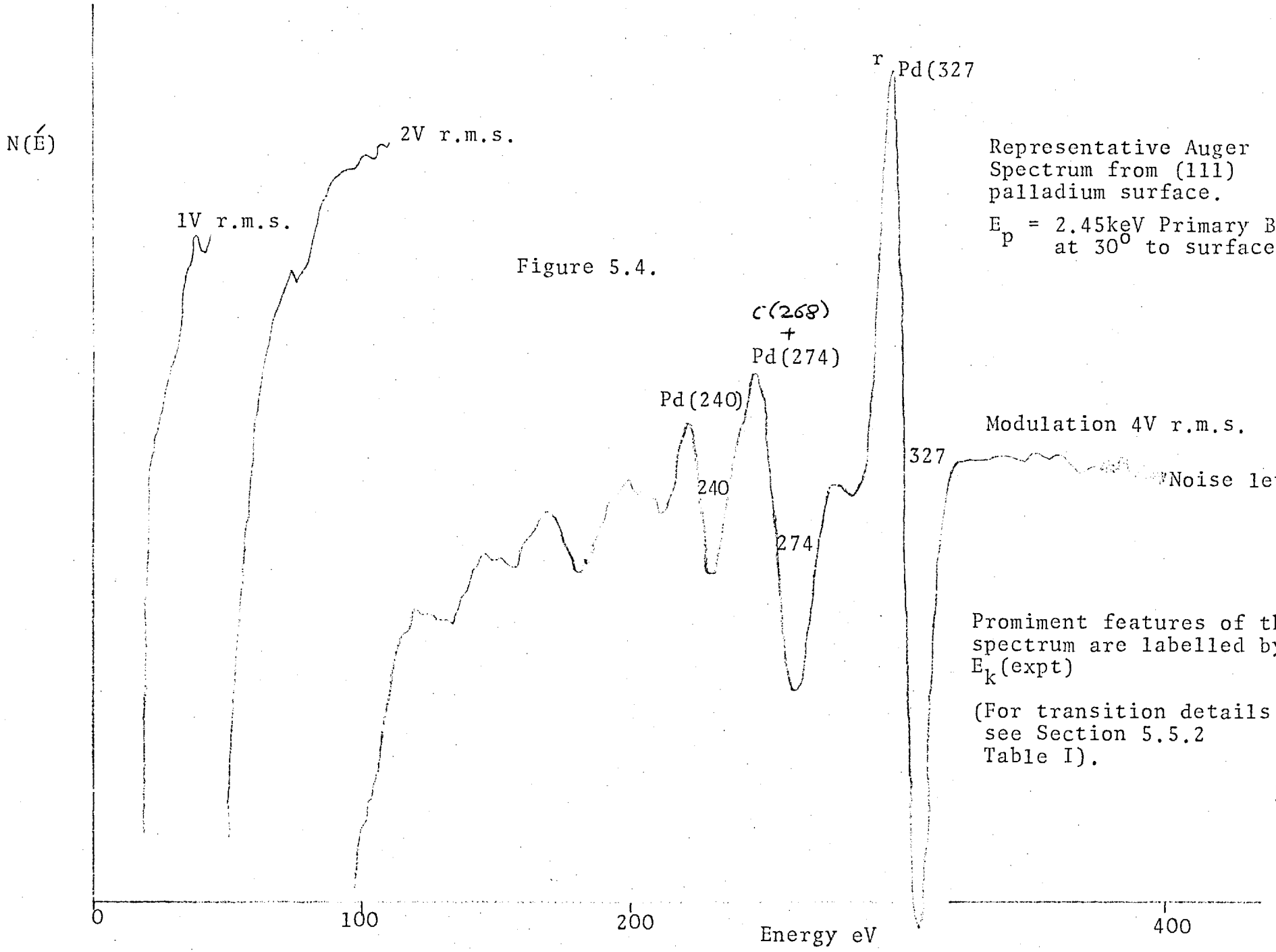


Figure 5.4.

Representative Auger Spectrum from (111) palladium surface.

E_p = 2.45keV Primary Beam at 30° to surface.

Promiment features of the spectrum are labelled by E_k(expt)

(For transition details see Section 5.5.2 Table I).

EXPERIMENTAL AND THEORETICAL AUGER TRANSITION ENERGIES
(Relative to Fermi level in eV)

TABLE I SILVER SPECTRUM

TRANSITION	E_k(Theory)	E_k(expt)	E_k(meas)
M_4 $N_{4,5}$ $N_{4,5}$	261 [1]	354	352 ±2
M_5 $N_{4,5}$ $N_{4,5}$	355		
M_4 N_3 $N_{4,5}$	307 [1]	297	294 ±2
M_5 N_3 $N_{4,5}$	301		
M_4 N_2 $N_{4,5}$			
N_5 N_2 $N_{4,5}$			
M_4 N_1 $N_{4,5}$	265.5 [1]	260	257 ±2
M_5 N_1 $N_{4,5}$	259.5		
N_1 $N_{4,5}$ $N_{4,5}$	83	79	73 ±1

PALLADIUM SPECTRUM

M_4 $N_{4,5}$ $N_{4,5}$	336 [1]	327	325 ±2
M_5 $N_{4,5}$ $N_{4,5}$	331		
M_4 $N_{2,3}$ $N_{4,5}$	283 [1]	274	271 ±1
M_5 $N_{2,3}$ $N_{4,5}$	278		
M_4 N_1 $N_{4,5}$	247.5 [1]	240	237 ±2
M_5 N_1 $N_{4,5}$	242.5		

[1] : Not resolved experimentally.

EXPERIMENTAL AND THEORETICAL AUGER TRANSITION ENERGIES

(Relative to Fermi level in eV)

TABLE II GOLD SPECTRUM

TRANSITION	E_k(Theory)		E_k(expt)	E_k(meas)
$N_7\ O_3\ O_{4,5}$	22	[1]	30	25 ±1
$N_6\ O_3\ O_{4,5}$	26			
$O_3\ O_{4,5}\ O_{4,5}$	44		44	39 ±2
$O_2\ O_{4,5}\ O_{4,5}$	62		58	54 ±2
$N_7\ O_{4,5}\ O_{4,5}$	73	[1]	70	66 ±2
$N_6\ O_{4,5}\ O_{4,5}$	77			
$O_1\ O_{4,5}\ O_{4,5}$	98		94	90
$N_5\ N_6\ N_6$	144	[1]	144	140
$M_3\ M_5\ N_5$	145.5			
$N_5\ N_6\ N_7$	148			
$N_5\ N_7\ N_7$	152			
$N_4\ N_6\ N_6$	162	[1]	164	160
$N_4\ N_6\ N_7$	166			
$N_4\ N_7\ N_7$	170			
$N_3\ N_4\ O_{4,5}$	175.5			

[1] : Not experimentally resolved

EXPERIMENTAL AND THEORETICAL AUGER TRANSITION ENERGIES
(Relative to Fermi level in eV)

TABLE III

ELEMENT	TRANSITION	E_k(Theory)	E_k(expt)	E_k(meas)
CARBON	K $L_{2,3}$ $L_{2,3}$	268	268	265
CHLORINE	$L_{2,3}$ $M_{2,3}$ $M_{2,3}$	182	189	185
SULPHUR	$L_{2,3}$ $M_{2,3}$ $M_{2,3}$	151	150	146

The transitions listed are also in agreement with those observed by BISHOP, RIVIÈRE (1969b) and PALMBERG, RHODIN (1968).

An experimentally determined value $E_k(expt)$ of the kinetic energy of the Auger electrons E_k resulting from a transition k may be obtained from equation 5.2.

$$E_k(expt) = 0.993\ E_k(meas) + \phi_n \qquad (5.2)$$

where E_k is defined by equation 3.28

$E_k(meas)$ is the potential difference applied between the retard grid of the analyser and the specimen

ϕ_n is the work function of the retard grid.

The factor of 0.993 is equation 5.2. results from field penetration of the grids of the electron detector as discussed by (TAYLOR, 1969). This was measured for the present apparatus by GIBSON (1973) who monitored the elastic peak in the secondary electron spectrum using the retarding field analyser.

The work function of nickel plated tungsten grids used in the present work was 5eV. If evaporant coats the grids this value will be in error.

Transitions which result from the presence of impurities at the specimen surface are listed in Table III.

In the present work in addition to monitoring the presence of contaminants, Auger electron spectroscopy was used to determine the mode of growth of the deposited

films section 5.6. and to investigate the degree of alloying occurring.

5.6. A Method of Investigating the Mode of Growth Using Auger Electron Spectroscopy.

In the present work the mode of growth of an overlayer film evaporated onto a substrate is investigated using Auger Spectroscopy.

The strong attenuation of both the incident electron beam and the created Auger electrons within the solid causes the Auger signal detected from each component of the specimen to be dependent on the position with respect to the surface of the excited atoms.

A calculation of the Auger current which considers only the attenuation of the Auger electrons within the specimen and the collection geometry has been shown to be capable of distinguishing between some different modes of growth. Hence a comparison of the observed Auger emission as a function of mean deposit thickness with the emission calculated for different modes of growth may allow the determination of the growth mode.

5.6.1. The Method of Calculation of Auger Signal Strengths

The method of calculation developed for application to data obtained using a retarding field analyser is due to DOBSON and REGAN (1976). A layer by layer calculation is made of the fraction of the created Auger electrons which are detected. This fraction is determined by collision processes within the specimen and the detector geometry. The attenuation of the Auger electrons over a path r is

is proportional to $\exp(\frac{-r}{\lambda_{ai}})$

where λ_{ai} is the mean free path of the Auger electrons and is dependent on the Auger electron energy E_k and the atomic number z of the absorbing material.

The detected Auger current I_{na} resulting from Auger electrons created in the n^{th} layer of the specimen Fig. 5.5. and emitted from atoms of the type A with an energy E_k is given by equation 5.3.

$$I_{na} = J N_n A_{na} \int_0^{\psi} \frac{\sin\theta}{2} \exp\left|\frac{-(n-0.5)d}{\lambda_a \cos\theta}\right| d\theta \qquad (5.3)$$

where J is the current density of the incident electron beam

N_n is the density per unit area of atoms of type A in the n^{th} layer of the specimen

A_{na} is the probability of creation of an Auger electron of energy E_k per electron incident (per electron incident on the species) per atom of type A in the n^{th} atomic layer of the specimen

d is the interlayer spacing.

The integral over the collection angle of the detector Fig. 5.5.

DOBSON & REGAN (1976) have shown that equation 5.3. may be rewritten

$$I_{na} = J \frac{A_{na}}{2} N_n (E_2(b) - \cos\psi E_2(b)) \qquad (5.4)$$

Retarding field analyser

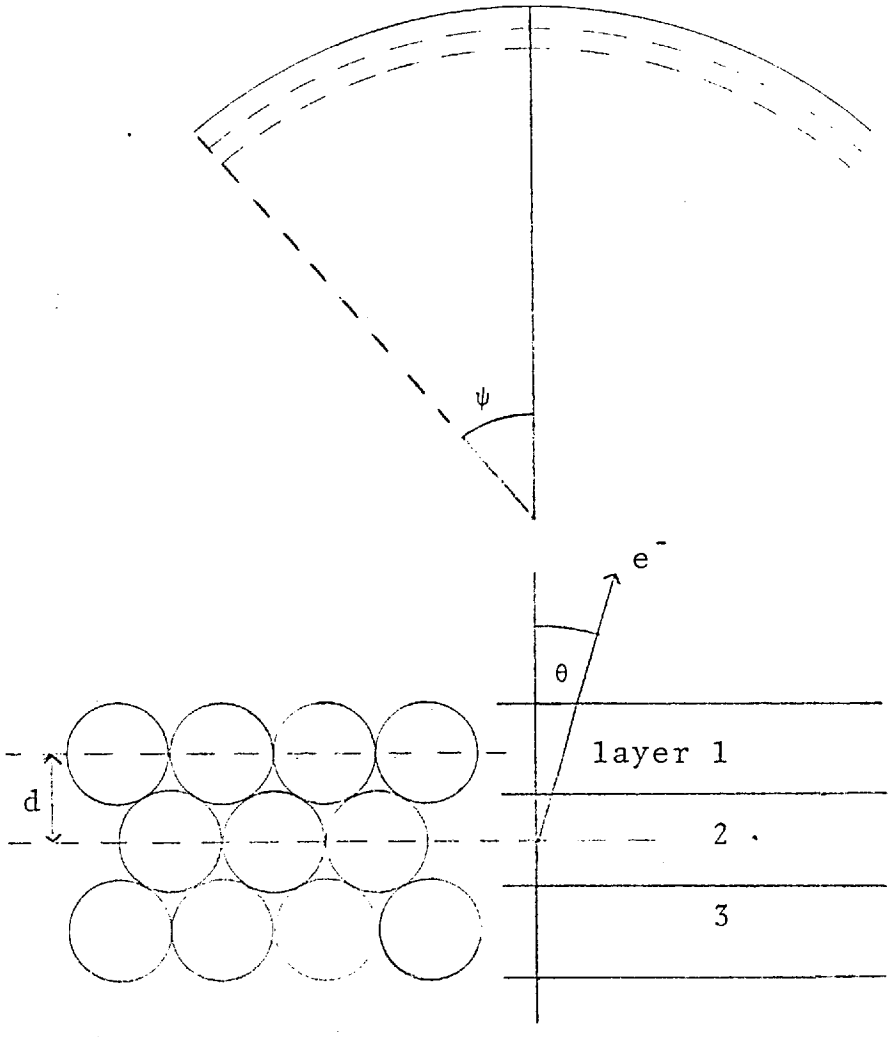


Figure 5.5.

where $E_2(b) = \int_1^\infty t^{-2} e^{-bt} dt$

and $b = \frac{(n-0.5)d}{\lambda_{ai}\cos\theta}$

$E_2(b)$ is an exponential integral tabulated by AMBRAMOWITZ & STEGUN (1965). The expression

$$(E_2(b) - \cos\psi\ E_2(b)) = i_{na} \qquad (5.5)$$

has been tabulated by DOBSON & REGAN (1976) for $\theta = 47^o$ which is applicable for most LEED systems supplied by VG. From equation 5.3. the probability of an Auger electron of energy E_k created in the n^{th} atomic layer being detected is $\frac{i_{na}}{2}$.

The mean free path of Auger electrons of energy E_k (20-500)eV lie in the range $\lambda \sim 3$ -15Å POWELL (1974) whereas the mean free path of primary beam electrons E = 2500eV is ≥ 30Å BRUNDLE (1974). It follows that A_{na} is a considerably more slowly varying function of n than i_{na}. We shall treat A_{na} as independent of n in the present calculation and replace A_{na} by A_a. The contribution of inelastically scattered primary electrons to Auger electron excitation partly offset the attenuation of the incident beam and improves this approximation.

The total Auger current detected I_a due to the emission of electrons of energy E_k may be written

$$I_a = \frac{N_n A_a J}{2} \sum_{n=1}^{\infty} i_{na} \qquad (5.6)$$

From Figure 5.6. it is seen that i_{na} is very small for large n and the equation may be approximated to

$$I_a = \frac{J}{2} \sum_{n=1}^{10} i_{na} \qquad (5.7)$$

Examination of reported values of λ_a reviewed by POWELL (1974) reveals a range of values reported for a particular energy of ~ ±2Å and little correlation in this spread with the atomic number of the absorbing material. This uncertainty in assigning a value to λ_a is probably the limiting factor on the accuracy of the model outlined above

In order to extend the calculation to characterise the Auger emission of specimens containing two atomic species, i.e. atoms of type A and B, some further definitions must be made.

N_n is the number of atoms of type A per unit area in the n^{th} layer of the speciman.

Similarly

M_n is the number of atoms of type B per unit area in the n^{th} layer of the specimen.

Also

A_a is the cross-section for the creation of Auger electrons of kinetic energy E_{ka} from atoms of type A.

B_b is the cross-section for the creation of Auger electrons of kinetic energy E_{kb} from atoms of type B.

A_a and B_b are defined for the flux of electrons incident on the specimen.

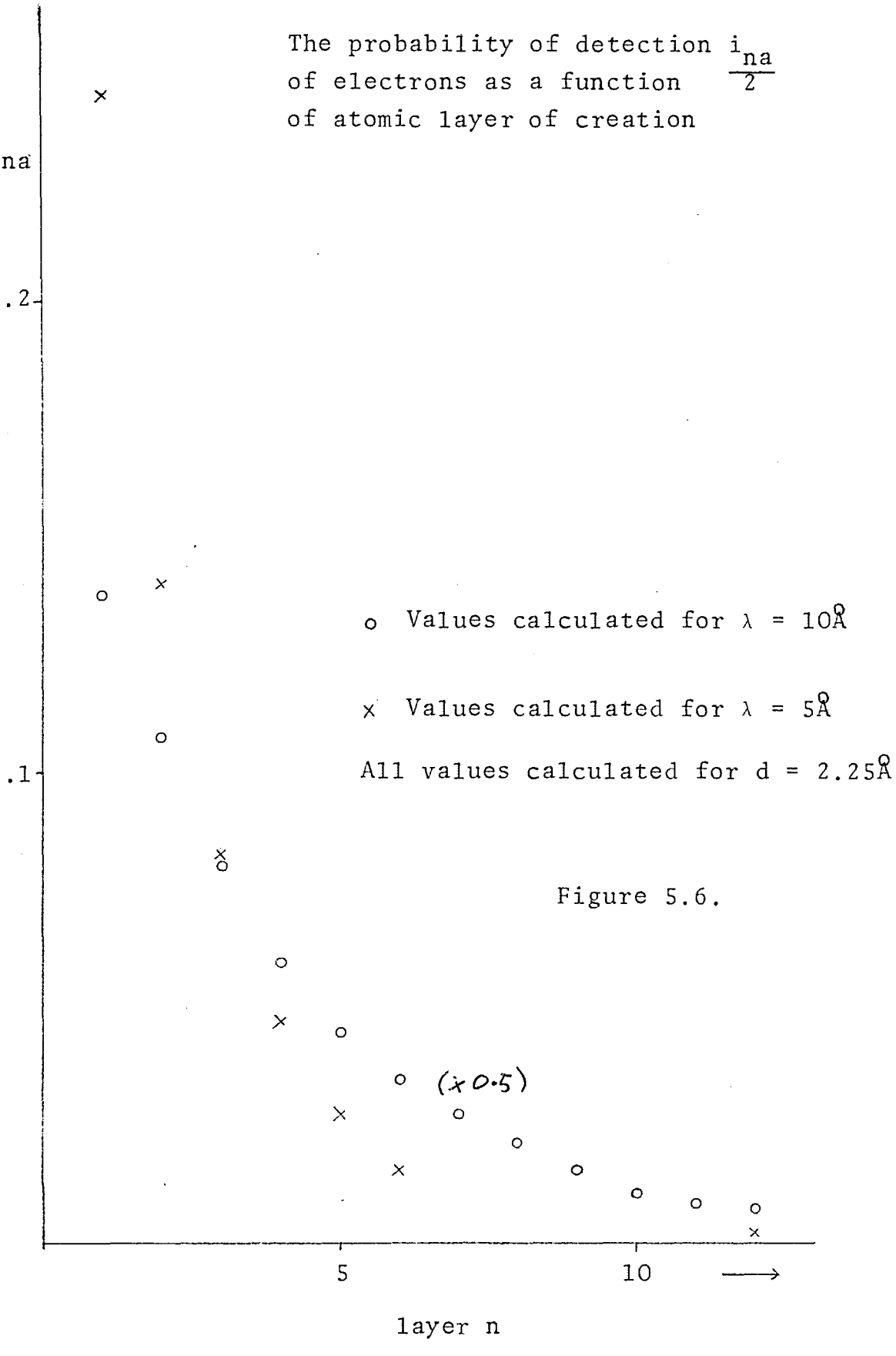

The probability of detection $i_{\frac{na}{2}}$ of electrons as a function of atomic layer of creation
na
.2
.1
o Values calculated for λ = 10Å
x Values calculated for λ = 5Å
All values calculated for d = 2.25Å
(x 0.5)
5
10
layer n

Figure 5.6.

In the present work the Auger emission from the substrate and overlayer combination is characterised by the ratio R_{ab} of the detected Auger signals from a substrate and an overlayer transition.

$$R_{ab} = \frac{A_a}{B_b} \sum_{n=1}^{10} \frac{N_n}{M_n} \frac{i_{na}}{i_{nb}} \qquad (5.8)$$

The use of the ratio R_{ab} to characterise Auger emission avoids the need to normalise the detected Auger signal with respect to the primary beam current. This requires only that the primary beam current remains constant during the recording of a single spectrum.

5.6.2. The Predicted Auger Signal Strengths

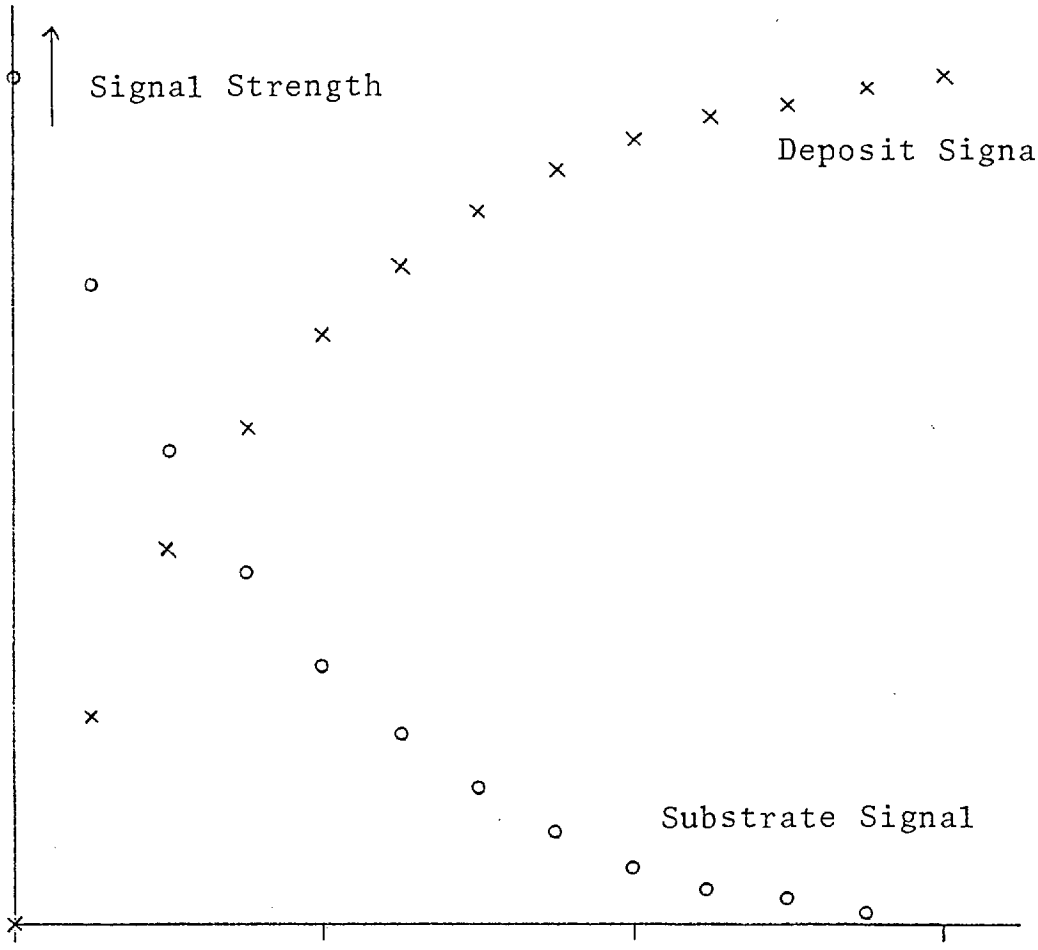
Using equation 5.8., the ratio of the Auger signal strength for palladium growing two-dimensionally on silver and gold is predicted in Figs. 5.7. and 5.8. For comparison with experimental data the mean free path for the Ag (352eV) Pd (325eV) and the Au(70eV) transitions to which the calculations are applied were taken to be 10Å, 10Å and 5Å respectively and the interplanar spacings 2.25Å.

The ratio R_{ab} of the Auger signal strengths from homogeneous two component alloys having a fractional composition x of component A is given by equation 5.9.

$$R_{ab} = \frac{A_a}{B_b} \frac{x}{(1-x)} \sum_{n=1}^{10} \frac{i_{na}}{i_{nb}} \qquad (5.9)$$

or

$$R_{ab} = \frac{x}{1-x} k \qquad (6.0)$$


Signal Strength
Deposit Signal
Substrate Signal

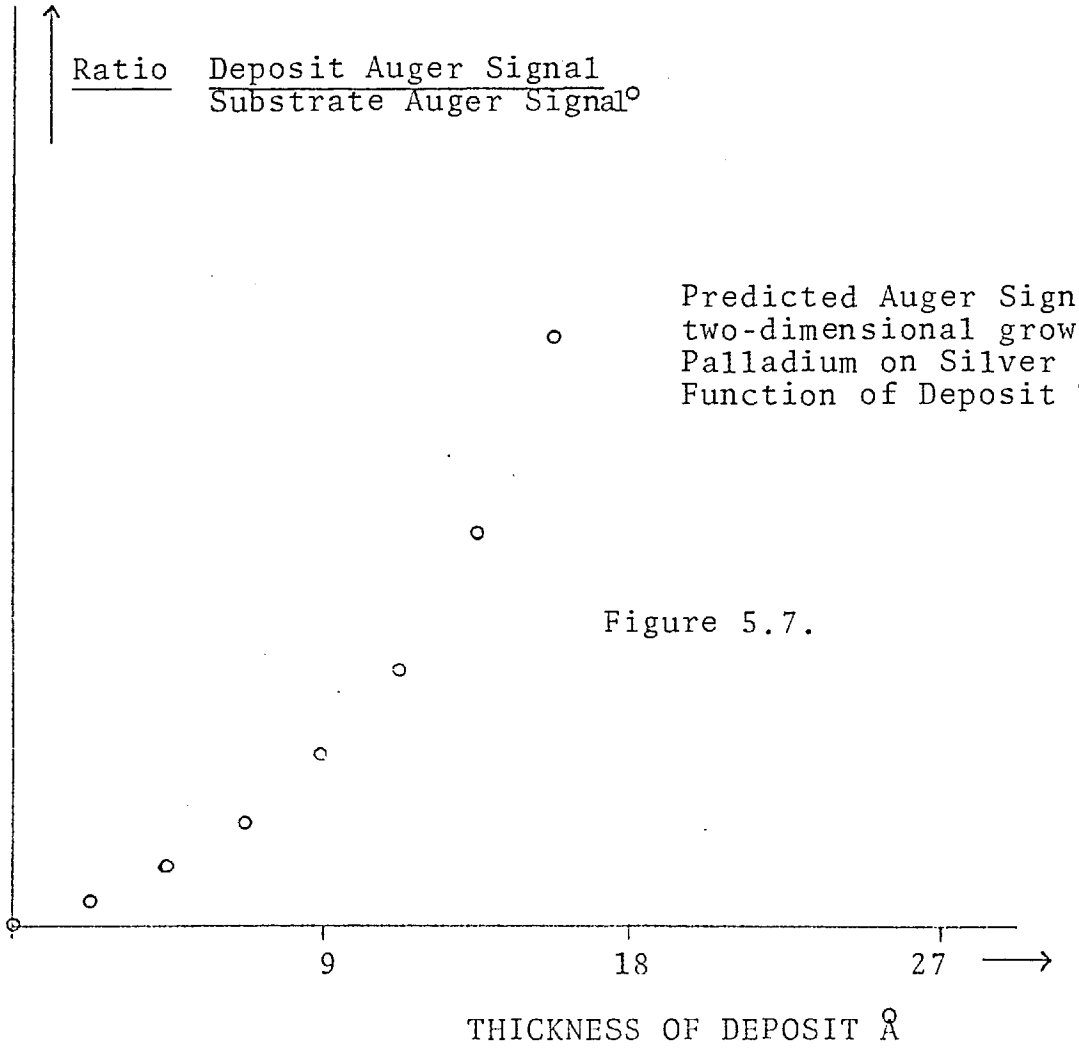
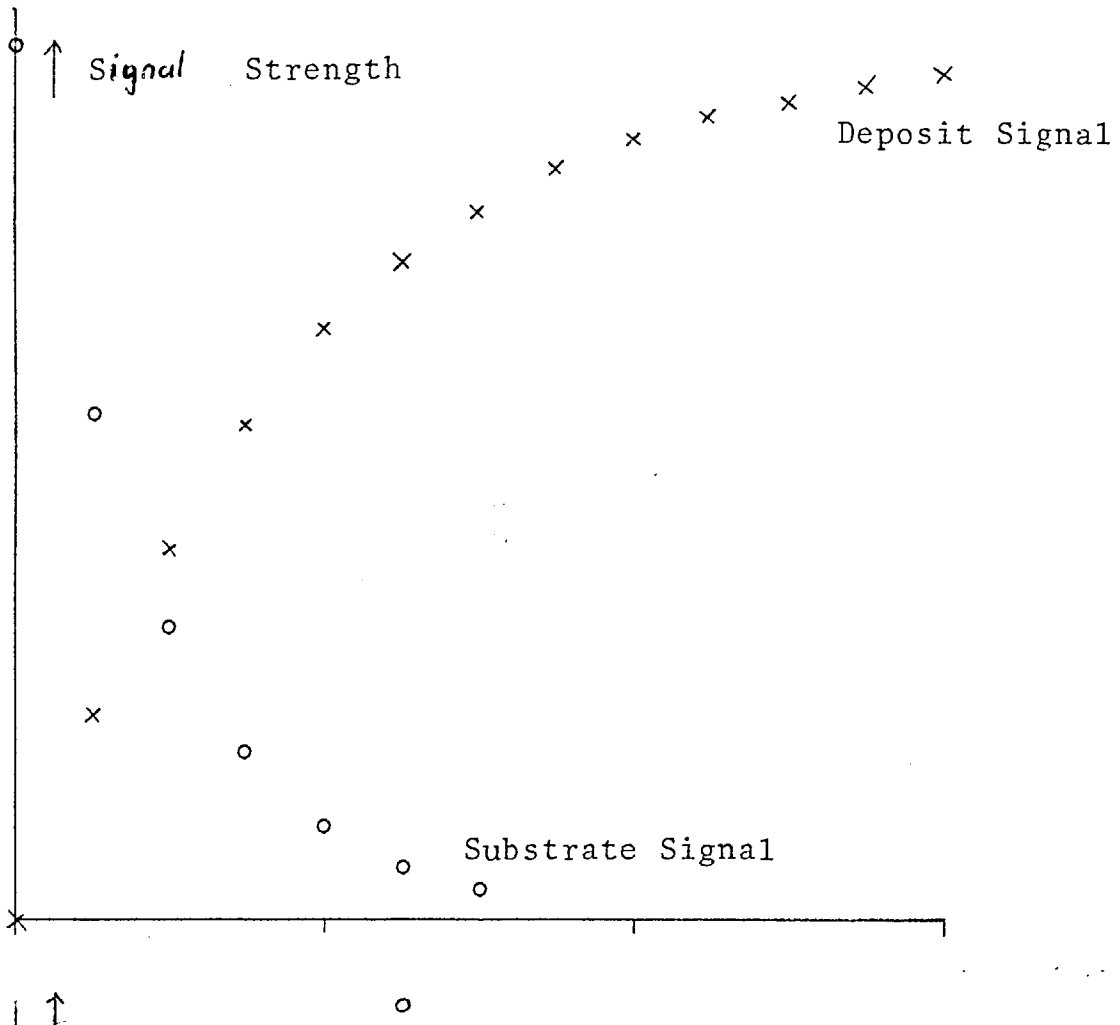
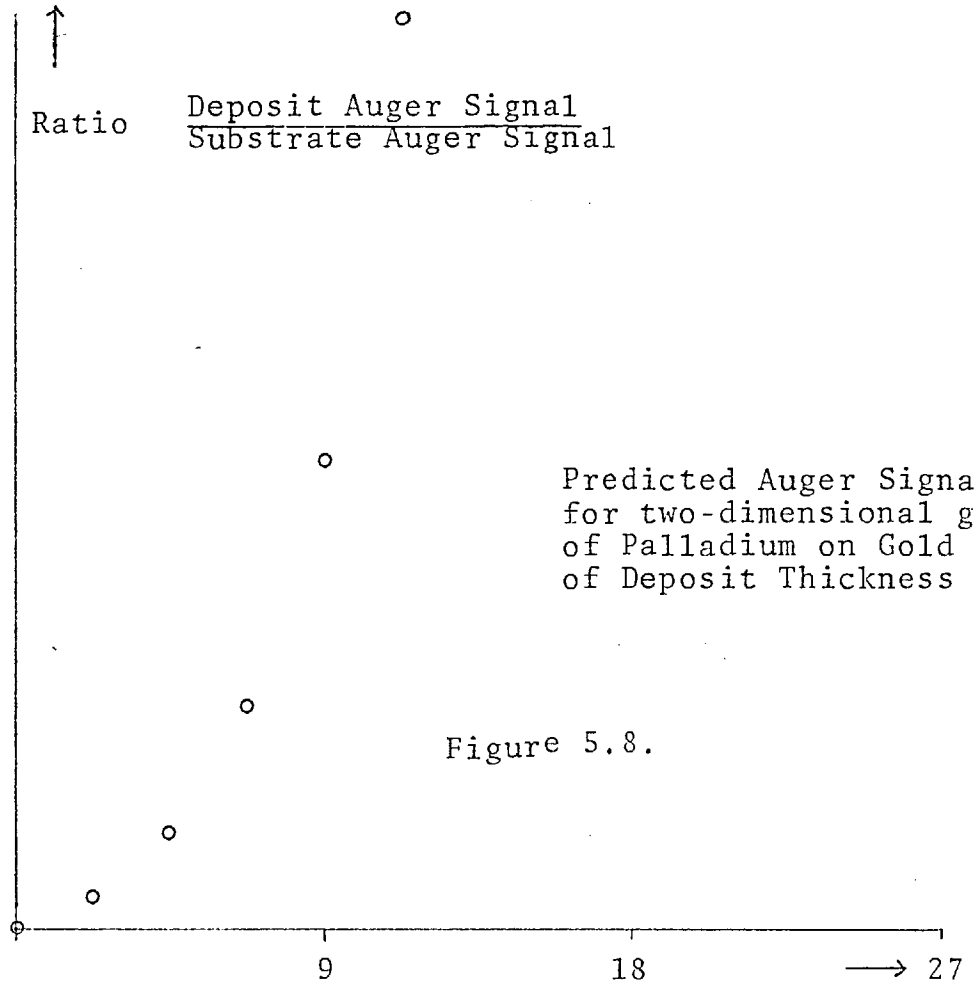

Ratio Deposit Auger Signal / Substrate Auger Signal
Predicted Auger Signals for two-dimensional growth of Palladium on Silver as a Function of Deposit Thickness
9
18
27
THICKNESS OF DEPOSIT Å

Figure 5.7.





Predicted Auger Signals
for two-dimensional growth
of Palladium on Gold as a function
of Deposit Thickness

Figure 5.8.

where k is a constant for any pair of transitions a and b. This method is particularly well suited to distinguishing the two-dimensional growth of immiscible materials from all other growth modes. Since for any mean deposit thickness and fixed λ_a and λ_b the ratio R_{ab} equation 5.8 from a two-dimensional configuration is a maximum over all other modes of growth, where the overlayer consists of atoms of type A and the substrate consists of atoms of type B.

5.7. Scanning Electron Microscope used in conjunction with Auger Electron Spectroscopy

A problem was encountered in positioning the electron beam exclusively on the specimen. This was a result of the narrow cut specimen configurations adopted for accurate RHEED misfit measurements (Section 5.3.1.). The difficulty was overcome by the construction of a scanning electron microscope SEM based on a design by ASHWELL et al (1973). The glancing incidence Auger gun was used and varying potentials were applied to its X and Y deflector plates to produce a raster scan of the electron beam over the specimen. The total secondary electron current from the specimen was detected using the screen of the LEED optics. The signal was then amplified and applied to the z input (beam intensity modulation control) of an oscilloscope. The X and Y inputs of the oscilloscope were driven by the same varying potentials which were applied to the electron gun deflector plates. A secondary electron emission SEM image of the specimen was then obtained on the oscilloscope display.

The SEM facility was used to centre the electron beam on the specimen for subsequent Auger analysis and it permitted a check of the homogeneity of the specimen surface to be made.

CHAPTER 6

The Growth of Palladium on Silver

6.1. Introduction

Both silver and palladium form close-packed cubic crystals having lattice parameters of 4.078Å and 3.882Å respectively. WYCKOFF (1963). The misfit of the system $M_o = 0.048$ is within the range of misfit values for which pseudomorphism has been reported and is less than the theoretical limit for the occurrence of pseudomorphism calculated by van der Merwe and others (section 2.3.2).

Recently YAGI et al (1976) have carried out a electron microscope investigation of the epitaxial growth of palladium on (100) silver and has reported a two-dimensional pseudomorphic growth mode. Few experimental details of this investigation were given.

Silver and palladium form a complete solid solution in one another, HANSEN (1958), and therefore allow alloy formation at elevated temperatures to occur.

The aim of the present work is to examine carefully the evidence for pseudomorphism in thesystem giving particular attention to the role of inter-diffusion.

6.2. RESULTS FOR ROOM TEMPERATURE DEPOSITIONS

Palladium films were evaporated in stages onto silver (111) substrates (section 5.5.1.) at room temperature. The first few monolayers $\sim$ < 20Å were deposited at a rate of $\simeq$ 1.5Å min^{-1} and this was increased for subsequent depositions to 5-10Å min^{-1}. The overlayer was found to grow epitaxially in an orientation parallel to the substrate.

The RHEED diffraction features, (observed at low angles of beam incidence) changed slowly and continuously as the overlayer thickness increased. The continuous streaks characteristic of silver substrates became increasingly modulated figures 6.1, 6.2, 6.3 and 6.4. In the case of thick films 110-225Å the diffraction pattern consisted of sharp elongated spots superimposed on streaks of lower intensity. The diffraction features from the palladium deposits < 45Å were broader than those of the silver substrate. However as additional palladium was deposited they became sharper again.

From AES data obtained during the initial stages of film growth figures 6.5 and 6.6. it is seen that the substrate signal is almost totally obscured by the deposition of 13.5Å. of palladium. Films at all stages of growth if maintained at room temperature for a number of hours, showed no change in their Auger spectrum.

The mismatch M of the overlayer with respect to the substrate was monitored by RHEED (section 5.1) at a number of stages of the film growth and found to change continuously as a function of deposit thickness. Fig. 6.7. A quartz crystal microbalance was used to determine the deposit thickness h (section 5.2).

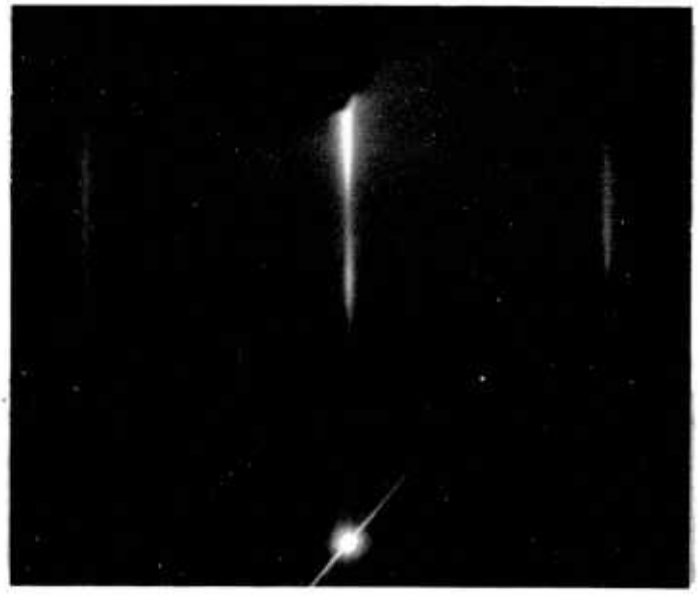


Figure 6.1

RHEED pattern from (111) silver substrate
E_p = 37 keV, <211> azimuth; $\alpha = 1.5^{o}$.

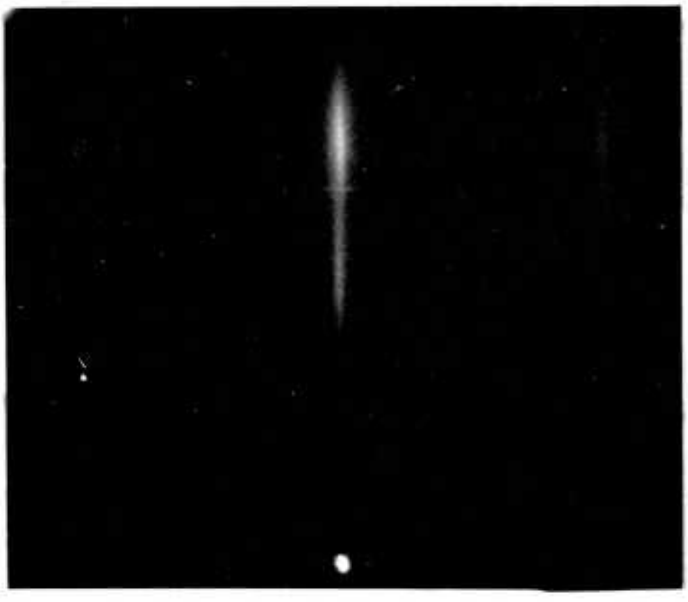


Figure 6.2

RHEED pattern from ~ 8Å of palladium deposited at 1.5Å min^{-1} onto a (111) silver substrate at room temperature.
E_p = 37 keV, <211> azimuth; $\alpha = 1.7^{o}$.

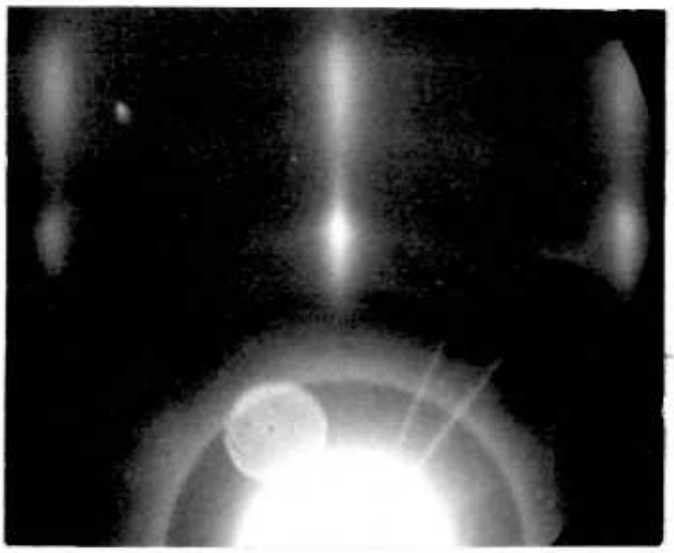


Figure 6.3

RHEED pattern from ∿ 38Å of palladium deposited onto a (111) silver substrate at room temperature.

E_p = 37 keV, <211> azimuth; $\alpha = 1.8^{o}$.

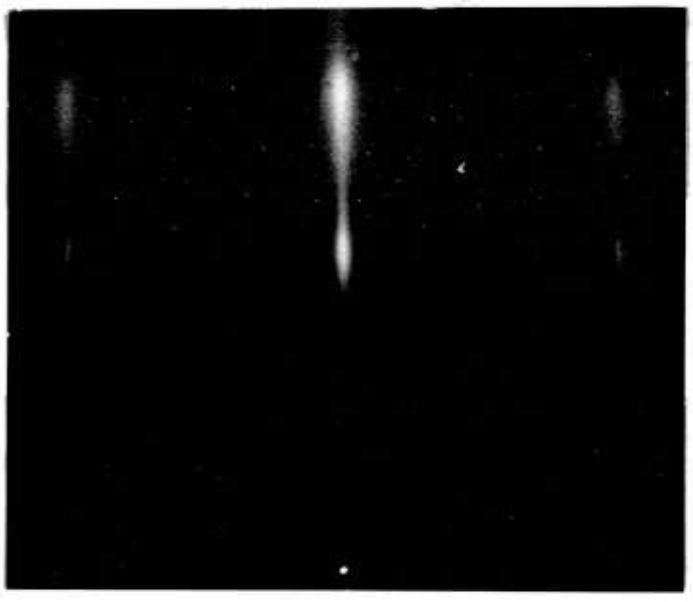
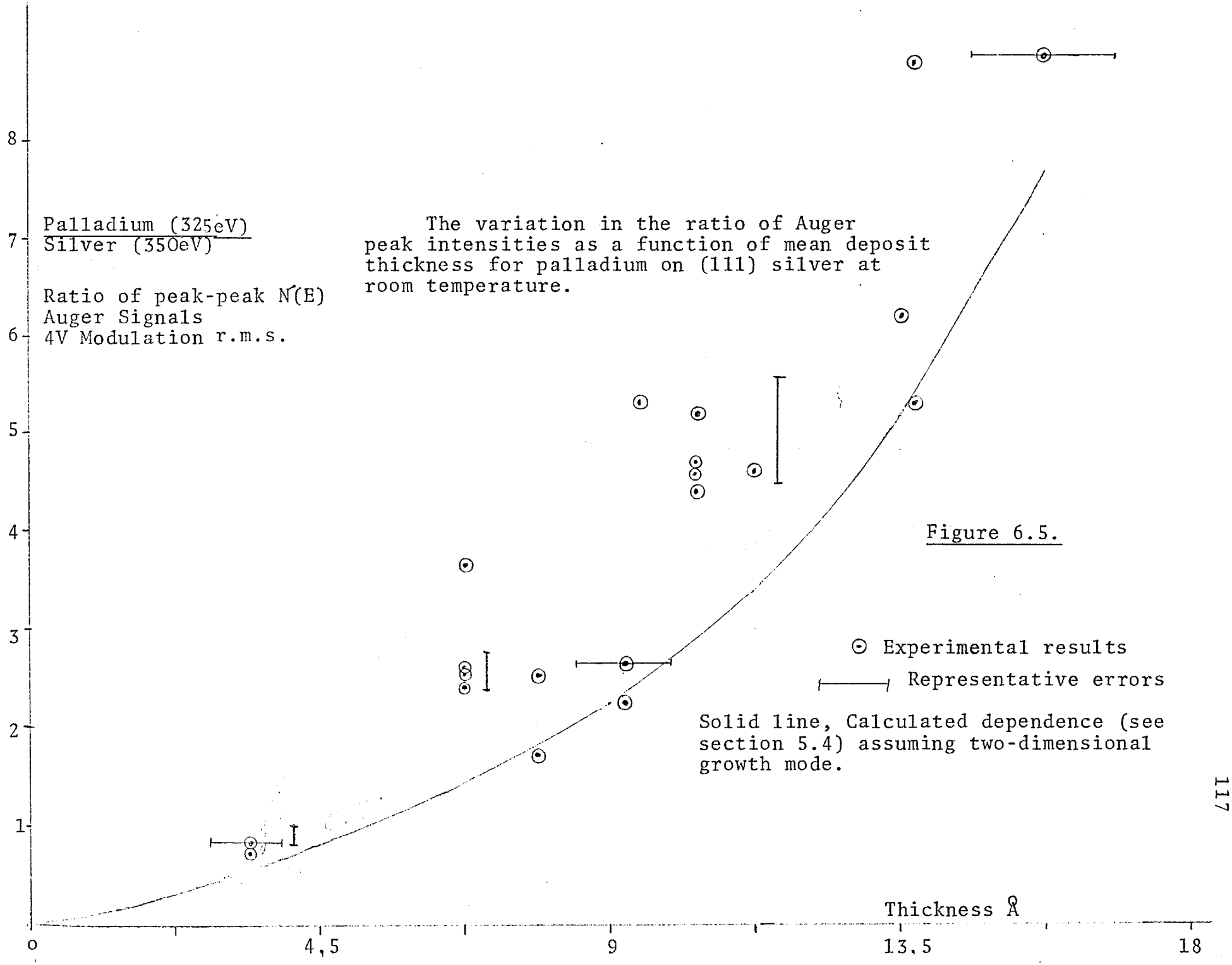


Figure 6.4

RHEED pattern from ∿ 215Å of palladium deposited onto a (111) silver substrate at room temperature.

E_p = 37 keV, <211> azimuth; $\alpha = 2.2^{o}$.



The variation in the ratio of Auger peak intensities as a function of mean deposit thickness for palladium on (111) silver at room temperature.

Figure 6.5.

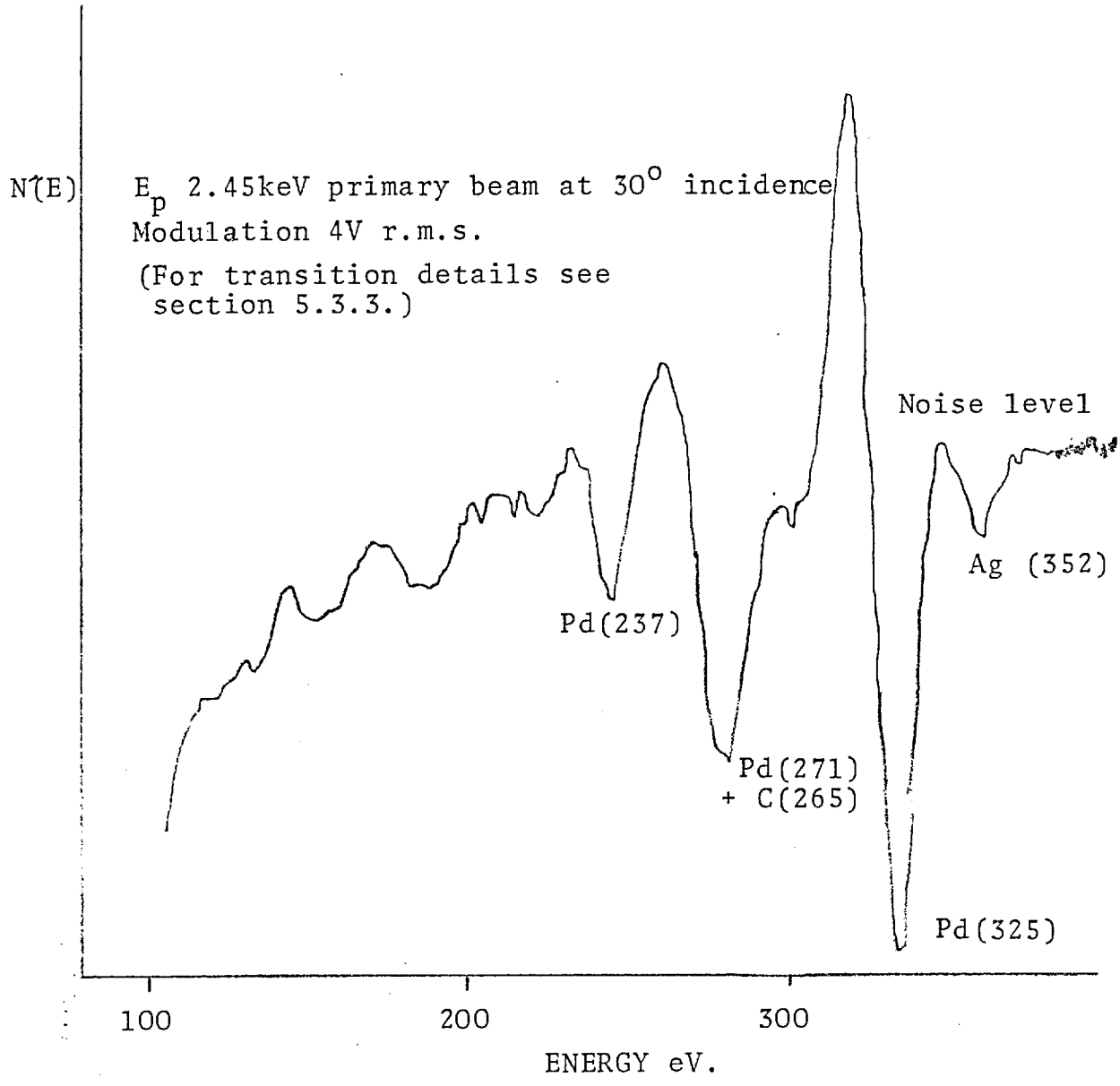
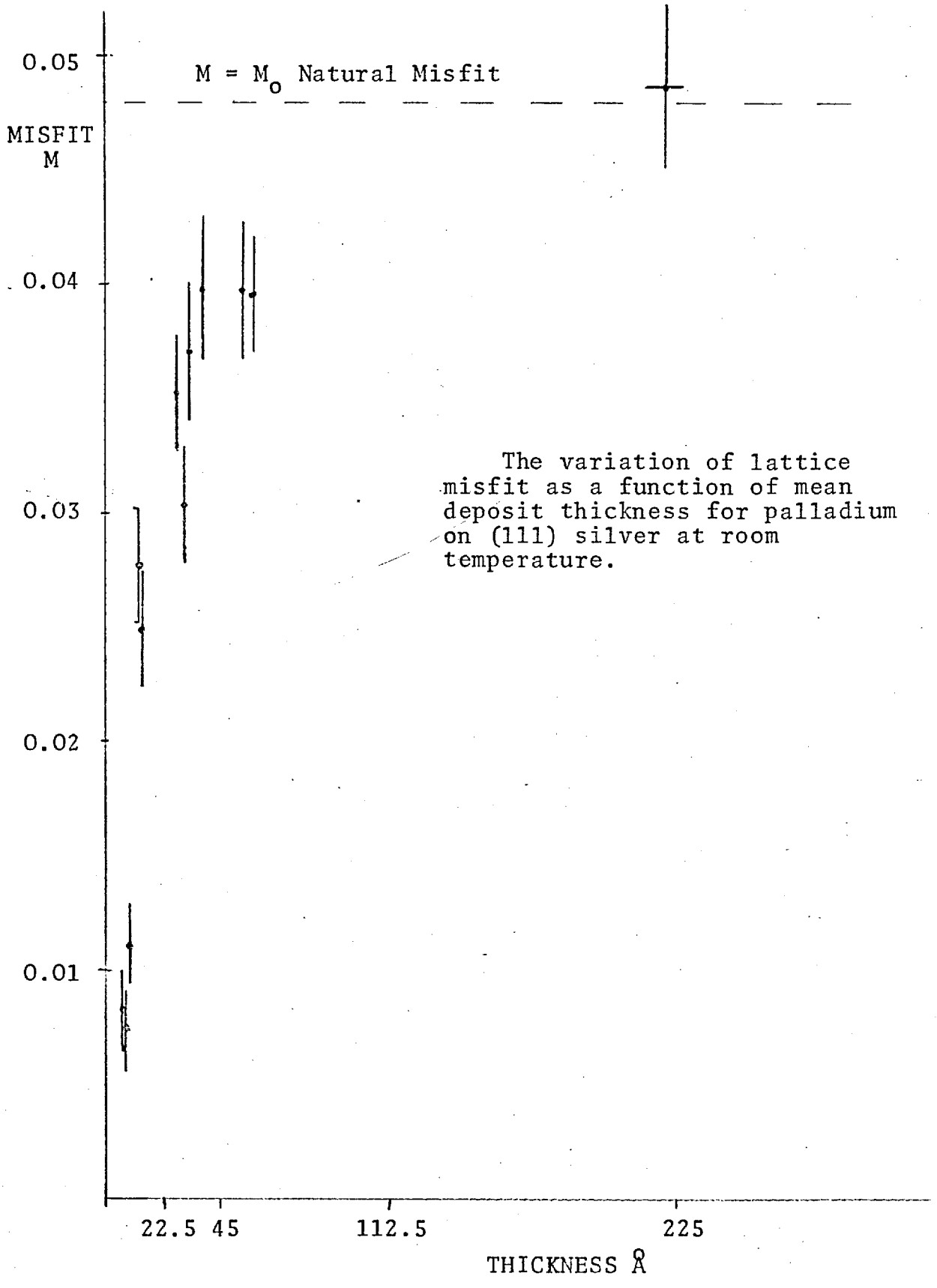


Figure 6.6

Auger spectrum after the deposition of 13.5Å of palladium on (111) silver at room temperature.



The variation of lattice misfit as a function of mean deposit thickness for palladium on (111) silver at room temperature.

Figure 6.7

6.3. RESULTS INDICATING THE ROLE OF DIFFUSION AT ELEVATED TEMPERATURES

Thick overlayers of Pd, 40-250Å, deposited on Ag at room temperature and described above were subjected to various annealing treatments and subsequently examined with RHEED and AES. On annealing these films at temperatures > 525K the substrate Auger signal reappeared and increased continuously as the annealing progressed Fig. 6.8.

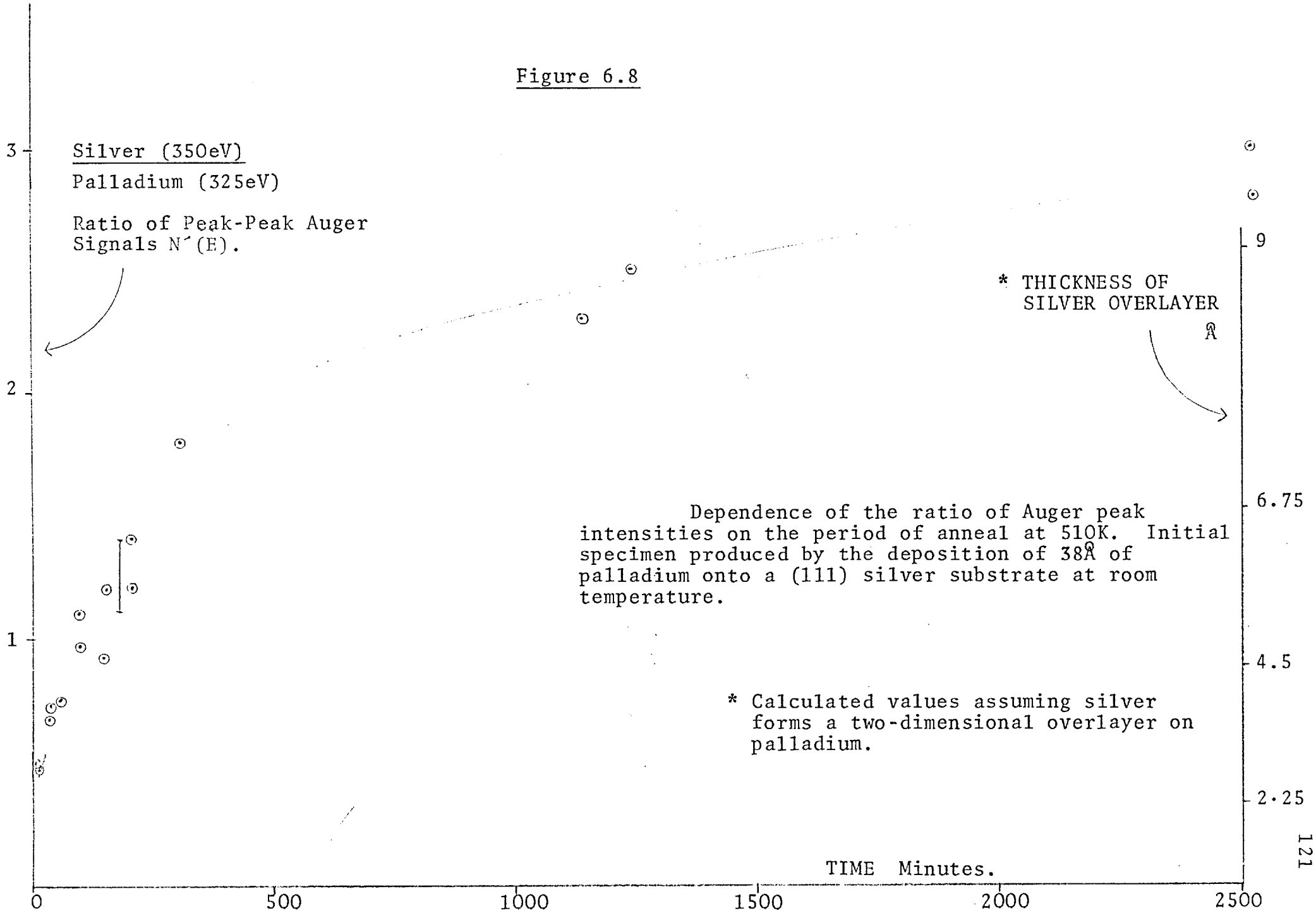
After annealing films for a number of hours the RHEED features reverted to unmodulated streaks Fig. 6.9. In addition the separation of the diffraction features changed towards that characteristic of a silver specimen.

The deposition of palladium onto a (111) silver substrate maintained at 440K produced results identical with those described in section 6.2. for substrates maintained at room temperature.

6.4. DISCUSSION OF GROWTH OF PALLADIUM ON SILVER

Both the dependence of Auger data on film thickness Fig. 6.5. and the changes in the modulation of RHEED features indicate that the first few monolayers of deposit grow approximately two-dimensionally. The small increase in streak modulation resulting from the deposition of a few monolayers suggests that the surface is only slightly rougher than the flat substrate. The agreement between the experimental and predicted dependence of Auger signal on film thickness Fig. 6.5 is good when two-dimensional growth is assumed.

Figure 6.8


Silver (350eV)
Palladium (325eV)
Ratio of Peak-Peak Auger Signals N´(E).
3
2
1
* THICKNESS OF SILVER OVERLAYER Å
9
6.75
4.5
2·25
Dependence of the ratio of Auger peak intensities on the period of anneal at 510K. Initial specimen produced by the deposition of 38Å of palladium onto a (111) silver substrate at room temperature.
* Calculated values assuming silver forms a two-dimensional overlayer on palladium.
TIME Minutes.
0
500
1000
1500
2000
2500

The good agreement is not critically dependent on the choice of the mean free paths of the Auger electrons. This is illustrated by the similarity of the predicted signals of the different systems Pd/Au, Pd/Ag. (Section 5.4).

Because the AES data resulting from annealing at room temperature displays no time dependence, inter-diffusion rates must be very small at room temperature.

The changes in modulation of RHEED features observed in thicker films, indicate that the specimen surface may have roughened considerably, having palladium islands growing out of a flattish palladium base.

The broadening of RHEED features obtained from thin deposit films may result from both small crystallite sizes and disorder in the form at inhomogeneous elastic strains. Section 3.3.2.

The observed dependence of mismatch on film thickness indicates that in the thinnest deposits the palladium are strained elastically to match the substrate. Fig. 6.7. The experimental procedures used ensure that the results obtained are not a consequence of contamination. This is confirmed by the low level of contaminants seen in the AES spectra, although the presence of small amounts of carbon can not be ruled out.

From the changes observed in RHEED and Auger data obtained after annealing to temperatures > 525K it is clear that diffusion processes are active. The reappearance of unmodulated RHEED streaks Fig. 6.9. probably results from the regeneration of a flat specimen surface. A consequence favoured by the associated reduction in surface area and hence the total surface energy of the specimen.

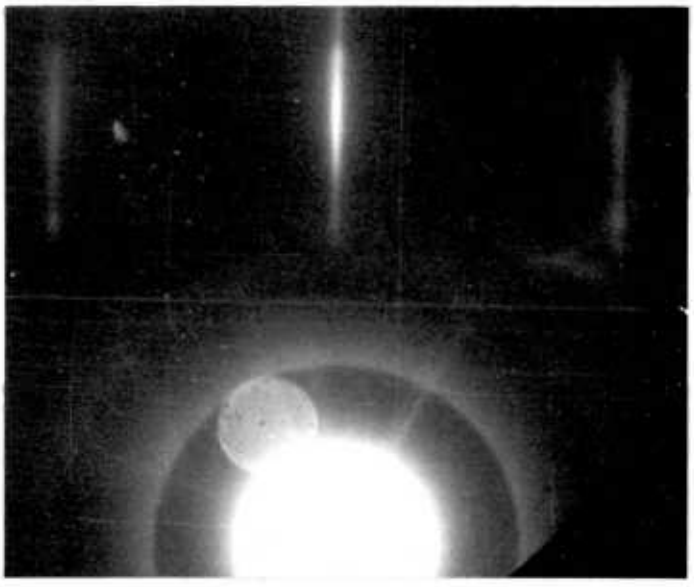


Figure 6.9.

As figure 6.3 but after annealing to 610K for 18 hours the 38Å of palladium deposited onto a (111) silver substrate at room temperature.
E_p = 37 keV, <211> azimuth; $\alpha = 2.5^{o}$.

The observed replacement of palladium by silver substrate atoms at the surface Fig. 6.8 further reduces the surface energy (surface energy of palladium $\sim$ 1.5 $J m^{-2}$

surface energy of silver $\sim$ 0.9 $J m^{-2}$)

WEAST (1974).

The change in specimen configuration by which substrate atoms reach the surface may consist of components of three fundamental processes:-

1) The break-up of the palladium overlayer into islands revealing the substrate surface. The overall change in the surface free energy of such a process is determined by the final surface area of the palladium islands formed and may be positive or negative accordingly.

2) The formation via grain boundary diffusion at a silver layer overlaying the palladium deposit. The total free energy of the specimen may be reduced by such a transition since silver has a lower surface free energy than palladium. The formation of a second silver palladium interface having an unknown interfacial energy must, however, be considered. As a consequence the change in free energy cannot be predicted.

3) The alloying of the substrate and deposit by lattice interdiffusion.

The formation of a flat surface as observed by RHEED on annealing is not compatible with the existence of palladium nuclei associated with (1) above.

Even when such a transition is energetically favourable the large activation energy resulting from an initial increase in surface area is expected to prevent it taking place.

Processes (2) and (3) cannot be distinguished in the present results; they may both occur, their contribution to the final state of thespecimen being determined by the kinetics of each process in combination with the surface smoothing process.

YAGI et al (1976) have reported results for the growth at Pd on Ag(III) in close agreement to those reported above, i.e. a two-dimensional pseudomorphic growth mode. However few further details were reported and therefore no comment can be made.

6.5. CONCLUSIONS

It is concluded that the room temperature deposition of palladium onto (111) silver substrates causes palladium to grow as a two-dimensional overlayer elastically strained in its thinner deposits $\sim$ 2.25Å to match the substrate. At temperatures greater than 525K diffusion between the palladium deposit and the silver substrate occurs.

CHAPTER 7

The Growth of Palladium on Gold

7.1. Introduction

Both palladium and gold form close-packed cubic crystals having lattice parameters of 3.889Å and 4.078Å respectively WYCKOFF (1963). The misfit between the lattices M_o = 0.046. Palladium and gold form a series of complete solid solutions HANSEN (1958).

YAGI et al (1971) have carried out an in-situ electron microscope investigation of the growth of thin evaporated palladium films on (111) gold between 575-675K in a vacuum of 10^{-4} Pa. From observations of the misfit dislocation density it was concluded that the overlayer grew pseudomorphically in a two-dimensional growth mode. A separate A.E.S. investigation by MATSUSHITA, YAGI et al (1974) carried out on Pd/Au films grown at room temperature also indicated a two-dimensional growth mode.

CHERNS, STOWELL (1975a,b: 1976) deposited palladium on (100) and (111) gold substrates between room temperature and 575K in a vacuum of 10^{-6} Pa. From a careful investigation of misfit as a function of thickness it was concluded that the first 6Å of palladium on (111) substrates and 10Å on (100) substrates grew pseudomorphically. It was also concluded that the overlayer grew two-dimensionally. Thickness measurements were made from X-ray microanalysis observation and the misfit determined from observations of the dislocation density.

7.2. The Growth of Palladium on Gold (111) at Room Temperature Results

Palladium was evaporated in stages onto gold (111) substrates (section 5.5). During the initial depositions $\sim$ < 10Å the rate of deposition was $\sim$ 1.5Å min.$^{-1}$. For subsequent film growth this was increased to 4-9Å min.$^{-1}$.

The palladium grew epitaxially with the (111) planes and <110> axis parallel to the substrate.

The appearance of the RHEED patterns (observed at low angles of incidence $\sim 2^{o}$) changed during the course of the experiment. The substrate pattern which consisted of almost continuous streaks became modulated. The modulation increased with increasing film thickness and in the thickest films examined 100-225Å a sharp spot pattern was observed superimposed on faint streaks. Figs. 7.1. 7.2.

The intrinsic width of the RHEED features changed as the overlayer thickness increased. The initial deposits < 45Å produced broadened streaks, but as more palladium was deposited the streaks became sharper. The diffraction features from films 100Å were similar in breadth to those of the substrate. At all stages of the experiment the widths of streaks of different diffraction orders were found to be equal to one another.

The Auger data obtained during the initial stages of overlayer formation is shown in Fig. 7.3. as a function of film thickness. It is seen that the deposit signal is much stronger than that of the substrate after the deposition of only 10Å. The Auger spectrum from the specimen was unchanged

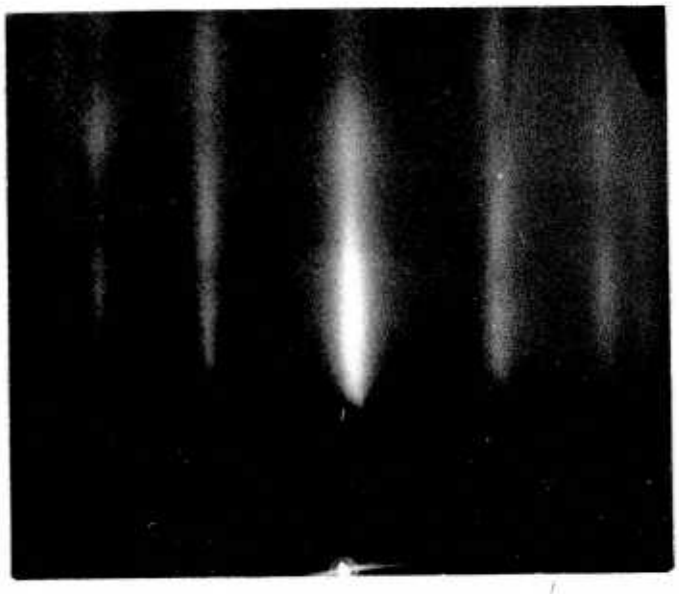


Figure 7.1.

RHEED pattern from $\sim 10\text{Å}$ of palladium deposited onto a (111) gold substrate at room temperature.

E_p = 37 keV, <211> and <110> azimuths superimposed due to 30° misorientation, $\alpha = 1.5^\circ$.

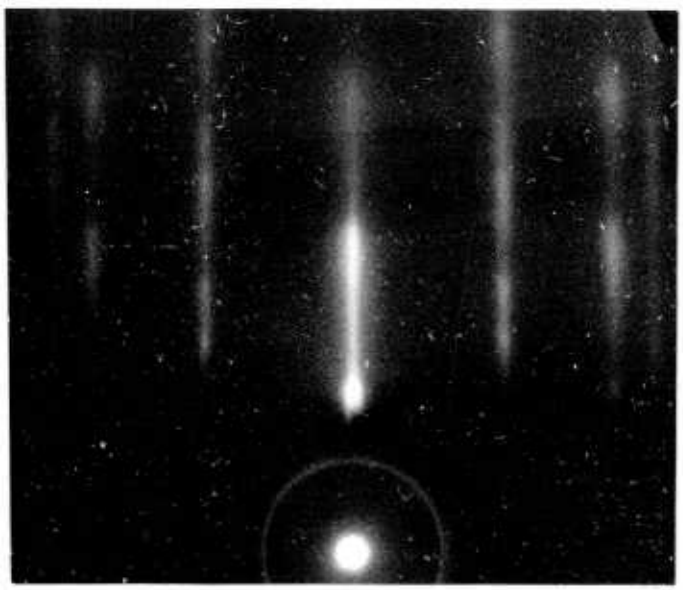


Figure 7.2.

RHEED pattern from $\sim 475\text{Å}$ of palladium deposited onto a (111) gold substrate at room temperature.

E_p = 37 keV, <211> and <110> azimuths superimposed due to 30° misorientation, $\alpha = 1.25^\circ$.

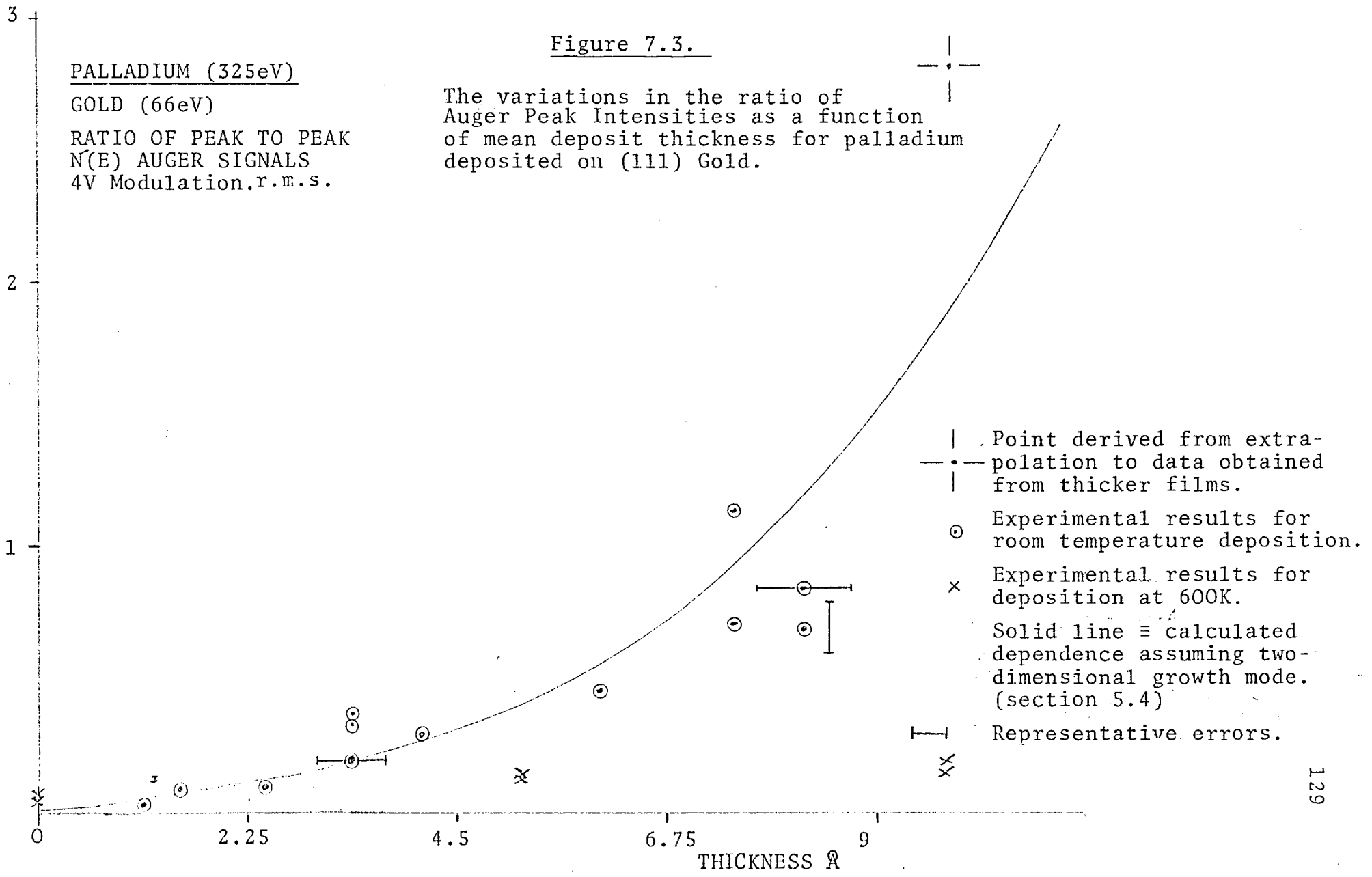


Figure 7.3.

The variations in the ratio of Auger Peak Intensities as a function of mean deposit thickness for palladium deposited on (111) Gold.

after annealing at room temperature for several hours. The first Auger spectrum was recorded within 6-7 minutes of completion of each deposition.

The mismatch M of the deposit the substrate was monitored throughout the experiment by RHEED - Section 5.1. It was found that the mismatch changed continuously with film thickness Fig. 7.4.

The deposit thickness h was determined by means of a calibrated quartz crystal oscillator - Section 5.2.

7.3. Results of Annealing Experiments at Elevated Temperatures on Palladium: Gold bicrystal Deposited at Room Temperature.

The bicrystal specimens used in this investigation consisted of thick films of palladium 100-225Å grown at room temperature on gold (111) substrates. The growth of these bicrystals is described in section 7.2. above.

After annealing in situ the specimens were observed with RHEED and A.E.S. Annealing for a few minutes at temperatures up to 500K produced no change. But on heating for a few minutes to temperatures > 555K the substrate Auger signal was observed to reappear. This signal was found to grow continuously relative to the palladium overlayer signal throughout the period of the anneal (2-3) days Fig. 7.5.

RHEED observation of the annealed films showed the spot diffraction pattern to have disappeared. The resulting RHEED pattern consisted of sharp almost continuous streaks. Fig. 7.6.

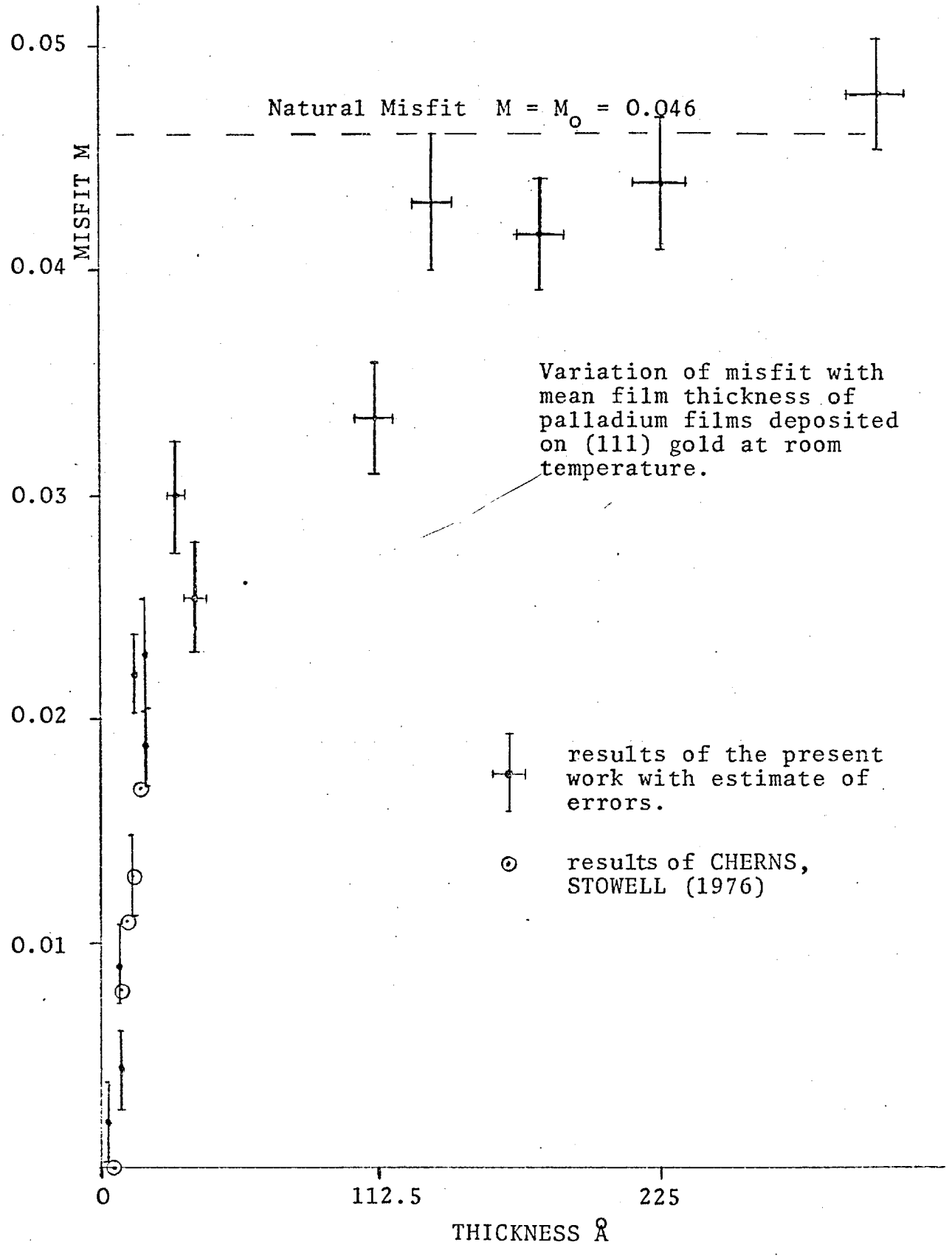
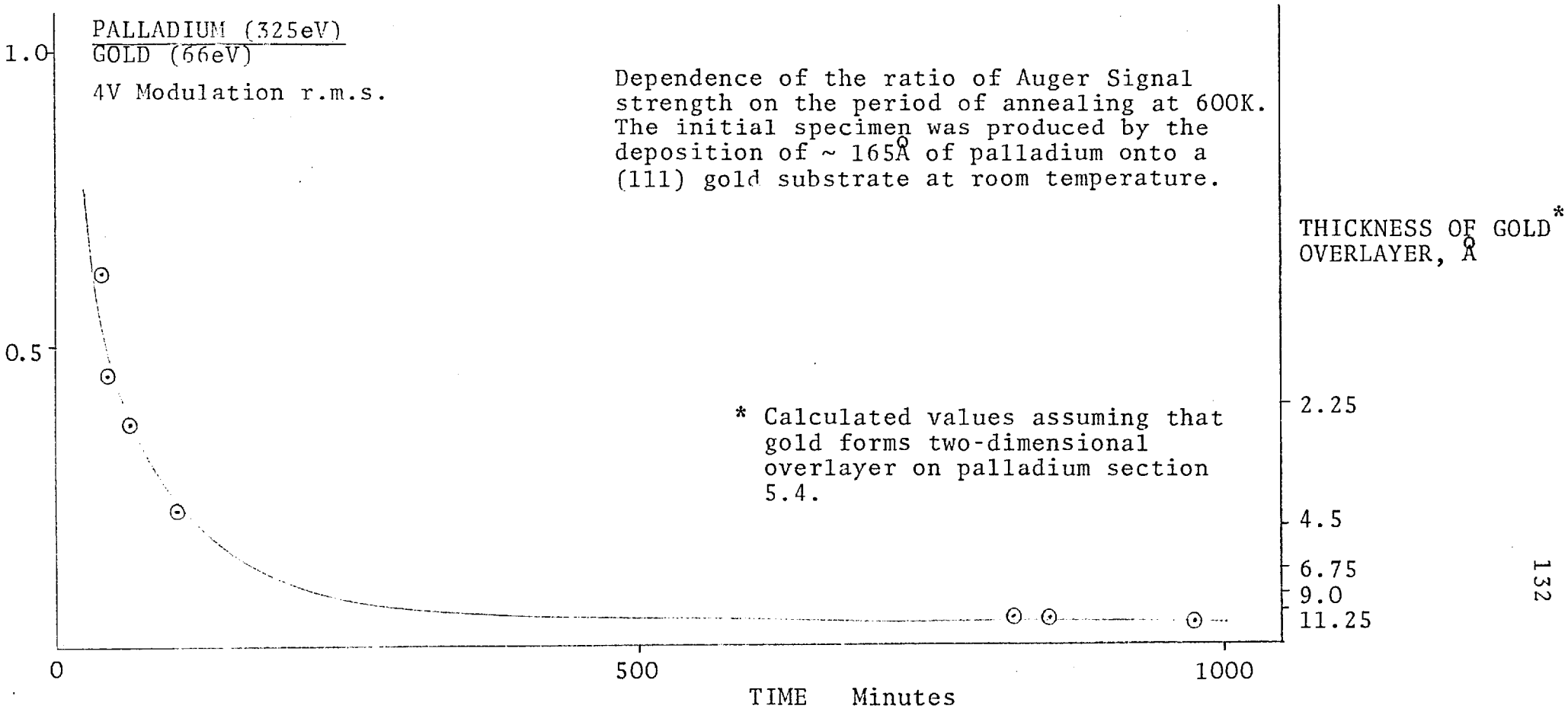

0.05
0.04
0.03
0.02
0.01
MISFIT M
Natural Misfit M = M$_o$ = 0.046
Variation of misfit with mean film thickness of palladium films deposited on (111) gold at room temperature.
results of the present work with estimate of errors.
results of CHERNS, STOWELL (1976)
0
112.5
225
THICKNESS Å

Figure 7.4.

Figure 7.5.



Dependence of the ratio of Auger Signal strength on the period of annealing at 600K. The initial specimen was produced by the deposition of ~ 165Å of palladium onto a (111) gold substrate at room temperature.

* Calculated values assuming that gold forms two-dimensional overlayer on palladium section 5.4.

RHEED measurements showed the lattice spacing at the specimen surface to have reverted within 0.06Å of the substrate spacing.

7.4. Discussion of Growth of Palladium on (111) Gold at Room Temperatures

Both the observed changes in modulation of RHEED streaks and the dependence of the Auger data on film thickness indicate that the first few monolayers of palladium, deposited on gold at room temperature grow two-dimensionally: layer upon layer. The increase in RHEED streaks modulation resulting from the deposition of 5-10Å of palladium suggests that only a small degree of roughness has developed. From the consideration of the reliability of the Auger technique used to predict the mode of growth section 5.4 the agreement between the predicted and experimental dependence of the Auger data on film thickness Fig. 7.3 is considered strong evidence for the occurrence of two-dimensional growth.

Because no change in the Auger spectrum is observed during the course of annealing at room temperature diffusion between the substrate and deposit can only have occurred on a small scale.

The changes in appearance observed in RHEED patterns during the growth of thick palladium films suggests that the surface becomes roughened. The patterns obtained from thick deposits of palladium > 100Å monolayers suggest that three-dimensional islands grow out of a two-dimensional deposit.

The broadening of RHEED features obtained from thin deposit films may result from both small crystallite sizes and disorder in the form of inhomogeneous elastic strains

section 3.3.2.

The measurement of the misfit M Fig. 7.4. shows that the thinnest layers of palladium are strained to match the gold substrate i.e. that they grow pseudomorphically.

7.5. Discussion of Results of Annealing Bicrystals Grown at Room Temperature T > 550K

The changes observed in specimens annealed at temperatures > 550K show that diffusion rates are significant in this temperature range. The appearance of continuous streaks in the RHEED patterns of annealed specimens suggests that the surface has become flatter. The transitions form a rough to a flat surface would be favoured by the associated reduction in the surface area and hence the total surface free energy of the specimen.

Auger examination showed that after annealing, gold substrate atoms had migrated to the specimen surface. Since the surface energy of palladium is greater than the surface energy of gold (surface energy of palladium 1.5 joules m^{-2}, surface energy of gold 1.2 joules m^{-2}) WEAST (1974) this process may also reduce the surface and total free energy of the system.

The movement of substrate atoms to the specimen surface may result from one of the following processes:-

1) The break-up of the overlayer film into islands exposing the gold substrate between the islands;

2) The formation via grain boundaries , dislocations and surface diffusion of a gold layer overlaying the deposit film.

3) The interdiffusion of the substrate and overlayer. The unmodulated streaks observed in RHEED patterns from annealed films are inconsistent with the formation of the three-dimensional islands of process (1). Even when such a transition is energetically favourable the large activation energy resulting from an initial increase in surface area is expected to prevent it taking place.

Processes (2) and (3) cannot be distinguished in the present work. Both processes may contribute to the final state, to an extent determined by the kinetics of each process. The final state is obtained by the above process occurring together with the surface smoothing.

Using the model described in section 5.4. the ratio of the Auger signal strengths was calculated for different structures and compared with the value obtained after prolonged annealing of Pd/Au bicrystals at temperatures > 625K. If the surface regions of the specimen was assumed to consist of a homogeneous Pd/Au alloy it is found to consist of $\sim$ 90% gold. However if a flat gold film is assumed to overlay the palladium it is calculated to have a thickness of 14Å.

The observed change in lattice spacing during the annealing process together with the observation of the growth of palladium at room temperature on annealed Au/Pd substrates suggests that the lattice spacing of the annealed substrates is characteristic of gold $\pm$ 0.01Å.

7.6. Results for the Growth of Palladium on (111) Gold at 600K

Palladium was deposited in stages onto a (111) palladium gold substrate maintained at 600K. The substrate was formed by the prolonged annealing of a palladium gold bicrystal described above in section 7.5.

The palladium grew epitaxially with the (111) planes and the <110> axis of the overlayer and substrate parallel.

The specimens are maintained at 600K for 1-2 hours between depositions while RHEED and AES observations were made. The initial Auger spectrum was obtained within $\sim$ 5 minutes of the completion of the deposition.

The appearance of the RHEED patterns were unchanged throughout the experiment. Figs. 7.6. 7.7.

After each deposition the ratio of the palladium Auger signal to the gold Auger signal was found to have increased with regard to its value before the deposition. During the annealing period between depositions the ratio was always found to decrease. The time dependence of the Auger data is shown in Fig. 7.8 for each deposition.

The mismatch M of the deposit surface with respect to the substrate surface obtained from RHEED measurements is shown as a function of film thickness in Fig. 7.9.

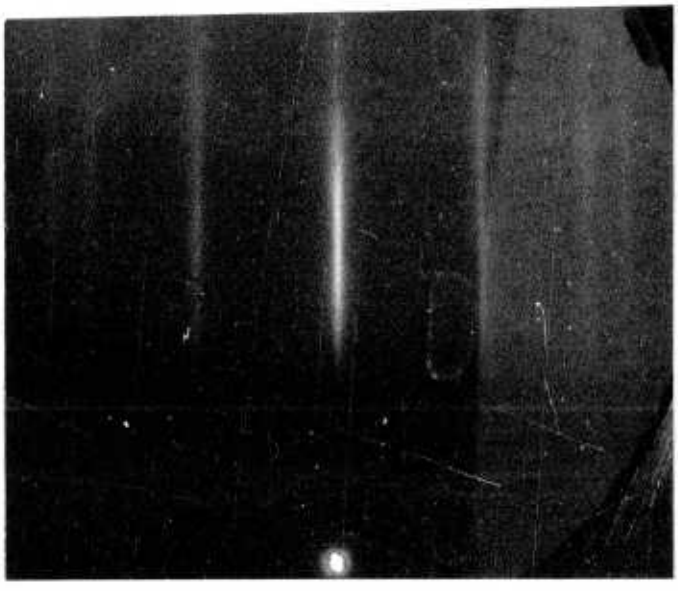


Figure 7.6.

RHEED pattern as figure 7.2. but after annealing at 615k for 37 hours.

E_p = 37 keV, <211> and <110> azimuths superimposed due to 30° misorientation, α = 1.8°.

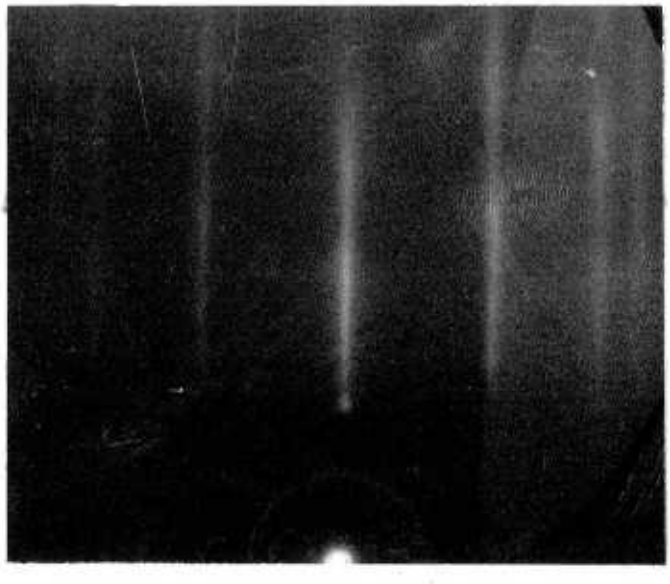
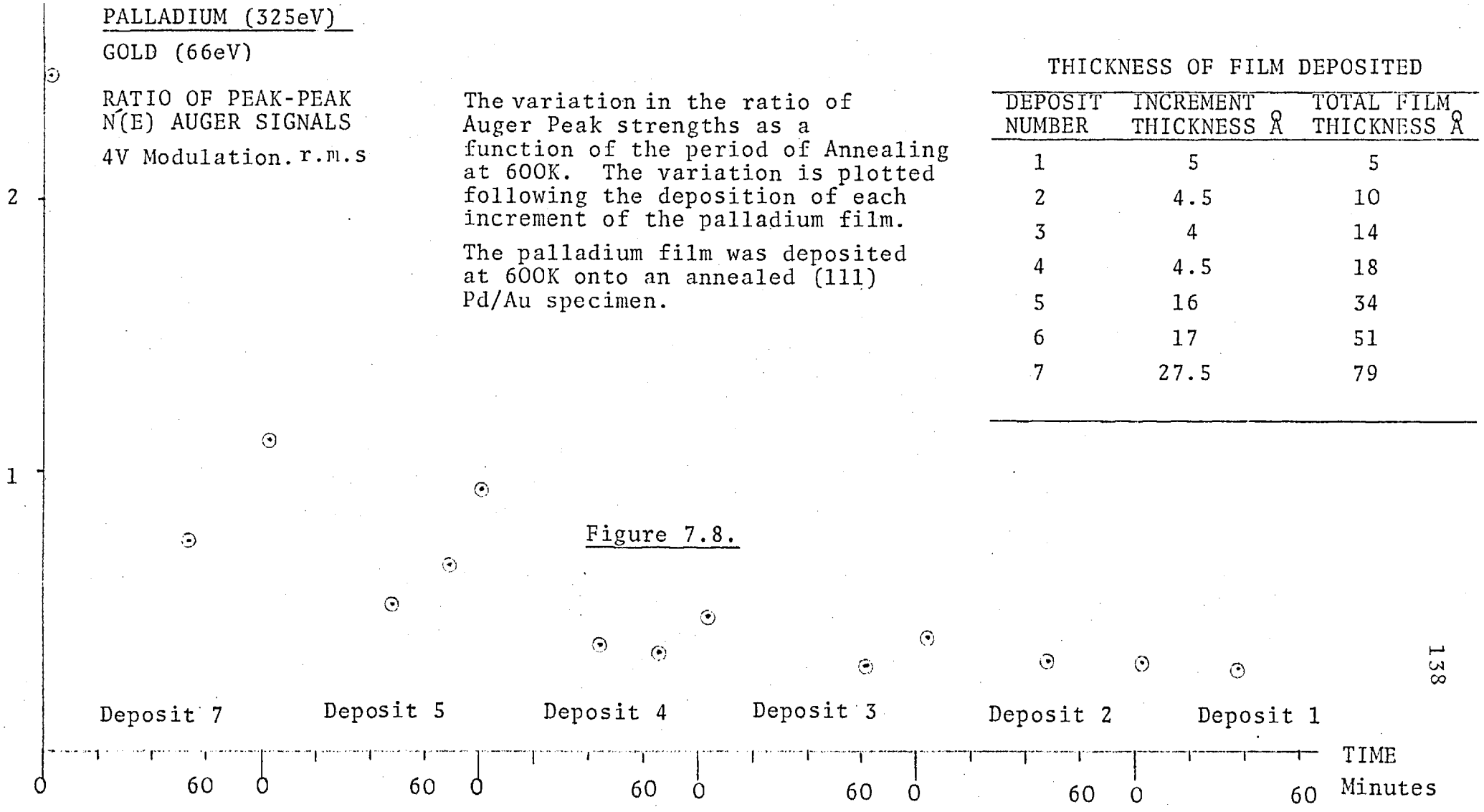


Figure 7.7

RHEED pattern from ~ 130Å of palladium deposited at 600K onto (111) annealed Pd/Au substrate (as in Fig.7.6)

E_p = 37 keV, <211> and <110> azimuths superimposed due to 30° misorientation, α = 1.5°.



The variation in the ratio of Auger Peak strengths as a function of the period of Annealing at 600K. The variation is plotted following the deposition of each increment of the palladium film.

The palladium film was deposited at 600K onto an annealed (111) Pd/Au specimen.

THICKNESS OF FILM DEPOSITED

DEPOSIT NUMBER	INCREMENT THICKNESS Å	TOTAL FILM THICKNESS Å
1	5	5
2	4.5	10
3	4	14
4	4.5	18
5	16	34
6	17	51
7	27.5	79

Figure 7.8.

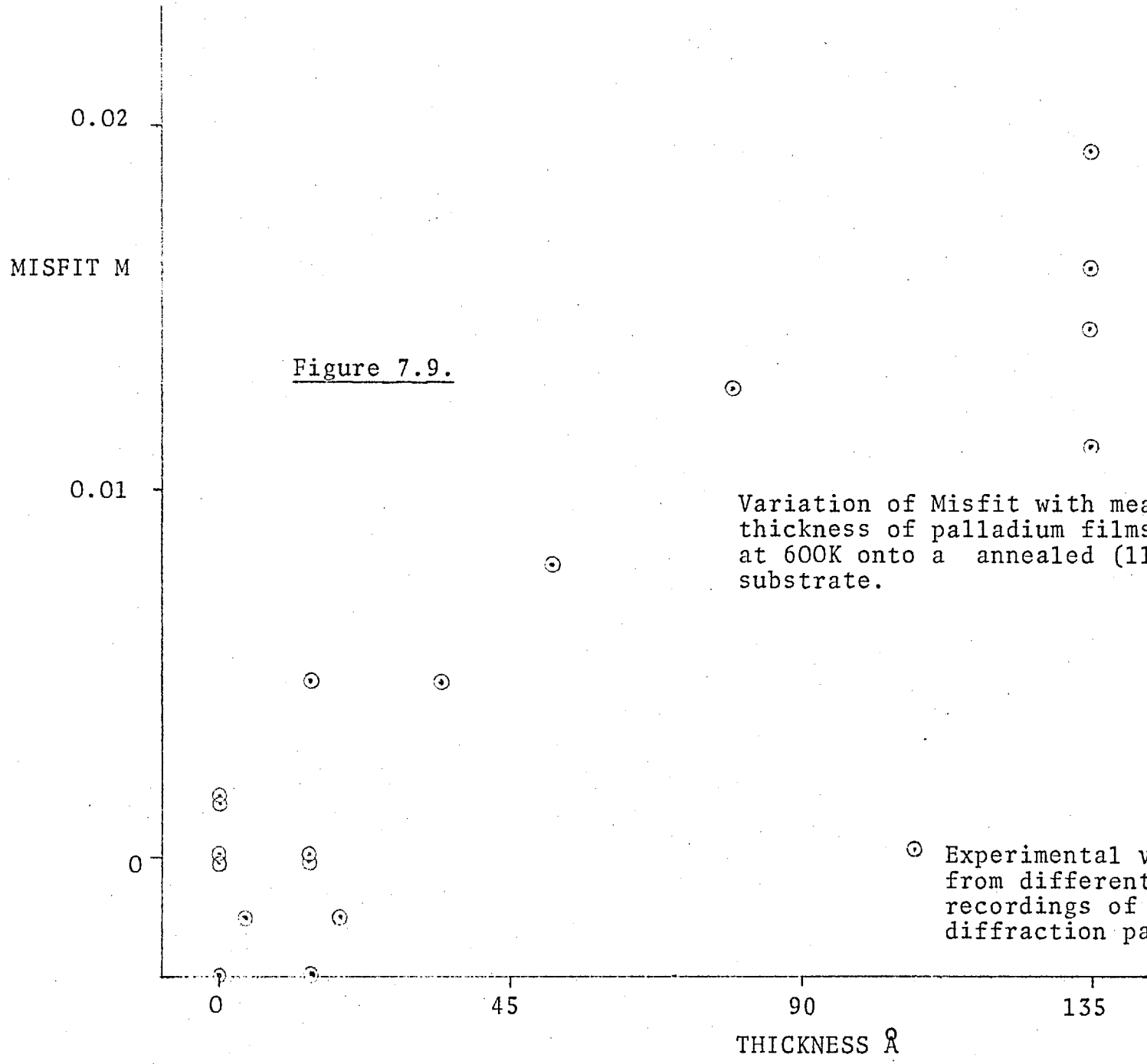


Figure 7.9.

Variation of Misfit with mean film thickness of palladium films deposited at 600K onto a annealed (111) Pd/Au substrate.

⊙ Experimental values obtained from different photographs recordings of corresponding diffraction pattern.

7.7. Discussion of the Growth of Palladium on Annealed Pd/Au Bicrystals at 600K

As a result of the discussion above section 7.5 we shall consider the substrate to act as a flat (111) gold crystal. The investigation with RHEED and AES of the growth of palladium at 600K on gold (111) shows that film growth proceeds in a manner substantially different from that observed at room temperature.

The RHEED patterns obtained throughout the experiment consisted only of unmodulated streaks. In contrast to the results of section 7.2. this suggests that a flat surface was maintained.

The time dependence of the Auger data observed while annealing between depositions indicates that diffusion processes are active. Fig. 7.10 displays the superposition of the time dependent Auger data obtained after different depositions to form a single curve. The smooth curve obtained is very similar to that of Fig. 7.5 suggesting that the same processes are active in both sets of observations. The Auger data obtained for the growth of palladium on gold at room temperature Fig. 7.3. was compared with that for the growth of palladium on gold at 600K Fig. 7.8. From this it can be seen that substantial diffusion occurs during the period of deposition.

The form of the change in lattice spacing observed by RHEED Fig. 7.9 is very different to that observed in Fig. 7.4. The variation observed in Fig. 7.9 is partly expected to depend on the extent to which alloying has taken place. It is expected that the dependence of misfit on film thickness at elevated temperatures is dependent on the increments of

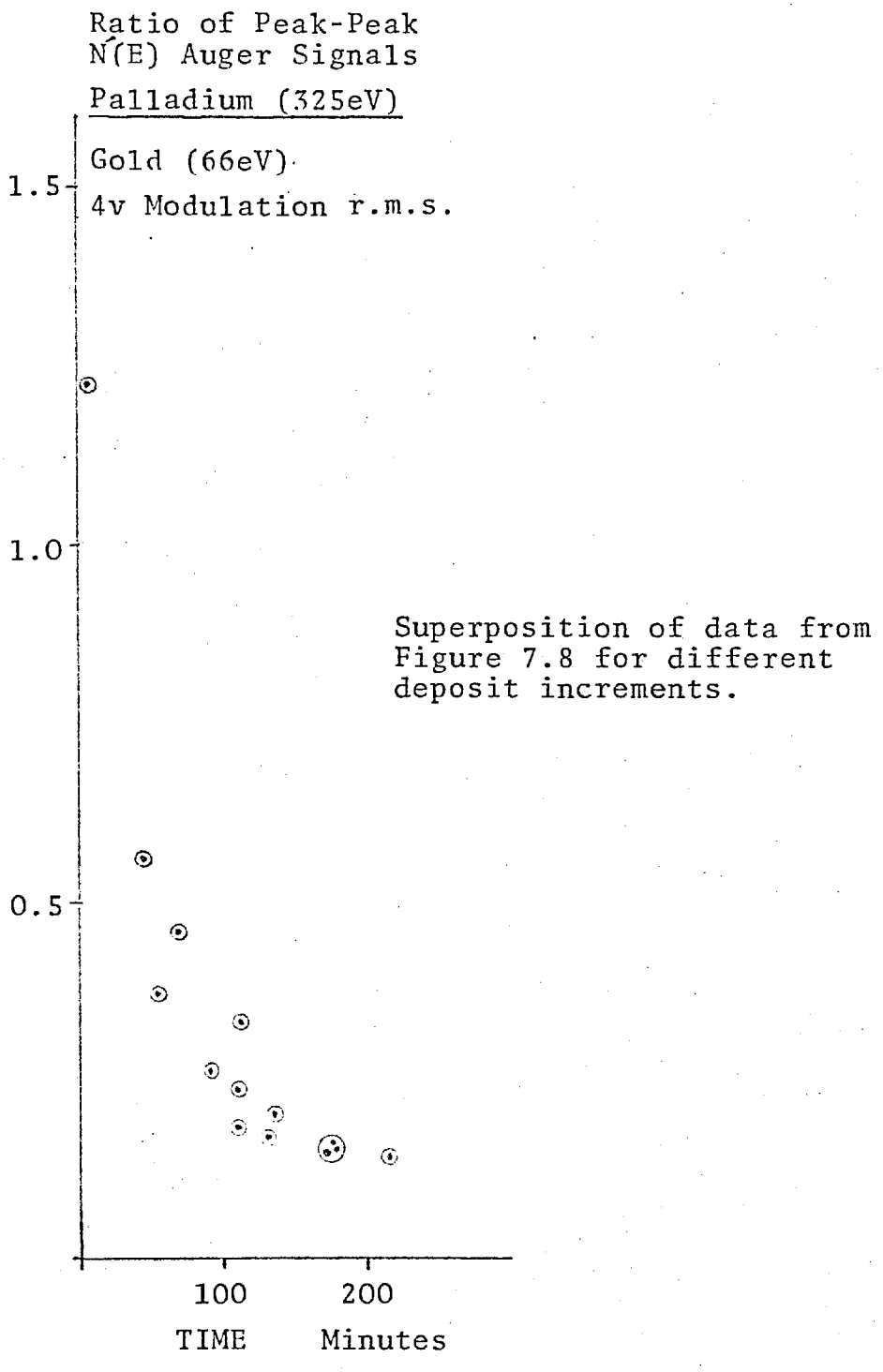

Ratio of Peak-Peak
N(E) Auger Signals
Palladium (325eV)
Gold (66eV)
4v Modulation r.m.s.
1.5
1.0
0.5
Superposition of data from
Figure 7.8 for different
deposit increments.
100
200
TIME
Minutes

Figure 7.10.

thickness deposited and the rate of deposition.

7.8. Discussion of the Results of the Present Work in Relation to other Investigations on the Same System

The present work shows palladium to grow initially on (111) gold at room temperature as a two-dimensional pseudomorphic overlayer. This result is in agreement with those of YAGI et al (1971) and CHERNS, STOWELL (1975a,b: 1976) although they carried out their depositions at elevated temperatures. However the work reported here also demonstrates the important influence of diffusion processes on film growth at elevated temperatures. It is therefore necessary to examine the possible effects of diffusion on their results.

The role of diffusion will depend on a number of factors BALLUFFI, BLAKELY (1975):-

1. Temperature
2. Time Scale
3. Film thickness
4. Single or staged deposition processes
5. Defects and dislocations.

The substrate temperatures investigated by YAGI et al (1971) 575-675K were higher than the temperature range for which diffusion was observed in the present work. CHERNS, STOWELL (1976) however worked mainly at lower temperatures 300-575K.

Specimens were annealed for longer periods in the present work than in that of CHERNS & STOWELL (1975a,b: 1976) who cooled their samples after deposition, a technique possibly adopted by YAGI et al (1971). In section 7.7 substantial diffusion effects were reported to occur during the process of deposition at 600K. These processes would be independent of subsequent annealing times, but would be dependent on the increments of thickness deposited and the rate of deposition.

The extent of rearrangement may be enhanced when the films are grown in stages. Because an extended annealing period may result. The films < 20Å thick examined by YAGI et al (1971) and CHERNS & STOWELL (1975a,b: 1976) were formed in a single evaporation.

Their experimental techniques were not suitable for determining the importance of diffusion processes, because no surface sensitive technique for chemical analysis was used and no systematic annealing experiments were reported. CHERNS & STOWELL (1975a,b: 1976) used an electron probe X-ray microanalysis technique for chemical analysis which is insensitive to the distribution of the atomic species within the specimen section 3.7. MATSUSHITA, YAGI et al (1974) did however make Auger observations of the growth at room temperature of Au/Pd and Pd/Au. The results obtained were in good agreement with the results reported in the present study. However they should not be assumed to be valid at the substrate temperatures used in the electron microscopy study of YAGI et al (1971). A fast interdiffusion process is reported by YAGI et al (1971) in electron microscopy

observations at temperatures above 675K, but was considered not to be significant in the temperature range 575-675K. In a later publication however MATSUSHITA, YAGI et al (1974) structural changes resulting from diffusion process above 525K are reported.

Some diffusion must have occurred in the specimens observed by YAGI et al (1971) but probably not in those of CHERNS & STOWELL (1975a,b: 1976). In the case of CHERNS & STOWELL (1976) this conclusion is supported by the good agreement between their results and the present work carried out at room temperature Fig. 7.4. YAGI et al (1971) however do not provide any results with which a comparison of this kind can be made.

7.9. Conclusions

It is concluded that the room temperature deposition of palladium onto (111) gold substrate causes palladium to grow as a two-dimensional overlayer elastically strained in its thinnest deposits $\sim$ 2.25Å to match the substrate. Diffusion processes have been shown to be significant when palladium-gold bicrystals are annealed at temperatures > 550K. It has also been shown that thin films of palladium deposited onto gold at temperatures > 600K have properties very different from those formed at room temperatures. This has been shown to be a result of alloying and diffusion processes.

REFERENCES

Ambramowitz, M., Stegun, I.A., (1965) Handbook of Mathematical functions. New York, Dover pp.228, 245-8.

Ashwell, G.W.B., Todd, C.J., R. Heckingbottom, (1973), J. Phys. E. Sci. Inst. Series 2, Vol. 6, p.435.

Ball, C.A.B., (1970) Phys. Status. Solidi, 42, 357.
(1970) Phys. Status. Solidi, 38, 335.

Ballufi, R.W., Blakely, J.M. (1975) Thin Solid Films, 25, 263.

Bauer, E. (1958) Z Kristallogr, 110, 372.-

Bishop, H.E., Rivière, J.C. (1969a) J. Appl. Phys. 40 1740.
(1969b) Brit. J. Appl.Phys. Series 2, Vol. 2, 1635.

Boyko, B.T., Palatruk, C.S., Lebedeva, M.V. (1968), Fiz. Met. Metalloued, 25, 845.

Bradley, D.E. (1963), "Replica and Shadowing Techniques from Techniques for Electron Microscopy", ed. D.H. Hag, (Blackwell, Oxford), p.96.

Brundle, C.R. (1974), J. Vac. Sci. Techn. 11, 212.

Cabrera, N. (1964) Surface Science, 2 320.

Chambers, A., Jackson, D.C. (1975), Phil. Mag. 31, 1357.

Chattopadhyay, B., Measor, J.C. (1969), J. Materials Science, 4, 457.

Cherns, D. (1974), Phil. Mag., 30, 549.

Cherns, D., Stowell, M.J., (1975), Thin Solid Films, 29, 107.
(1975), Thin Solid Films, 29, 127.

Cherns, D., Stowell, M.J., (1976), Thin Solid Films, 37, 249.

Chih Shui Lu (1975) J. Vac. Sci. Techn. 12, 578.

Coghlan, W.A., Clausing, R.E. (1973), Atomic Data, 5, 317.

Dickson, E.W., Jacobs, M.H., Pashley, D.W., (1965), Phil. Mag., Vol. 11, p. 575.

Dobson, P.J., Regan, B., (1976), J. Phys. E. Sci. Inst. Series 2, Vol. 9, p. 694.

Eernesse, E.P., (1972), J. Appl. Phys., 43, 1330.

Ehrlich, G., (1974), Int. Rev. Solid State Sci., 4, 205.

Eshelby, J. P. (1949), Phil. Mag., 40, 903.

Federenko, A.I., Vincent, R., (1971), Phil. Mag., 17, 461.

Fernier,R.P., Murray, R.T., (1966), J. Reg. Micro Soc., 85, 323.

Fletcher, N.H., (1967), Phil. Mag., 16, 159.

Fletcher, N.H., Lodge, K.W., (1975) from "Epitaxial Growth", Part B., Chapter 7, Ed. J.W. Matthews (Academic Press - New York).

Gallon, T.E. (1972), J. Phys. D. Appl. Phys. 5, 882.

Gibson, M.J. (1973), Ph.D. Thesis, University of London.

Gibson, M.J., Dobson, P.J., (1975) J. Phys. F. Metal. Phys. 5, 1828.

Gibson, M.J., Dobson, P.J., to be published.

Gradmann, U., (1964) Ann. Phys. Leipzig, 13, 213
(1966) Ann. Phys. Leipzig, 17, 91.

Gradmann, U. Humnerle, W., Jillmanns, P. (1976), Thin Solid Film, 34, 249.

Hales, R., (1976), Oxidation of Metals, 10, 29.

Hansen, P.H., (1958), "Constitution of Binary Alloys", 2nd Ed. (McGraw-Hill).

Harris, L.A., (1968), J. Appl. Phys. 39, 4802.

Harris, L.A. (1969), Surface Science, 15, 73.

Hirsch, P.B.,Howie, A., Nicholson, R.B., Pashley, D.W., Whelan, M.J., (1965), "Electron Microscopy of Thin Crystals", (Butterworths, London).

Horng, C.T., Vook, R.W., (1976), Surface Science, 54, 309.

Jackson, D.C., Gallon, T.E., Chambers. A., (1973), Surface Science, 36, 381.

Jesser,W.A., Kuhlmann-Welsderf, D., (1967) Phys. Status Solidi, 19, 95., 21, 533.

Jesser, W.A., Matthews, J.W., (1967), Phil. Mag., 15, 1097.
(1968a), Phil. Mag., 17, 461.
(1968b), Phil. Mag., 17, 595.
(1968c), Acta. Met., 16, 1307.
(1968d), Phil. Mag., 17, 475.

Jesser, W.A., Van der Merwe, J.H., (1971), Phil. Mag., 24, 295.

King, W.H., (1971), "Application of Quantum Vacuum Microbalance Tech." Vol. 8, P.183, 1971, ed. A.W. Crzanderra, (Plenum Press).

Kruger, J., Yolken (1964), Corrosion, 20, 29.

Kuntze, R., Chambers, A., Prutton, M., (1969), Thin Solid Films, 36, 381.

Matsushita, Y., Yagi, K., Narusawa, T., Hanjo, G., (1974), Japanese Journal of Appl. Phys. Suppl.2., Part 1., 1974, p.567.

Matthews, J., (1966), Phil. Mag., 13, 1207.
(1970), Thin Solid Films, 5, 369.
(1972a), Surface Science, 31, 241.
(1973), from "A Treatise on Dislocations" ed. Nabarro, F.R.M., (Dekker-New York).
(1975), Epitaxial Growth", Chapter 8.

Matthews, J.W., Crawford, J.L., (1970), Thin Solid Film, 5, 187.

Matthews, J.W., Jesser, W.A., (1967), Acta Met. 15, 595.

Markov, I., Karschew, R., (1976), Thin Solid Films, 32, 163.

McDavid, J.M, Fain, S.C., (1975), Surface Science, 52, 161.

McGuire, E.J., (1972), Phys. Rev. A., 5, 1052.

Menadue, J.F., (1972), Acta Crysta. A., 28, 1.

Menter, J.W., (1958), Adv. in Physics, 7, 299.

Meyer, I., Vrakking, J.J., (1974), Surface Science, 45, 409.

Misell, D.L., (1973), Adv. Electron Phys., 32, 63-191.

Mlynczak, A., Niedermeyer, R., (1975), Thin Solid Films., 28. 37-58.

Neave, J.H., Foxon, C.T., Joyce, B.A., (1972), Surface Science, 29, 411.

Newman, R.C., Pashley, D.W., (1955), Phil. Mag., 46, 927.

Palmberg, P.W. Rhodin, T.N., (1968), J. Appl. Phys., 39, 24-25.

Pashley, D.W., (1956), Phil. Mag. Suppl. Vol.5, No.8, 173.

Pashley, D.W., (1959), Phil. Mag. Vol. 4, p.316.

Poppa, H., Moorhead, R.D., Heinemann, K., (1972), Nucl. Instr. Meth., 102, 521.

Poppa, H., Heinemann, K., Elliott, A.G., (1972), J. Vac. Sci. Technol., 102, 149.

Powell, C.J., (1974), Surface Science, 44, 29.

Rhodin, T.N., (1950), J. Amer. Chem. Soc., 72, 5102.
(1951), J. Amer. Chem. Soc., 73, 3143.

Sass, S.L., Balluffi, R.W., (1976), Phil. Mag., 33, 703.

Sass, S.L., Ton, T.Y., Balluffi, R.W., (1975), Phil. Mag., 31, 559.

G. Sauerbrey, (1959), Z. Physik, 155, 206.
(1964), Z. Physik, 178, 457.

Sewell, P.B., Mitchell, D.F., Cohen, M., (1969), "Developments in Applied Spectroscopy" Vol. 7a, ed. Grove, E.L., and Perkins, A.J. Plenum Press, New York - London 1969.

Sewell, P.B., Mitchell, D.F., Cohen, M., (1972) "Surface Science", 33, 535.

Simmons, G.W., Dwyer, D.J., (1975), "Surface Science", 48, 373.

Stoddart, C.T.H., Moss, R.C., and Pope, P., (1975), Surface Science, 53, 241.

Stowell, M.J., (1975), Chapter 5 from "Epitaxial Growth", Part B., ed. Matthews, J.W., (Academic Press, New York).

Taylor, A., (1961), "X-ray Metallography", (Wiley, N.Y.).

Taylor, N.J., (1969), Rev. Sci. Inst., 40, 792.

Van der Merwe, J.H., (1950), Proc. Phys. Soc., London A63, 616.
(1963a), J. Appl. Phys., 34, 117.
(1963b), J. Appl. Phys., 34, 123.
(1970), J. Appl. Phys., 41, 4725.

Varnshilein, B.K., (1964), "Structure Analysis by Electron Diffraction", Pergamon Press, Oxford. p.158.

Vrakking, J.J., Meyer, F., (1975), Surface Science, 47, 50.

Warner, A.W., Stockbridge, C.D., (1963), "Vacuum Microbalance Techniques", Vol.3., ed. K.H. Behrndt, (Plenum Press, New York).

Wassermann, E.F., Jablonski, H.P., (1970), Surface Science, 22, 69.

Weast, R.C., (1974), "Handbook of Chemistry and Physics", C.R.C. Press.

Weber, R.E., Peria, W.T., (1967), J. Appl. Phys., 38, 4355.

Wyckoff, W.G., (1963), "Crystal Structures", Vol.2., (Interscience - New York).

Yagi, K., Takagonagi, K., Kobagashi, K., Honjo, G., (1971), J. Crystl. Growth., 9, 84.

Yagi, K. Takagonagi, K., Kobagashi, K., Honjo, G., (1976), Thin Solid Films, 32, 185.

S.C. Yung, (1971), Phys. Review B. 3, 4160.